Carbon Fibre Reinforced Polymer Composites with Enhanced Ductility

Hele Diao

2014

A dissertation submitted in partial fulfilment of the requirements for the degree of

Doctor of Philosophy of Imperial College London

Department of Chemical Engineering

Imperial College London

South Kensington Campus,

SW7 2AZ London, UK

Abstract

Carbon fibre reinforced polymers (CFRPs) have high strength and stiffness, low density, long fatigue life in the fibre direction and good corrosion resistance. Nowadays, CFRPs are been used in aeronautics, wind turbine blades, sports goods and civil industry. However, one fundamental limitation of CFRPs is their brittleness (low ductility): CFRPs fail catastrophically at a relatively low strain (1.5% to 1.8%) under the tension with little warning or residual load-carrying capacity. To overcome this weakness, there is considerable interest to enhance the ductility of CFRPs exhibiting increased failure strains under tension and more progressive, graceful failure modes.

In this work, three different methods were developed to improve the ductility of unidirectional (UD) CFRPs. The first method was to introduce fibre waviness into UD composites. The fibre alignment angles of the resulting composites and control composites were assessed and it was found that fibre waviness in UD composite did result in a stepwise tensile failure mode and an enhanced strain to failure. The second method was using an air-assisted fibre tow spreading and commingling technology to manufacture continuous intermingled carbon fibre/glass fibre hybrid tows. After defining and quantifying the degree of hybridisation (at the filament level) of two carbon fibre/glass fibre hybrid tows, the one with the higher degree of hybridisation was selected to manufacture intermingled UD hybrid composites. It was found that hybridising of continuous glass and carbon fibres resulted in the composites with an increased failure strain. Moreover, these hybrid composites failed more gradually. The final method investigated for introducing ductility was the introduction of ply cuts into PEEK interleaved UD carbon fibre/PEEK composites, which were manufactured by compression moulding. The resulting cut-ply interleaved carbon

fibre/PEEK composite possessed a non-linear tensile stress-strain curve and ductility strain of 0.4%, which is due to shearing of the PEEK interleaves in the overlap regions between the cut carbon fibre plies.

Declaration of Originality

This dissertation is a description of the work carried out by the author in Department of Chemical Engineering, Imperial College London between October 2010 and November 2014 under the supervision of Prof. Alexander Bismarck and Prof. Paul Robinson. Except where acknowledged, the material presented is the original work of the author and no part of it has been submitted for a degree at this or any other university.

Signature

Date

Copyright Declaration

The copyright of this thesis rests with the author and is made available under a Creative Commons Attribution Non-Commercial No Derivatives licence. Researchers are free to copy, distribute or transmit the thesis on the condition that they attribute it, that they do not use it for commercial purposes and that they do not alter, transform or build upon it. For any reuse or redistribution, researchers must make clear to others the licence terms of this work.

Acknowledgement

First of all, I would like to thank my PhD supervisors, Profs Alexander Bismarck and Paul Robinson from Imperial College London and Prof. Michael Wisnom from the University of Bristol for their patient guidance, consistent encouragement and helpful discussions during the past four years. They have been sharing their extensive knowledge, great passion and valuable expertise in composite materials, which inspired me and also improved my work skills for the future.

I would like to express my gratitude to UK Engineering and Physical Sciences Research Council (EPSRC) for providing financial support to part of my research via Programme Grant EP/I02946X/1 on High Performance Ductile Composite Technology (HiperDuCT).

I am grateful to Dr. John Hodgkinson for valuable and prompt modification of my PhD thesis manuscript, helpful suggestions about mechanical testing methods for composite materials and expert advice on the characterisation of fibre misalignment angles. I am indebted to Dr. Soraia Pimenta for her modelling skills in predicting tensile behaviour of hybrid carbon/glass fibre composites and cut-ply interleaved carbon fibre/PEEK composites. I would like to thank Gary Senior, Jonathan Cole and Mark Grant for their help on composite manufacturing and sample preparation, Joseph Meggyesi for his patient tuition on mechanical testing of composite materials, Dr. Jesper Ankersen and Dr. Carla Gispert for their assistance with DIC measurements.

I would like to express my gratitude to all the members in Polymer and Composite Engineering (PaCE) group, who were always helpful and provided joy not only in research but also in daily life. I would like to thank (not in any particular order) Dr. Kingsley Ho, Dr. Siti Rosminah Shamsuddin, Dr. Koon Yang Lee, Dr. Sheema Riaz,

Dr. Henry Maple, Dr. Robert Woodward, Dr. Derrick Fam, Dr. Hui Qian, Dr. Atif Javaid, Dr. Natasha Shirshova, Su Bai, Dr. Edyta Lam, Jing Li, Michael Tebboth, Francois De Luca, Dr. Tomi Herceg, Wan Wan Nawawi, Dr. Jonny Blaker, Dr. Min Tang, Dr. Andreas Mautner, Dr. Ling Ching Wong, Dr. Qixiang Jiang and Dr. Nadine Graeber. Also, I would like to thank all the supervisors (Prof. Michael Wisnom, Prof. Ian Bond, Dr. Sameer Rahatekar, Prof. Kevin Potter, Prof. Paul Weaver, Prof. Alexander Bismarck, Prof. Paul Robinson, Prof. Milo Shaffer, Dr. Pimenta Soraia, Prof. Paul Curtis and Dr. Silvestre Pinho) and researchers (Dr. Omar Bacarreza Nogales, Dr. David Anthony, Francois De Luca, Dr. Gael Grail, Dr. Gergely Czel, Dr. HaNa Yu, Dr. James Serginson, James Trevarthen, Jonathan Fuller, Dr. Meisam Jalalvand, Dr. Siti Rosminah Shamsuddin and Stefano Del Rosso) involved in HiperDuCT project, a true collaboration between Imperial College and the University of Bristol, for their helpful discussions and advice during the monthly meetings.

Last, but not the least, I am deeply grateful to my parents, Riming Diao and Hongwen He. They nurtured my interest in science and engineering when I was a child and encouraged and supported me to study overseas when I grew up. During all those years, they gave me their deepest and endless love. Without them, I would not have finished my PhD successfully. Thanks for everything you did for me!

Table of contents

Abstract 2

Declaration of Originality 4

Copyright Declaration 5

Acknowledgement 6

Table of contents 8

List of figures 13

List of tables 19

List of abbreviation 21

1 Introduction 22

1.1 Aims and objectives 23

1.2 Structure of thesis 25

2 Indication of the potential of making UD CFRPs with the enhanced tensile strain via introducing fibre waviness 26

2.1 Introduction 26

2.2 Literature review 27

2.2.1 The effect of fibre waviness and misalignment on the tensile behaviour of UD composites 27

2.2.2 Manufacturing techniques to produce composites containing wavy fibres 30

2.2.3 Methodology of measuring fibre waviness and fibre misalignment 33

2.3 Materials and methods 36

2.3.1 Materials 36
2.3.2 Manufacturing UD carbon fibre/PA-12 with fibre waviness 36
2.3.3 Single-fibre tensile tests on as-received and gas-textured carbon fibres 41
2.3.4 Tensile tests of control, gas-textured and non-constrained annealed carbon fibre/PA-12 tapes 43
2.3.5 Measuring fibre alignment angle in carbon fibre/PA-12 composites 44
2.4 Results and discussion 46
2.4.1 Effect of gas-texturing on the tensile properties of carbon fibres 46
2.4.2 Tensile behaviour of control, gas-textured and non-constrained annealed carbon fibre/PA-12 tapes 47
2.4.3 The fibre alignment angle in the control, gas-textured and non-constrained annealed carbon fibre/PA-12 tapes 50
2.5 Summary 53
3 Intermingled carbon fibre/glass fibre thermosetting hybrid composites 55
3.1 Introduction 55
3.2 Literature review 57
3.2.1 The definition and classification of fibre hybrid composites 57
3.2.2 Tensile behaviour of UD fibre hybrid composites 58
3.2.3 Manufacturing of UD fibre hybrid composites 66
3.3 Materials and methods 69
3.3.1 Materials 69
3.3.2 Air-assisted fibre tow spreading and intermingling technology 70

3.3.3 Microscopy analysis of carbon fibre/glass fibre hybrid tows 74

3.3.4 Determination of fibre diameters 75

3.3.5 Manufacturing of carbon fibre/glass fibre reinforced epoxy hybrid composite 76

3.3.6 Tensile test of carbon fibre/glass fibre reinforced epoxy composite 77

3.4 Results and discussion 78

3.4.1 Spreading and comingling of carbon fibre/glass fibre tows 78

3.4.2 Characterisation of the degree of the hybridisation of carbon fibre/glass fibre tows 86

3.4.3 Degree of hybridisation of carbon fibre/glass fibre hybrid fibre tows 97

3.4.4 Tensile properties of carbon fibre/glass fibre reinforced epoxy composites 99

3.5 Summary 101

4 Ductile cut-ply interleaved carbon fibre/PEEK composites 103

4.1 Introduction 103

4.2 Literature review 105

4.3 Materials and method 106

4.3.1 Materials 106

4.3.2 Cut-ply interleaved carbon fibre/PEEK design 107

4.3.3 Manufacturing method of cut-ply interleaved carbon fibre/PEEK 109

4.3.4 Tensile test method of cut-ply interleaved carbon fibre/PEEK 113

4.3.5 Fractography 115

4.4 Results and discussion....116

4.4.1 The micro-structure of cut-ply interleaved carbon fibre/PEEK composite ……..116

4.4.2 Tensile behaviour of cut-ply interleaved carbon fibre/PEEK composite ……..120

4.4.3 Fractographic analysis of the cut-ply interleaved carbon fibre/PEEK composite....124

4.5 Summary....124

5 Conclusions and future work....126

5.1 Summary of findings....126

5.1.1 Introducing fibre waviness into UD composites....126

5.1.2 Intermingled UD carbon fibre/glass fibre hybrid composites....127

5.1.3 Interleaved cut-ply carbon fibre/PEEK composites....128

5.1.4 Comparison of the three approaches to produce CFRP with enhanced ductility ……..128

5.2 Suggestions for future work....130

5.2.1 Introducing fibre waviness into UD composites....130

5.2.2 Intermingled UD carbon fibre/glass fibre hybrid composites....131

5.2.3 Interleaved cut-ply carbon fibre/PEEK composite....132

Appendix I....134

Appendix II....137

Appendix III....139

References.....140

List of figures

Figure 2.1 Predicted and experimental tensile stress-strain curves of $(\pm\theta)_S$ carbon fibre/PEEK composite [22].....27

Figure 2.2 (a) Schematic drawing of representative volume and coordinates for UD composite with uniform fibre waviness, (b) photo showing UD composite with uniform fibre waviness and (c) predicted and experimentally obtained tensile stress-strain curves for UD composite with uniform fibre waviness but various fibre waviness ratios [30] 29

Figure 2.3 Schematic diagrams of manufacturing techniques to produce thermosetting composites containing ply waviness (a) [31], (b) [32, 33, 35], (c) and (d) [35, 36]....31

Figure 2.4 Schematic drawing of a sinusoidal-model waved fibre [30].....33

Figure 2.5 Unidirectional carbon/epoxy composite with out-of-plane ply waviness[48] 34

Figure 2.6 (a) Optical micrograph of UD composite with a domain and pixel array highlighted and (b) schematic depiction of a set of domains within which the average 35

Figure 2.7 (a) Photo and (b) flow chart of setup of manufacturing route of UD carbon fibre/PA-12 composite tape 36

Figure 2.8 Design of gas-texturing device (a) photo (b) schematic diagram.....37

Figure 2.9 Setup of (a) 13 pins used in wet-impregnation bath and (b) 3 heated shear pins.....38

Figure 2.10 Schematic diagram of layup process of carbon fibre/PA-12 tapes during non-constrained annealing 39

Figure 2.11 Mould temperature during the non-constrained annealing process.....40

Figure 2.12 Top views of the carbon fibre/PA-12 tape (a) before and (b) after non-constrained annealing.....40
Figure 2.13 Mounting for single fibre tensile test specimen (a) Dimensions of mounting (b) Mounting with specimen bonded in place 42
Figure 2.14 Setup of single-fibre tensile test 42
Figure 2.15 The dimensions of the tensile specimen.....43
Figure 2.16 Setup for tensile tests of UD composite tapes 43
Figure 2.17 (a) Schematic diagram of cutting sample (b) Typical microscopy image of polished sample surface 44
Figure 2.18 Distribution of the apparent fibre alignment angles of a typical gas-textured carbon fibre/PA-12 sample 45
Figure 2.19 Typical tensile stress-strain plots of as-received and gas-textured carbon fibres 46
Figure 2.20 (a) The cumulative failure curve and (b) Weibull plots of as-received and gas-textured carbon fibres.....47
Figure 2.21 Tensile stress-strain curves of (a) control, (b) gas-textured and (c) non-constrained annealed carbon fibre/PA-12 tapes.....50
Figure 2.22 True fibre alignment angle distributions of (a) control (b) gas-textured and (c) non-constrained annealed carbon fibre/PA-12 composites 51
Figure 3.1 Classification of fibre hybrid composites: (a) laminated, (b) woven and (c) intermingled 58
Figure 3.2 Theoretical tensile strength of fibre hybrid composite [63] 66
Figure 3.3 Schematic figure of air-assisted fibre spreading process [101].....70
Figure 3.4 Setup of fibre tow spreading machine (a) photo (b) flow chart 71
Figure 3.5 Schematic figure of air-assisted fibre hybridisation process.....73

Figure 3.6 Manufacturing of intermingled carbon fibre /glass fibre tow 74
Figure 3.7 Typical micrograph of a carbon fibre/glass fibre hybrid tow (type B).....75
Figure 3.8 (a) Schematic diagram and (b) photo of the setup used to measure fibre diameters using the modified-Wilhelmy technique 76
Figure 3.9 (a) Schematic and (b) photo of the mould used to manufacture carbon fibre/glass fibre reinforced epoxy hybrid composite 77
Figure 3.10 Dimensions of the specimen used for the tensile testing.....77
Figure 3.11 Photos of carbon fibre and glass fibre tows taken during fibre spreading83
Figure 3.12 Appearance of same spread carbon fibre (CF-H) tow with and without twists 84
Figure 3.13 Appearance of carbon fibre/glass fibre hybrid tows (a) Type A and (b) Type B.....85
Figure 3.14 Schematic diagrams of ideal intermingled fibre hybrid tow containing two fibre types in the (a) hexagonal fibre package and (b) cubic fibre package 87
Figure 3.15 Schematic of the model to describe randomly-distributed, comingled two fibre-type hybrid tow 87
Figure 3.16 Probability distribution of $AP_{CF,Model}$ for a model fibre hybrid tow type B when the model was run 1, 10, 100 and 1000 times at the sizes of analysis windows of (a) 3x3 (b) 6x6, and (c) 14x14 fibres 89
Figure 3.17 Coefficient of variation in $AP_{CF,Model}$ for fibre hybrid tow type B at as function of the size of the analysis window and number of times the model was run 90
Figure 3.18 Flow chart of the program to evaluate the distribution of carbon fibre and glass fibre in micrographs of cross-sections of carbon fibre/glass fibre hybrid tows..91

Figure 3.19 Detection of carbon fibres and glass fibres from original micrograph using an image recognition program: (a) original micrograph, (b) carbon fibre within the micrograph and (c) glass fibre within the micrograph 92
Figure 3.20 Schematic of subdividing the micrograph into square analysis windows 93
Figure 3.21 Probability distributions of $AP_{CF,Model}$ and $AP_{CF,Experiment}$ for fibre hybrid tow type B as function of the size of analysis windows (a) $(3D_{nominal})^2$, (b) $(6D_{nominal})^2$and (c) $(14D_{nominal})^2$ 96
Figure 3.22 Coefficients of variation in $AP_{CF,Model}$ and $AP_{CF,Experiment}$ as a function of $\sqrt{\text{size of analysis window}}$ 97
Figure 3.23 Characteristic optical micrographs of cross-sections of fibre hybrid tow A (a and b) and fibre hybrid tow B (c and d) 99
Figure 3.24 Typical tensile stress-strain curves of control carbon fibre/epoxy, carbon fibre/glass fibre/epoxy and control glass fibre/epoxy (V_f =30-40%, V_{CF}:V_{GF} = 1.55:1) 100
Figure 4.1 Schematic diagram of cut-ply interleaved carbon fibre/PEEK composite 104
Figure 4.2 Schematic diagrams of UD discontinuous tow composite laminates [116] 106
Figure 4.3 Analysis of the unit cell in the cut-ply interleaved carbon fibre/PEEK composite 108
Figure 4.4 Photo of the mould for manufacturing small-scale interleaved carbon fibre/PEEK composite 110
Figure 4.5 (a) Schematic diagram and (b) photo of the mould for manufacturing large-scale cut-ply interleaved carbon fibre/PEEK composite 112
Figure 4.6 Schematic diagrams of cutting template (a) A and (b) B 113

Figure 4.7 (a) Schematic diagram from the side view and (b) photo of the tensile test setup 114

Figure 4.8 Definition of initial modulus, σ_y, ε_y, ε_u and ε_d 115

Figure 4.9 Schematic diagram of fracture surface of cut-ply interleaved carbon fibre/PEEK 115

Figure 4.10 The thicknesses of PEEK region in small-scale interleaved carbon fibre/PEEK composites manufactured from the PEEK films with the thicknesses of (a) 100 μm and (b) 50 μm via various temperature and pressure used in compression moulding 117

Figure 4.11 The micrographs of small-scale interleaved carbon fibre/PEEK composites made from (a) 50-μm-thick PEEK film (sample: S-8)and (b) 100-μm-thick PEEK film (sample :S-4) 118

Figure 4.12 The micro-structure of the large-scale cut-ply interleaved carbon fibre/PEEK composites obtained using cutting templates (a) A and (b) B..... 119

Figure 4.13 The schematic diagram of micro-structural changes in cut-ply interleaved carbon fibre/PEEK composite caused by compression moulding 120

Figure 4.14 The typical tensile stress-strain curves measured from the front and back view at the gauge length of 10 mm 121

Figure 4.15 The micrographs of a cut-ply interleaved carbon fibre/PEEK composite observed from the (a) front and (b) back views 122

Figure 4.16 A typical plot of the effect of the gauge length on the strain to failure and modulus of the cut-ply interleaved carbon fibre/PEEK composite 123

Figure 4.17 The typical tensile stress-strain curves of cut-ply interleaved carbon fibre/PEEK composite at the gauge length of 6,8 10 and 12mm 123

Figure 4.18 The SEM images of PEEK fracture surface of cut-ply interleaved carbon fibre/PEEK composite at the magnifications of (a) 1000 x and (b) 1600 x.....124
Figure 5.1 Schematic diagram of interleaved cut-ply carbon fibre/PEEK composite containing multiple overlapping regions 133

List of tables

Table 2.1 Operation parameters of polishing process.....44

Table 2.2 Tensile properties of as-received and gas-textured carbon fibre 47

Table 2.3 Tensile properties of control, gas-textured and non-constrained annealed carbon fibre/PA-12 composite tapes.....48

Table 2.4 Parameters of the Gaussian fitting curves of the distribution of the fibre alignment angles of control, gas-textured, non-constrained annealed carbon fibre/PA-12 composite 52

Table 3.1 Overview of the investigations on the hybrid effect of continuous UD fibre hybrid composites 61

Table 3.2 Comparisons of ultimate failure strain of the hybrid composites and their corresponding un-hybridised composites 65

Table 3.3 The detail information of carbon fibres 69

Table 3.4 The detail information of glass fibres 70

Table 3.5 Summary of function, component and operating parameters of fibre tow spreading machine 71

Table 3.6 The manufacturing parameters of spreading carbon fibre and glass fibre tows.....72

Table 3.7 Fibre types, number of filaments of each fibre type and volume ratio between carbon fibre and glass fibre in the carbon fibre/glass fibre hybrid tows 73

Table 3.8 The manufacturing parameters of hybridising carbon fibre/glass fibre tows 74

Table 3.9 Grading system used to quantify stability of the spread fibre tow width 79

Table 3.10 Summary of the appearance of spread carbon fibre and glass fibre tows..80

Table 3.11 Diameters of the fibres used in hybridisation 88

Table 3.12 Tensile strength, modulus, strain to initial and final failure of control CF/epoxy, CF/GF/epoxy and control GF/epoxy composites. 101
Table 4.1 Properties of carbon fibre/PEEK prepreg and PEEK [7, 118] 107
Table 4.2 Manufacturing parameters of compression moulding of small-scale interleaved carbon fibre/PEEK composite 110
Table 4.3 The micro-structure of cut-ply interleaved carbon fibre/PEEK (produced by cutting templates and measured in the micrographs) 120
Table 4.4 The tensile properties of cut-ply interleaved carbon fibre/PEEK composite 120
Table 5.1 The tensile properties of the composites produced using wavy fibres, hybrid tows and by ply cutting and interleaving 129

List of abbreviation

CF	Carbon fibre
CFRP	Carbon fibre reinforced polymer
CPL	Composite production line
CV	Coefficient of variation
CTE	Coefficient of thermal expansion
DI	Deionised
DIC	Digital image correlation
FE	Finite element
FRP	Fibre reinforced polymer
GF	Glass fibre
GFRP	Glass fibre reinforced polymer
HDPE	High density polyethylene
N_2	Nitrogen
NDE	Non-destructive evaluation
PA-12	Polyamide-12
PEEK	Polyether ether ketone
PP	Polypropylene
PSU	Polysulfone
PTFE	Poly-tetrafluoro-ethylene
ROM	Rule of mixtures
SEM	Scanning electron microscopy
UD	Unidirectional

1 Introduction

Conventional fibre reinforced polymer composites (FRPs) possess high strength and stiffness, low density, long fatigue life in fibre direction and an excellent resistance to corrosion. By carefully selecting the type and amount of reinforcement, its alignment and orientation in a polymer matrix, these composites offer a wide range of mechanical properties, which hence provide immense design possibilities. Within the last fifty years the production of fibre reinforced polymer composites has rapidly increased. It is estimated that the global consumption of carbon fibre reinforced polymers (CFRPs) will reach $25.2 billion by 2020 [1] and the market for glass fibre reinforced polymers (GFRPs) will be worth $16.4 billion in 2016 [2]. In the early days, the application of carbon fibre reinforced polymer composites was mainly confined to the aeronautics industry [3]. In the recent decades, CFRPs have become widely used in other areas such as wind turbine blades, pressure vessels, luxury automobiles, civil construction, marine applications and a vast variety of sports goods. Despite the advantages of high performance CFRPs, such as their high specific strength and stiffness, these materials have a fundamental limitation, which is their inherent brittleness. Conventional UD CFRPs deform elastically to the strain of ~1.5% [4-7] and then fail catastrophically with no prior warning or little residual load-carrying capacity. In contrast, some ductile materials, such as some metals and polymers, can deform plastically with much higher strains to failure and hence dissipate significant strain energy[8]. The terminology “ductility” is initially used to describe the ability of solid material to deform plastically under tension without fracture [9-11]. However, this definition is not quite suitable to describe the ductility of UD CFRPs, because the tensile properties of UD CFRPs in fibre direction are dominated by carbon fibre, which has no ductility. In this thesis, the definition of

ductility for UD CFRPs is mainly referred to whether the CFRPs have an improved failure strain under tension with a progressive and graceful failure mode.

Due to the lack of ductility of conventional CFRPs, the CFRPs have very limited residual load carrying capacity after the initial failure occurs. To overcome this limitation, it is necessary to increase the ductility of CFRPs and this could be achieved by creating composites with enhanced strain to failure and a more progressive failure mode. However, to-date much of the research focussed on improving FRP composite materials has been directed towards improving their through-thickness properties, i.e. improving delamination resistance and impact performance, and, more recently, the development of multifunctional [12-15] and green FRPs [16-20]. Despite achieving plastic deformation of CFRPs using angle-ply composites [21-23], it seems that little work has been directed towards improving the ductility of CFRPs. Much more work was published related to enhancing the ductility of CFRPs used in construction materials [24-26]. However, even in civil engineering, there has only been a very limited work done for this purpose. In Bank's review paper [8] about ductility of FRP composites for civil construction, he stated that "*there has been insufficient attention to exploiting and enhancing progressive failure and energy absorption in the FRP composites themselves*". It is therefore necessary to develop methods to enhance the ductility of FRP exhibiting increased failure strains and more progressive, graceful failure modes.

1.1 Aims and objectives

In 2011, Imperial College London and University of Bristol launched a six-year research programme, i.e. high performance ductile composite technology (HiperDuCT), to design, realise and evaluate composite architectures that display a

ductile or pseudo-ductile response to mechanical load while maintaining high strength and stiffness.

As part of HiperDuCT programme, the research stated in this thesis is aimed to develop CFRP composites with enhanced ductility, which exhibit increased failure strains and a more progressive failure mode. Three different approaches (corresponding to three technical chapters in the thesis) have been explored to achieve this objective. The three approaches include introducing fibre waviness into UD composite (Chapter 2), mixing carbon and glass fibres at the filament level to create ideally intimately intermingled UD hybrid composites (Chapter 3) and adding polymer interleaves into cut-ply UD composites (Chapter 4).The specific objectives are listed below:

a) Chapter 2
    - Create UD CFRP with randomly distributed wavy fibres
    - Characterise the fibre alignment angles and tensile properties of such composites

b) Chapter 3
    - Manufacture continuous UD intermingled carbon/glass fibre hybrid composites and characterise their tensile behaviour
    - Define and quantify the degree of hybridisation (at filament level) in such composites

c) Chapter 4
    - Produce a cut-ply interleaved carbon fibre/PEEK composite and characterise its tensile behaviour

1.2 Structure of thesis

The thesis is divided into five chapters. Chapter 1 provides a general introduction and defines the aims and objective of this research. Chapter 2, 3 and 4 describe the three approaches taken to develop CFRPs with enhanced ductility. Each of these three chapters includes an introduction, an individual literature review, descriptions of the manufacturing techniques, test methods and test results, a discussion and a summary of the key findings. The final chapter of this thesis provides an overall summary and conclusion of this research as well as the suggestions for future work.

2 Indication of the potential of making UD CFRPs with the enhanced tensile strain via introducing fibre waviness

2.1 Introduction

Unidirectional (UD) carbon fibre reinforced polymers (CFRPs) have high specific strength and stiffness, but they fail in a brittle manner with little warning when subjected to uniaxial tension. This inherent brittleness means that the material has no load-carrying capacity after the initial failure occurs. Changing the failure mode of UD CFRPs from catastrophic one into gradual one and improving the failure strain of UD CFRPs, therefore, could potentially reduce the required safety factors. The tensile properties of UD CFRPs in the fibre direction are dominated by the fibre properties. It has already been demonstrated that the waviness and fibre misalignment can enhance the tensile failure strain and produce a non-linear tensile behaviour [22, 23, 27-30], and this will be discussed in section 2.2. One of the possible failure mechanisms of a composite containing fibres with various waviness and misalignment is that straight and well-aligned fibres fail first while the tensile load can stretch and align the wavy, misaligned fibres in direction of the applied strain until they eventually fail. However, most work described in previous literature [22, 23, 27-30] focused on theoretical prediction of the tensile behaviour of UD composite with uniform fibre waviness. There is little published work available on the experimental tensile behaviour of UD composites with small fibre misalignment angle and random fibre waviness.

In this chapter, the literature about the effect of fibre misalignment and fibre waviness on the tensile behaviour of CFRPs, the manufacturing techniques and characterisation of fibre misalignment and fibre waviness in CFRPs, are reviewed first. Inspired by the possibility of tailoring the tensile strain to failure and producing a non-linear failure behaviour, two manufacturing methods were explored for producing UD composites

containing wavy fibres with small degrees of fibre misalignment. Gas-texturing the carbon fibre tow and non-constrained annealing carbon fibre/PA-12 were used to produce such UD composites. The fibre alignment angles and tensile properties of these two composites and their control samples were characterised.

2.2 Literature review

2.2.1 The effect of fibre waviness and misalignment on the tensile behaviour of UD composites

Before investigating the effect of fibre or ply misalignment and waviness on the tensile behaviour of UD composite, researchers firstly began to study the tensile behaviour of angle-ply $(\pm\theta)_S$ composites to evaluate the effect of fibre alignment angle on the tensile behaviour of composites [22, 23, 27, 28]. As can be seen in Figure 2.1 [22], the tensile stress- strain behaviour of UD angle-ply $(\pm\theta)_S$ composites exhibits a significant non-linearity. Even though larger fibre alignment angles result in a significant reduction of the tensile strength and modulus compared with UD composites, introducing $(\pm\theta)_S$ fibre alignment angles does provide composites with non-linear tensile stress-strain curves and a more progressive failure behaviour.

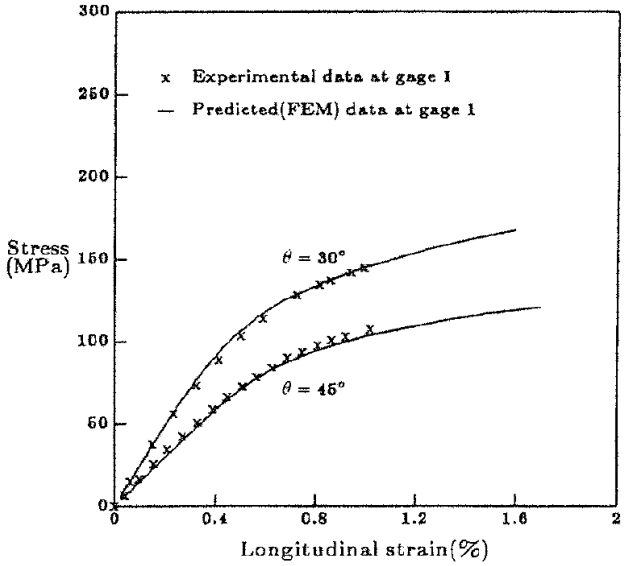
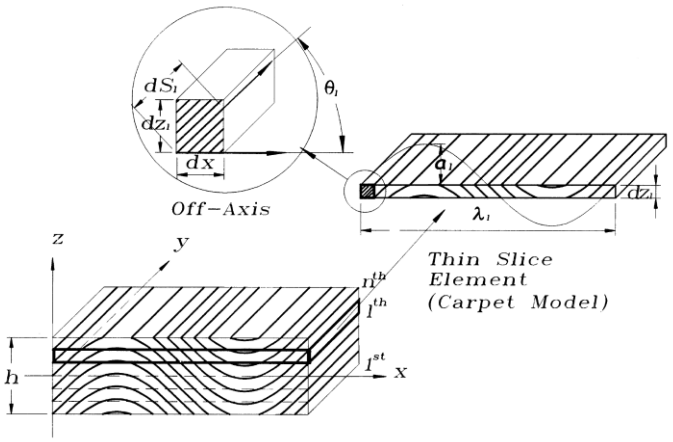


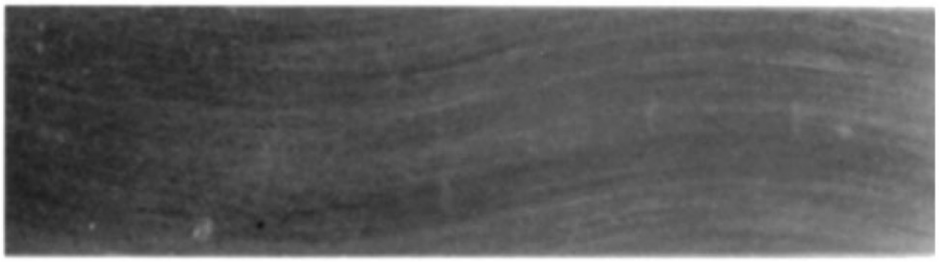
Figure 2.1 Predicted and experimental tensile stress-strain curves of $(\pm\theta)_S$ carbon fibre/PEEK composite [22]

Compared with $(\pm\theta)_S$ angle-ply composite, the tensile behaviour of UD composites with ply waviness is more complex, because composites with ply waviness contain different fibre alignment angles within a single ply. Chou and Takahashi [29] predicted using an elastic constitutive model that Kevlar or glass fibre reinforced elastomers containing uniform out-of-plane ply waviness exhibit a non-linear tensile behaviour and enhanced tensile failure strain. Later, Chun et al. [30] built a model to investigate the tensile behaviour of UD carbon fibre/epoxy composites with uniform out-of-plane fibre waviness and validated the model experimentally, as shown in Figure 2.2 (a) and (b). They found that the apparent modulus of such composite was reduced as the tensile stress increased. The non-linear tensile behaviour and the failure strain increased with increasing fibre waviness [30], as shown in Figure 2.2 (c). Unfortunately, both models showed that introducing uniform fibre waviness reduced the tensile strength and modulus compared with the UD composites.

(a)



(b)



(c)

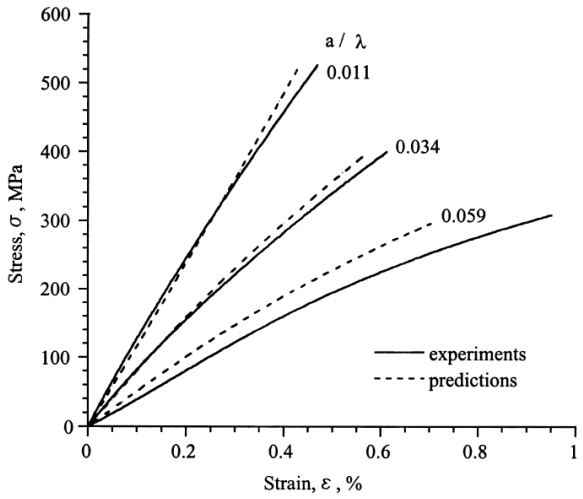


Figure 2.2 (a) Schematic drawing of representative volume and coordinates for UD composite with uniform fibre waviness, (b) photo showing UD composite with uniform fibre waviness and (c) predicted and experimentally obtained tensile stress-strain curves for UD composite with uniform fibre waviness but various fibre waviness ratios [30]

In order to minimise the reduction in the tensile strength and modulus caused by introducing uniform fibre waviness into the UD composites and to produce composites with an enhanced failure strain exhibiting a non-linear tensile behaviour, it is desirable to design UD composite containing wavy and straight fibres, In such a

composite, the straight fibres will fail first but the undamaged wavy fibres can still carry the load. Such composite, therefore, would fail in steps rather than in a catastrophic manner.

2.2.2 Manufacturing techniques to produce composites containing wavy fibres

2.2.2.1 Producing thermosetting composites containing wavy fibres

In the 1990s, researchers began to develop processes to introduce fibre waviness or ply waviness into carbon fibre/epoxy composites. Kuo et al. [31] manufactured an out-of-plane wavy UD carbon fibre/epoxy composite by using a sinusoidal matching mould, shown in Figure 2.3(a). Later, some investigators added carbon fibre/epoxy strip into UD composite when laying up UD prepregs to create a UD carbon fibre/epoxy with out-of-plane ply waviness, as seen in Figure 2.3 (b) [32, 33]. Potter et al. [34] reported that fibre misalignment and in-plane waviness in uncured UD carbon fibre/epoxy prepregs (maximum fibre misalignment angle of 3.8°) is mainly caused by the variation in tension applied on the carbon fibres tows when manufacturing UD prepregs, the twisting within fibre tows, the presence of broken fibres, which lay across the fibre direction of the prepreg and winding the prepreg for the storage and delivery. Later, they also produced out-of-plane wavy-ply carbon fibre/epoxy composites by a carefully designed moulding process. They added a carbon fibre/epoxy strip (Figure 2.3(b)), one or two UD discontinuous carbon fibre/epoxy layers (Figure 2.3(c) and (d)) into a number of continuous UD carbon fibre/epoxy prepregs during the layup process to form a composite with controlled out-of-plane ply waviness [35]. They found that the presence of ply-waviness can cause delamination initiating at the ply drops, which negatively affected the compressive strength of the UD composites [36].

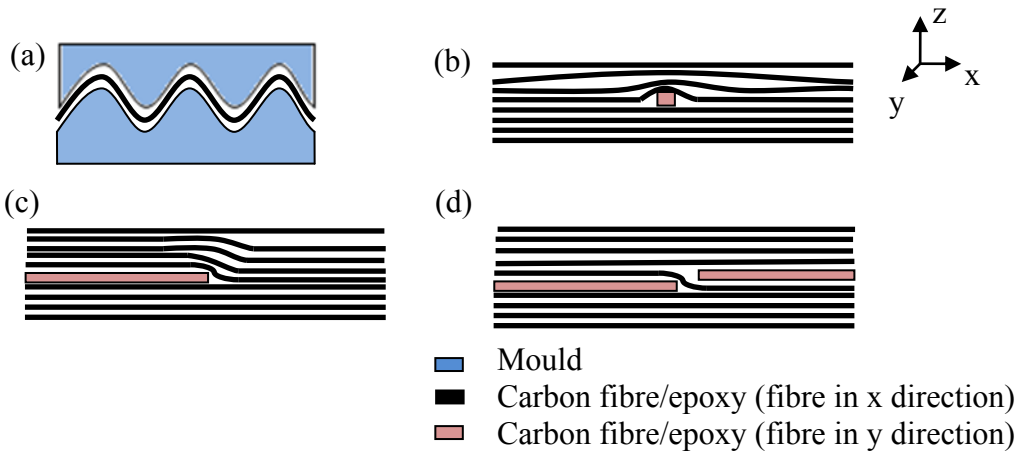


Figure 2.3 Schematic diagrams of manufacturing techniques to produce thermosetting composites containing ply waviness (a) [31], (b) [32, 33, 35], (c) and (d) [35, 36]

2.2.2.2 Producing thermoplastic composites containing wavy fibres

UD carbon fibre/thermoplastic composites with out-of-plane ply waviness were reported by Mrse and Piggott, who designed a crimping moulding method to introduce ply waviness into carbon fibre/PEEK composites [37]. The authors found that this process damaged the carbon fibres, which had a negative effect on the compressive strength of the composite [37]. O'Hare and Hyer [38] developed a three-step moulding method to manufacture flat cross-wavy ply carbon fibre/polysulfone (PSU) composites. This moulding method involved creating the wavy ply using a curved matched mould, then using strips made of carbon fibre/PSU to fill the gaps between the curved layer and the nearby flat layers to form a flat sub-laminate, finally laying up the sub-laminate with other carbon fibre/PSU layers and consolidating them into laminate [38].

As stated above, using curved moulds can only introduce waviness into UD carbon fibre/thermoplastic composite at ply level, some published work shows that some continuous UD fibre reinforced thermoplastic composites manufactured by fibre commingling by gas-texturing can contain a degree of waviness at fibre level [39-42]. In the 1990s, fibre gas-texturing technology was developed to commingle reinforcing

fibre yarns and thermoplastic polymer fibre yarns to form a hybrid roving, which was then processed into continuous fibre reinforced thermoplastic polymers using pultrusion process [39]. Lauke et al. [6] reported that the longitudinal tensile strength of UD glass fibre reinforced polyamide produced by consolidation of glass fibre/polyamide fibre hybrid tows was lower than the value predicted by the rule of mixture but they did not provide tensile stress-strain curves of this composite. The authors thought that the reduction in tensile strength was caused by the fibre misalignment in the composite, because some fibre misalignment was observed in the fibre hybrid tow. However, it seems likely that the damage on the glass fibres caused by gas-texturing process is another factor contributing to the reduction of tensile strength of such composite.

Thermal expansion, on the other hand, can produce waviness at filament level without damaging the fibre. Some investigations show the coefficient of thermal expansion (CTE) mismatch between the composite materials and mould tools [43], CTE mismatch between fibre and thermoplastic matrix [44] can cause the residual thermal stress in fibres, which is large enough to create fibre waviness in UD composite. Kugler and Moon observed a fibre waviness with a maximum degree of fibre misalignment of 8.4° in a carbon fibre/PSU composite when investigating the effect of different processing parameters (mould materials, moulding temperature and time) on fibre waviness in the resulting composites [43]. The heating/cooling history during processing of fibre reinforced thermoplastics can affect the magnitude of the fibre waviness or misalignment in the composite [43]. Cohen et al. [45] observed fibre waviness in a single glass fibre reinforced polycarbonate sample, which was caused by polymer melt flow during the consolidation process.

2.2.3 Methodology of measuring fibre waviness and fibre misalignment

The magnitude of fibre waviness affects the mechanical behaviour of UD composites. One of the major problems in characterising fibre waviness is the need to determine or define the shape of a wavy fibre. Many researchers assumed a sinusoidal form (Figure 2.4) when modelling wavy fibres [30, 46-48]. The magnitude of the ideal fibre waviness can be quantified by the wavelength (λ) and the amplitude (A) of a sinusoidal wavy fibre. The maximum fibre misalignment angle is a function of wavelength and amplitude (Equation 2.1):

$$\theta_{max} = \tan^{-1}\left(\frac{2\pi A}{\lambda}\right) \qquad \text{Equation 2.1}$$

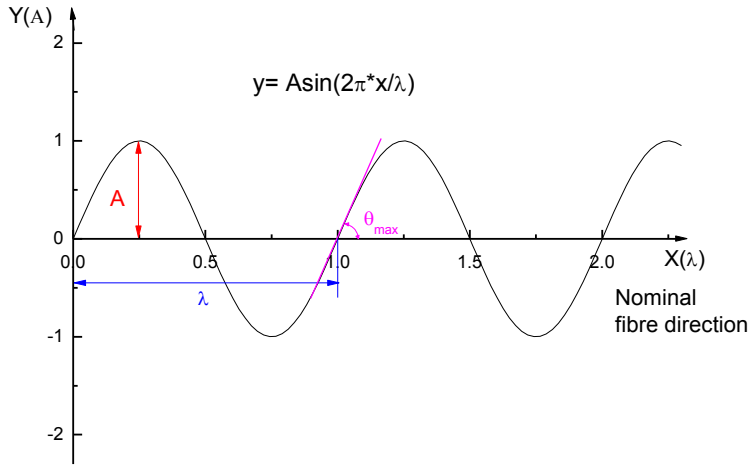


Figure 2.4 Schematic drawing of a sinusoidal-model waved fibre [30]

However, the problem is that most wavy fibres are in reality not sinusoidal, which makes it difficult to determine fibre misalignment angles using Equation 2.1. Most researchers, therefore, measured the ply or fibre misalignment angle directly to quantify ply or fibre waviness. The out-of-plane ply misalignment can be easily observed and measured from micrographs of cross-section of the composite in through-thickness direction [35, 38, 48], as seen in Figure 2.5. Recently, Pain and Drinkwater [49] also developed a non-destructive evaluation method to detect and locate the ply waviness using ultrasonic array scattering. In this method, the average

ultrasonic array scattering matrix of a UD composite without ply waviness was generated from experimental ultrasonic scanning and statistics-based signal processing, which was treated as a baseline; the ply waviness in a UD composite was detected and located by comparing the signals obtained from experimental ultrasonic scan on this wavy composite with the baseline.

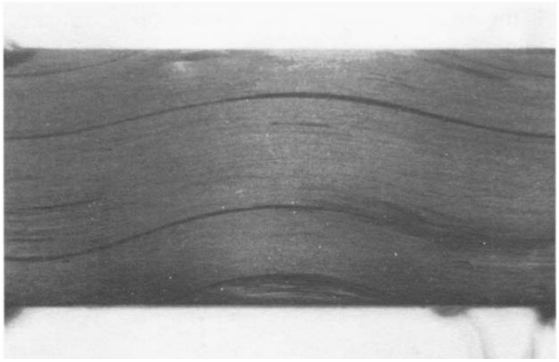


Figure 2.5 Unidirectional carbon/epoxy composite with out-of-plane ply waviness[48]

However, measuring fibre misalignment angles of individual fibres is more challenging than measuring the ply waviness, because it requires a detection technique with higher resolution. Since the 1980s, several researchers have investigated the characterisation of fibre misalignment from the micrographs of polished section of composites [50-54]. Two of the most popular methods for measuring fibre misalignment are Yurgartis' method [50] and multi-field image analysis [52, 54]. Yurgartis used the fact that a fibre with a circular cross section will be an ellipse when cut at an angle other than 90° and 0° to the fibre direction. By measuring the major and minor axial dimensions of the ellipsoid, the individual fibre alignment angle can be obtained. The accuracy of this method was reported to be ± 0.25º [50]. This method will be discussed in detail in section 2.2.3. Creighton and Sutcliffe [52, 54] designed a multi-field image analysis to determine the degree of fibre misalignment in a composite from a low magnification microscope image. In their method, the fibre alignment angle in a domain (250 x 250 μm) of a longitudinal

section of a UD composite was inferred from the alignment of the elongated features, which can be a fibre filament, fibre bundle or the matrix between the fibres, as shown in Figure 2.6. This method is less time-consuming and more effective in measuring the fibre misalignment in a large domain than Yurgartis' method, but the results obtained were less reliable when the domain size was decreased [52, 54].

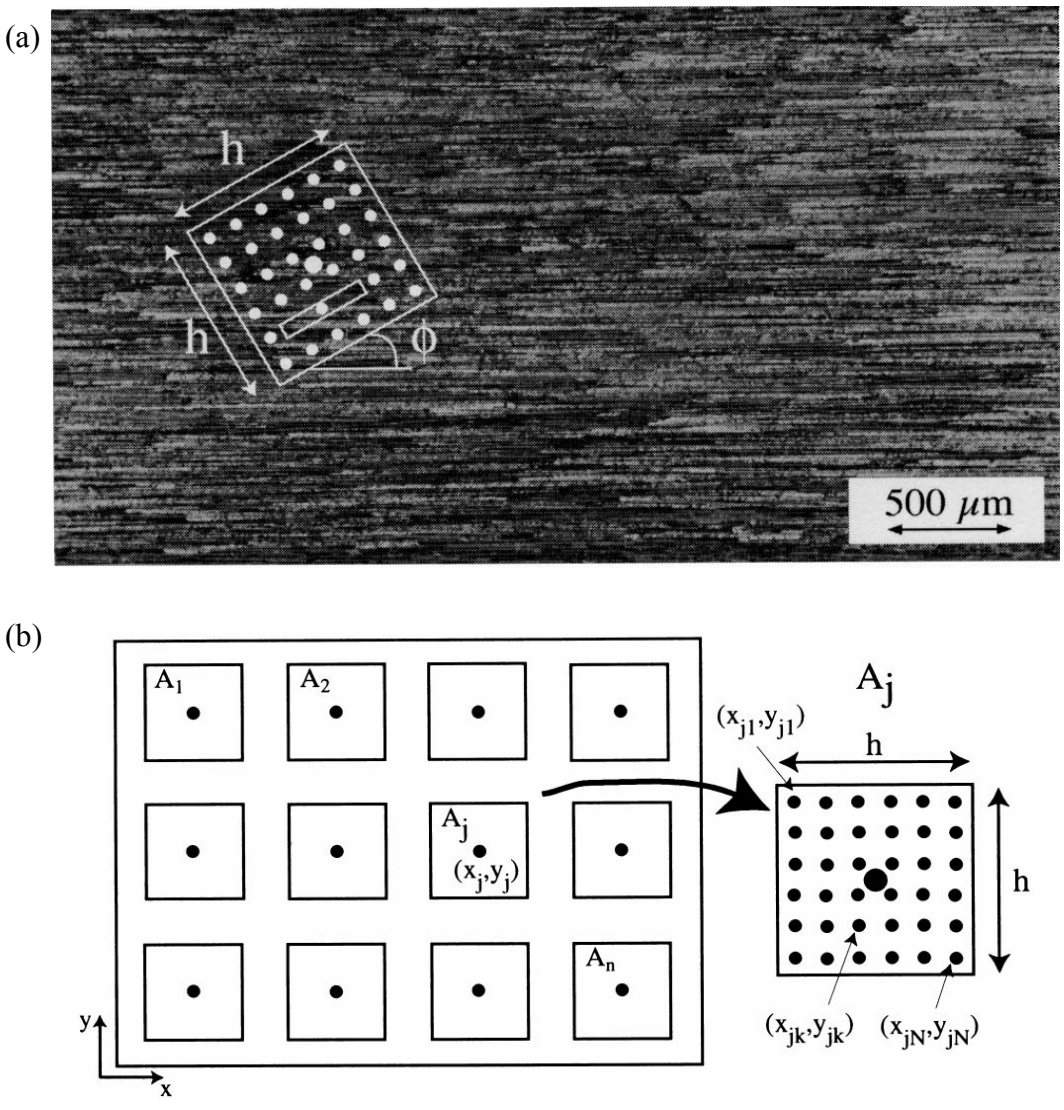


Figure 2.6 (a) Optical micrograph of UD composite with a domain and pixel array highlighted and (b) schematic depiction of a set of domains within which the average fibre orientation φ is to be measured [52]

2.3 Materials and methods

2.3.1 Materials

Continuous carbon fibre tows (HexTow®IM7-12K) kindly provided by Hexcel Co. (Cambridge, UK) were used as reinforcement. Polyamide (PA)-12 in powder form (Vestosint®-2159, Evonik Degussa GmbH, Weiterstadt, Germany) was used as matrix. Nitrogen (BOC UK Co. London, UK) was used in the gas-texturing process.

2.3.2 Manufacturing UD carbon fibre/PA-12 with fibre waviness

2.3.2.1 Manufacturing unidirectional carbon fibre/PA-12 composite tapes using gas-texturing method followed by wet-powder impregnation

Gas-textured carbon fibre/PA-12 tape was manufactured using a modular custom-built composite production line (CPL) [55] (developed by Polymer and Composite Engineering Group in Imperial College London), shown in Figure 2.7.

(a)



(b)

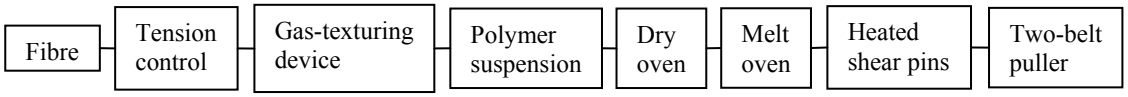


Figure 2.7 (a) Photo and (b) flow chart of setup of manufacturing route of UD carbon fibre/PA-12 composite tape

A 2 L PA-12 suspension (5 wt.%) was prepared for the wet-impregnation bath in the CPL. In order to aid the dispersion of the polymer powder and avoid cake formation during rest periods, 0.1 wt.% surfactant (Cremophor® A-25, BASF Company, Manchester, UK) was added to the suspension. In order to ensure that PA-12 powder

was homogenously distributed in the impregnation bath, this suspension was stirred for 2.5 h. Similarly, 1L concentrated PA-12 suspension (15 wt%) was prepared as the top-up material to maintain the polymer concentration in the wet-impregnation bath during the manufacture process as otherwise the dispersion would deplete.

Two carbon fibre tows were passed over a perforated PTFE bar (Figure 2.8). A N_2 (pressure=2.5 bar) flow passing through these small holes ($Ø_{hole}$ = 1 mm) in the bar caused the carbon fibre tows to spread into filaments or small bundles and some fibre misalignment. These spread carbon fibre tows were combined into one carbon fibre tow after the gas-texturing process.

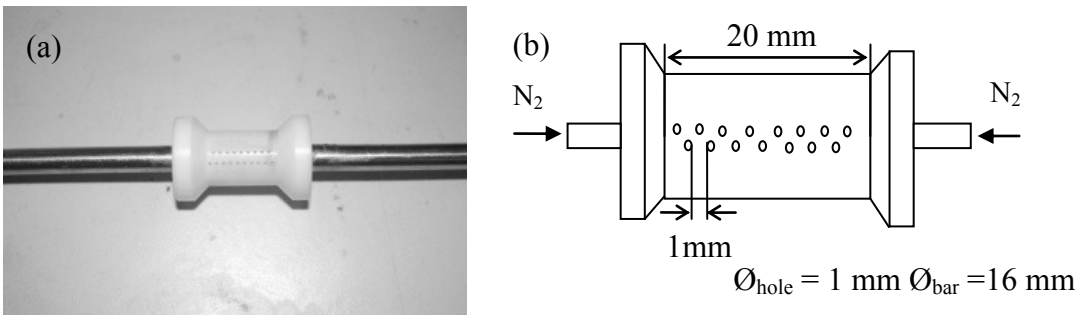


Figure 2.8 Design of gas-texturing device (a) photo (b) schematic diagram

The tow was then passed through the PA-12 wet-impregnation bath alternating under and over 13 pins (Figure 2.9(a)) to increase the space between the filaments in the tow to allow them to pick up PA-12 powder from the suspension. Two 1 m long infra-red heating ovens were used to remove the water carried by the fibre tow (set temperature: 120°C) and melt the polymer powder (set temperature: 205°C), respectively. The fibre tow with the polymer melt passed over and under three heated shear pins (set temperature: 220°C; Figure 2.9(b)), which provided the composite tape with a smooth surface. Finally, it was consolidated between the two room-temperature steel rollers. A two-belt puller was used to control the speed of this manufacturing process at 0.5 m/min.

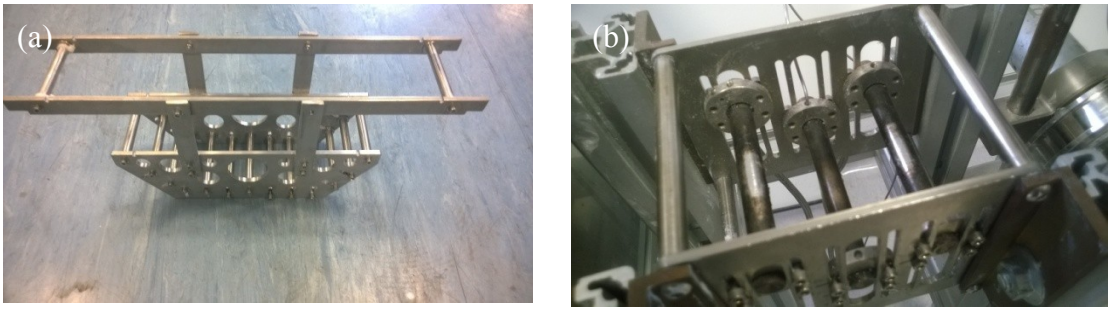


Figure 2.9 Setup of (a) 13 pins used in wet-impregnation bath and (b) 3 heated shear pins

Control carbon fibre/PA-12 composite tapes were manufactured using the same method as the gas-textured carbon fibre/PA-12 except that the fibre tow did not pass over the gas-texturing device. During this process, the concentration of polymer powder in the wet-impregnation bath decreases, which results in an increasing fibre volume fraction in the composite. In order to maintain the powder concentration 50 mL concentrated PA-12 suspension (15 wt.%) was, therefore, added into the bath every 15 min. The fibre volume fraction of the composite (V_f), calculated using Equation 2.2, was monitored by weighing 1 m of the composite tape:

$$V_f = \frac{\rho_m W_f}{\rho_f (W_c - W_f) + \rho_m W_f} \qquad \text{Equation 2.2}$$

where ρ is the density of the materials (g/m^3), W the linear weight of the tape (g/m). The subscripts c, m and f represent composite, polymer matrix and fibre, respectively. Only composite tapes with V_f = 58-62% were selected in this research.

2.3.2.2 Manufacturing of carbon fibre/PA-12 composite tape using non-constrained annealing

In order to introduce fibre misalignment into carbon fibre/PA-12 without damaging carbon fibres, the composite tapes were annealed at temperature from 220 °C to 20 °C when non-constrained. In this process, two factors cause carbon fibre misaligned after moulding: a) PA-12 remains a viscous melt for a sufficient long time allowing the carbon fibres to move as the melt flows; b) the CTE mismatch between carbon fibres

and PA-12 and the CTE mismatch between composite and mould causes residual thermal stress in carbon fibres, which in turn cause the carbon fibres to become misaligned and wavy during the consolidation.

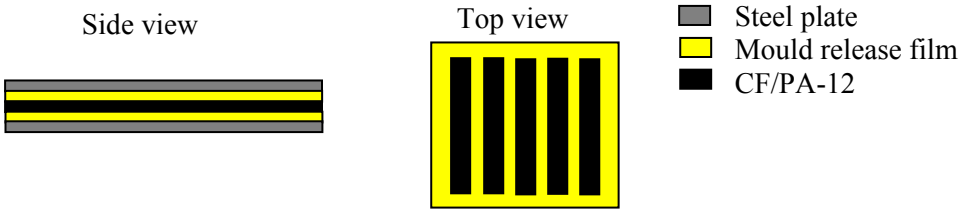


Figure 2.10 Schematic diagram of layup process of carbon fibre/PA-12 tapes during non-constrained annealing

The carbon fibre/PA-12 tape with a width of 6-8 mm was cut into 200 mm long sections. These tape sections were sandwiched between release films (Upilex® 25S, UBE Industries Ltd., Tokyo, Japan) and placed between two steel plates, as seen in Figure 2.10. The whole assembly was heated in a pre-heated hot press (Model# 4126, Carver Inc., Indiana, USA) at 220°C with contact-only pressure (i.e. no actual pressure applied) for 2 h. It was slowly cooled down to room temperature in 8 hours. The temperature change of the unit was monitored by a thermocouple (RS 615-8206, RS Components Co., UK), which is shown in Figure 2.11. After the non-constrained annealing, some visible fibre misalignment was introduced into the carbon fibre/PA-12 tape, as seen in Figure 2.12. However, the magnitude of the fibre misalignment angle cannot be clearly quantified from Figure 2.12 due to the low magnification of the images.

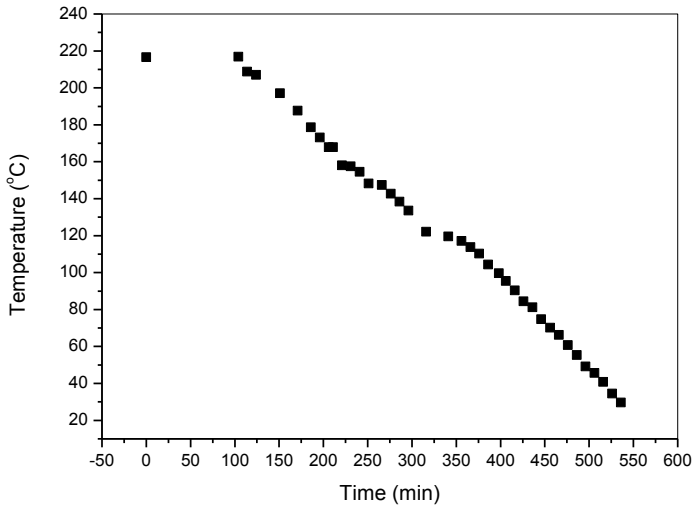


Figure 2.11 Mould temperature during the non-constrained annealing process

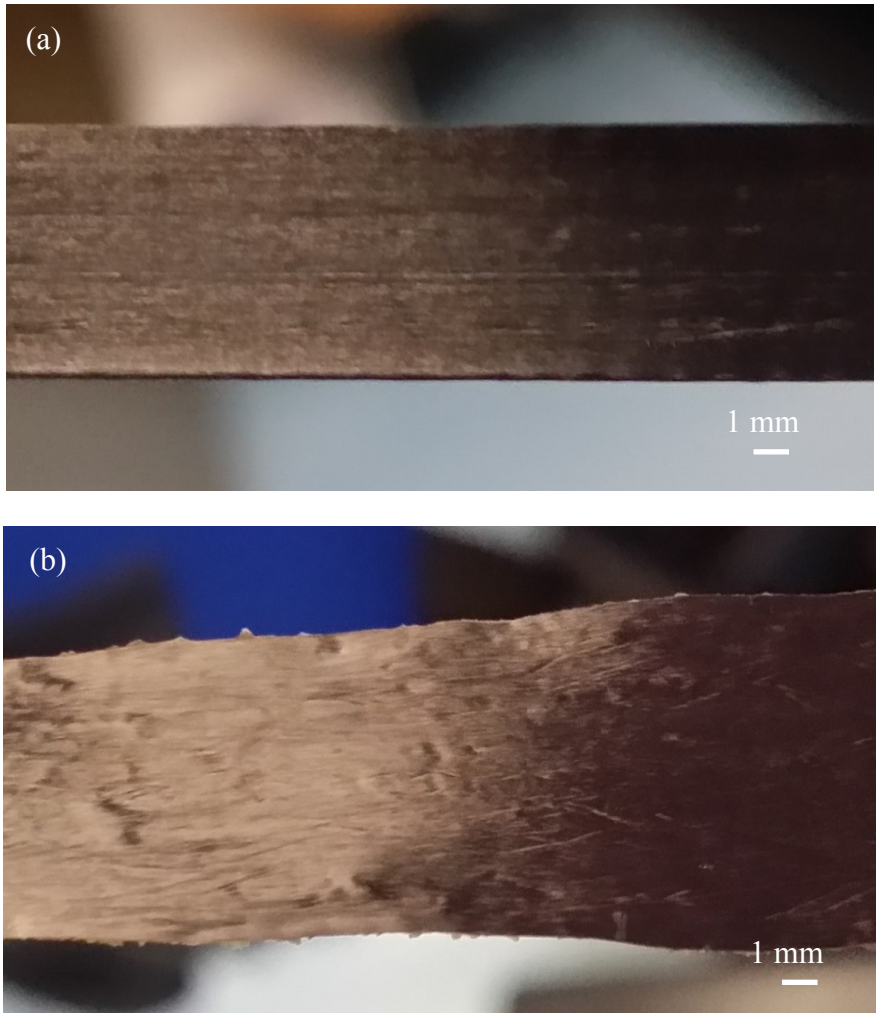


Figure 2.12 Top views of the carbon fibre/PA-12 tape (a) before and (b) after non-constrained annealing

2.3.3 Single-fibre tensile tests on as-received and gas-textured carbon fibres

A Linkam TST350 tensile tester (Linkam Scientific Instrument Ltd, Surrey, UK) with 20N load cell was used to measure the tensile strength and the apparent modulus of as-received and gas-textured carbon fibre according to the ISO 11566 standard [56]. Single fibres were mounted onto paper cards (seen in Figure 2.13) to minimize the stress concentration on the fibre in the gripping area. A single fibre was placed at the centre of the testing card and bonded at both ends of the mounting using an epoxy adhesive (Araldite® Rapid, Huntsman Advanced Materials GmbH, Switzerland). The fibre specimen on the paper mount was fixed in the grips, shown in Figure 2.14. Then, both sides of the cardboard holder were cut at the mid gauge. The single fibres were loaded at a crosshead rate of 15 μm/s. The load-crosshead displacement curve was recorded until the fibre failed. 25 single fibres from each group, i.e. as-received and gas-textured, were tested in order to obtain a representative result. The tensile strength ($\hat{\sigma}$) and strain to failure ($\hat{\varepsilon}$) of the fibres were calculated using Equation 2.3 and Equation 2.4, respectively.

$$\hat{\sigma} = \frac{4F_{\max}}{\pi d^2} \qquad \text{Equation 2.3}$$

$$\hat{\varepsilon} = \frac{\delta}{L} \qquad \text{Equation 2.4}$$

where F_{max} is the maximum measured tensile load, d the fibre diameter, δ the crosshead displacement when the fibre fails and L the gauge length. The apparent tensile modulus E is the slope of the linear fit to the tensile stress-strain curve.

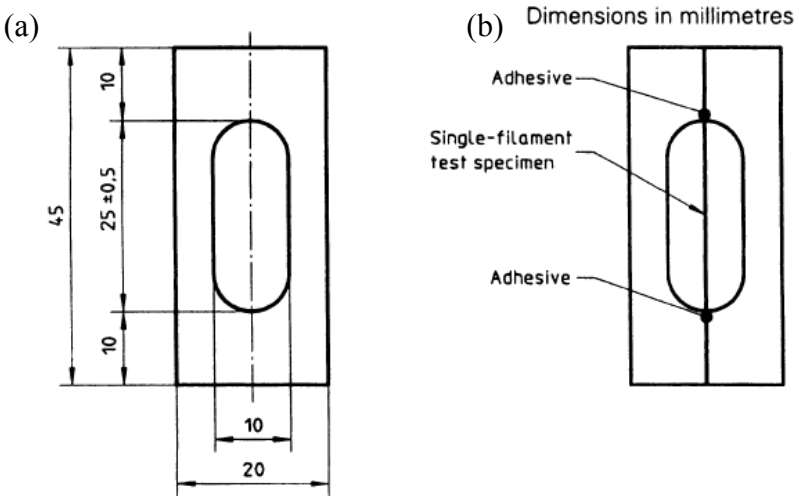


Figure 2.13 Mounting for single fibre tensile test specimen (a) Dimensions of mounting (b) Mounting with specimen bonded in place

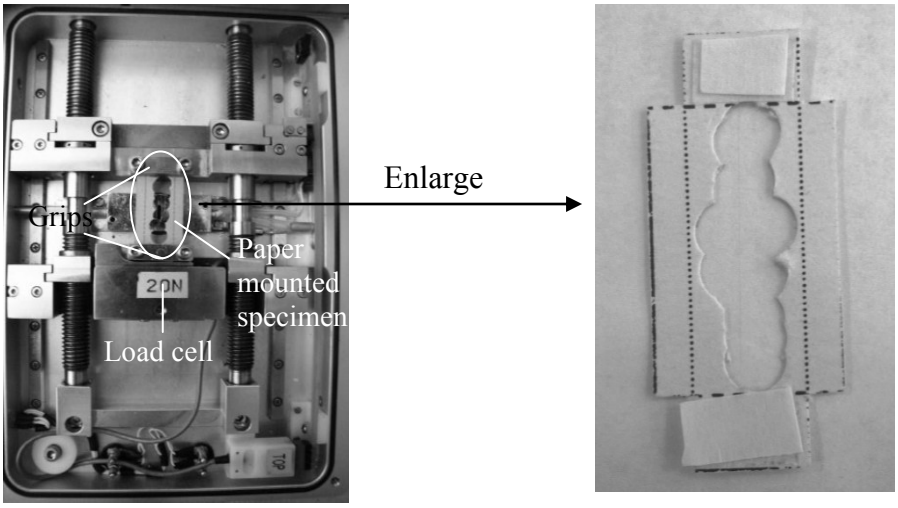


Figure 2.14 Setup of single-fibre tensile test

In order to evaluate the variation and distribution of the carbon fibre tensile strength, the cumulative failure probability $P_{R,i}$ of the i[th] fibre was calculated using Equation 2.5. The Weibull-modulus (m) of the fibre strength is given by the slope of $\ln[-\ln(1-P_{R,i})]$ as function of $\ln\hat{\sigma}_i$ plot, see Equation 2.6 [57],

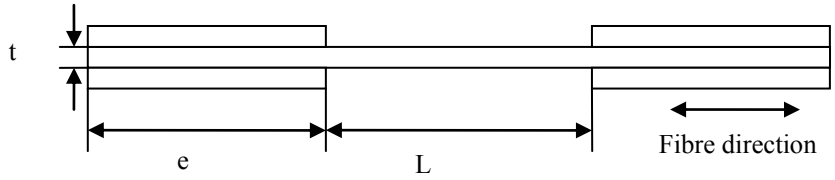
$$P_{R,i} = \frac{R_i}{N+1} \qquad \text{Equation 2.5}$$

$$\ln[-\ln(1-P_{R,i})] = m\ln\hat{\sigma}_i + C \qquad \text{Equation 2.6}$$

where R_i is the rank of the i[th] fibre, N the total number of tested fibres, $\hat{\sigma}_i$ the strength of the i[th] fibre and C a constant.

2.3.4 Tensile tests of control, gas-textured and non-constrained annealed carbon fibre/PA-12 tapes

All the carbon fibre/PA-12 tapes were cut into 200 mm-long sections and end tabbed with glass fibre/epoxy laminate with a thickness of 1.5 mm. The end tabs were bonded to the tape using cyanoacrylate adhesive (CN-general, Techni Measure Co, Japan). The dimensions of the tested samples are shown in Figure 2.15. The samples were tested under uniaxial tensile load (Model 4566 or 5969, Instron Ltd, Bucks, UK, depending on availability) at a crosshead rate of 0.5 mm/min. Digital image correlation (ARAMI-2M, GOM UK Ltd, Coventry, UK) was used to record the strain over the whole gauge length in the control and gas-textured carbon fibre/PA-12 samples. A video-gauge system (Imetrum Ltd, Bristol, UK) was used to measure the strain in the non-constrained annealed carbon fibre/PA-12. The setup for the tensile tests is shown in Figure 2.16.



Thickness (t) =0.08mm. Width (w) = 6-8mm Free length (L) =100mm Length of end tabs (e) =50mm

Figure 2.15 The dimensions of the tensile specimen

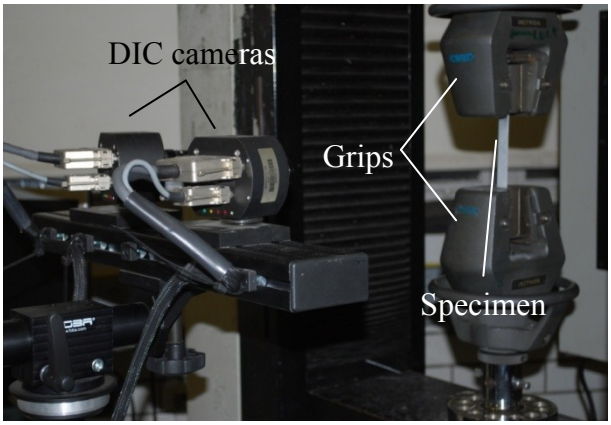


Figure 2.16 Setup for tensile tests of UD composite tapes

2.3.5 Measuring fibre alignment angle in carbon fibre/PA-12 composites

2.3.5.1 Microscopy sample preparation

After tensile testing, samples were cut from the undamaged end-tab regions at an angle of 5º nominal to the fibre direction (Figure 2.17(a)). The cut samples were embedded in a transparent epoxy resin (EpoCure®, Buehler Ltd., Düsseldorf, Germany) and cured at room temperature for 24 h. The samples were polished using a disc polish machine (Motopol-12, Buehler Ltd., Düsseldorf, Germany) with different grades of sand paper and diamond suspensions (details are given in Table 2.1). The polishing pressure and speed were 0.2 MPa and 150 rpm, respectively.

Table 2.1 Operation parameters of polishing process

Polishing sequence	Polishing grade	Time (min)
1	P120 SiC (with water as medium)	10
2	P320 SiC (with water as medium)	5
3	P800 SiC (with water as medium)	5
4	P2500 SiC (with water as medium)	5
5	Nylon cloth (with 6 μm diamond suspension as medium)	2
6	Nylon cloth (with 3 μm diamond suspension as medium)	2
7	Nylon cloth (with 1 μm diamond suspension as medium)	2

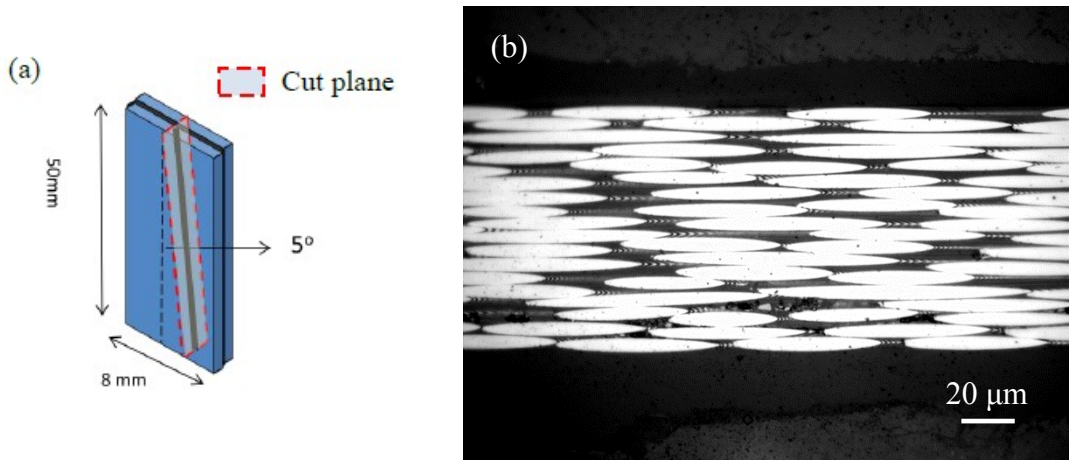


Figure 2.17 (a) Schematic diagram of cutting sample (b) Typical microscopy image of polished sample surface

2.3.5.2 Microscopy analysis

The cut surfaces of tested samples were investigated using a reflective microscope (AX10, Zeiss Ltd., Cambridge, UK) at 50x magnification. Twenty microscopy images

were taken from each sample. A typical optical micrograph is shown in Figure 2.17(b). By measuring the major and minor axial dimensions of the cut fibre surfaces, the apparent fibre angle can be determined using Equation 2.7 [50]:

$$\theta_{apparent} = \sin^{-1}\frac{d}{l} \qquad \text{Equation 2.7}$$

where $\theta_{apparent}$ is apparent fibre alignment angle, l and d the major and minor axial dimensions of the cut fibre surfaces, respectively.

For each image, 10 fibres were randomly selected for measurement. Two hundred fibre alignment angles, therefore, were measured for each sample. As stated above, 4 samples in each group were tested in the uniaxial tensile test, so 800 apparent fibre alignment angles in each group (i.e. control, gas-textured and non-constrained annealed carbon fibre/PA-12) were characterised to obtain a representative result.

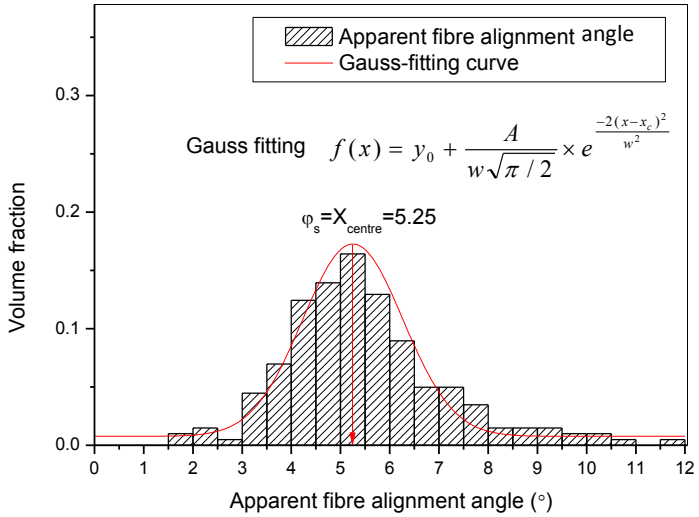


Figure 2.18 Distribution of the apparent fibre alignment angles of a typical gas-textured carbon fibre/PA-12 sample

The apparent fibre alignment angle $\theta_{apparent}$ is a function of the fibre alignment angle in the composite and the sectioning angle φ_s. However, the sectioning angle cannot be determined with a high accuracy by measuring the angle between the cut surface and fibre direction. Figure 2.18 shows the distribution of apparent fibre alignment angle of a typical gas-textured carbon fibre/PA-12 tape. It is worth noting that only very few

fibres have an apparent fibre alignment angle smaller than 3°, which skews the apparent fibre alignment angle distribution. When the apparent fibre alignment is very small (less than 3°), the sectioned fibre segment shows as a quasi-rectangle, which has a length exceeding the length of microscopy measuring field. These fibre segments, therefore, were not countable in the measurement. In order to minimise the distortion caused by the limited microscopy measuring field, the sectioning angle is the median value (X_{centre}) of the gauss-fitting curves of the apparent alignment angle distribution instead of the average value of the measured apparent fibre alignment angles. The true fibre alignment angle (θ) is determined via Equation 2.8.

$$\theta = \theta_{apparent} - \varphi_s \qquad \text{Equation 2.8}$$

2.4 Results and discussion

2.4.1 Effect of gas-texturing on the tensile properties of carbon fibres

The typical tensile stress-strain plots of as-received and gas-textured carbon fibre are shown in Figure 2.19. The tensile properties of as-received and gas-textured carbon fibre are shown in Table 2.2. The tensile strength and strain to failure of gas-textured carbon fibres is 15% lower than for as-received carbon fibres. As expected, the tensile modulus of the carbon fibres is hardly affected by the gas-texturing process.

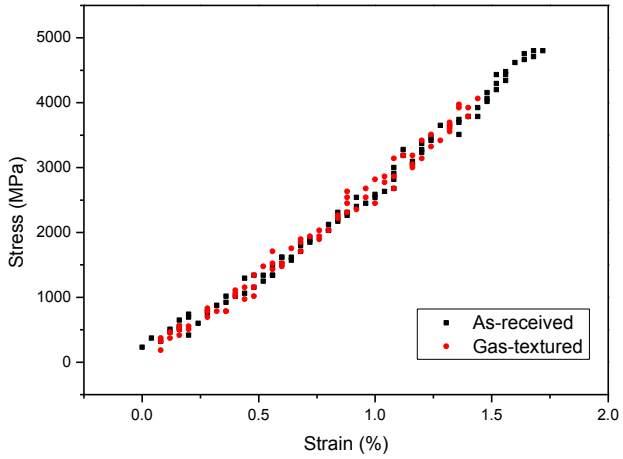


Figure 2.19 Typical tensile stress-strain plots of as-received and gas-textured carbon fibres

Table 2.2 Tensile properties of as-received and gas-textured carbon fibre

	Strength (MPa)	Strain to failure (%)	Modulus (GPa)	Weibull modulus of strength
As-received	4843 ±192	1.72±0.07	273.7±2.5	5.34
Gas-textured	4152± 201	1.48±0.08	267.4±4.2	4.37

The plots of tensile cumulative failure probability P_R as function of the tensile strength σ of as-received and gas-textured carbon fibres fit well to the Weibull probability distribution (Figure 2.20). The Weibull modulus of as-received carbon fibres is 22% higher than that of gas-textured carbon fibres, which means that the scatter in the strength of the as-received fibres is lower.

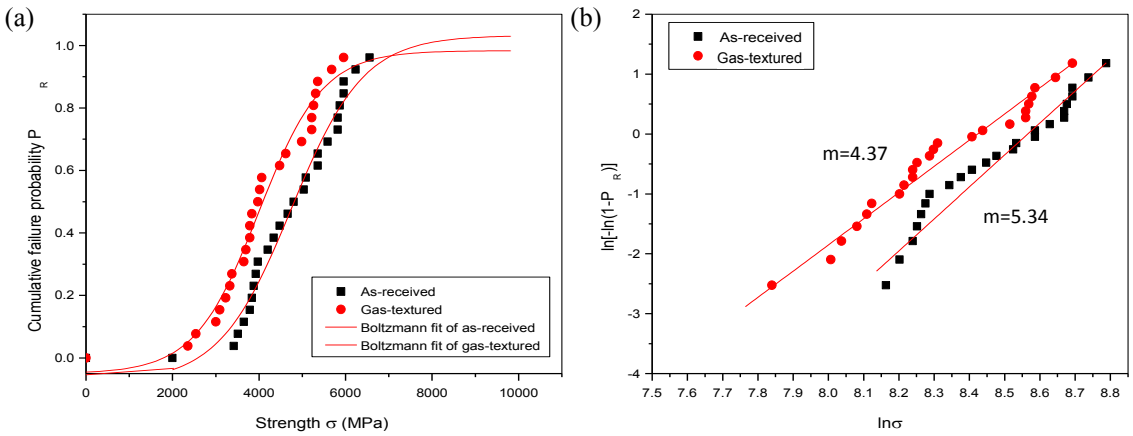


Figure 2.20 (a) The cumulative failure curve and (b) Weibull plots of as-received and gas-textured carbon fibres

2.4.2 Tensile behaviour of control, gas-textured and non-constrained annealed carbon fibre/PA-12 tapes

The tensile strength, modulus and strain to failure of the control, gas-textured and non-constrained annealed carbon fibre/PA-12 tapes are summarised in Table 2.3. Because the tensile modulus of gas-textured carbon fibre was same as that of as-received carbon fibre, the initial tensile modulus of gas-textured carbon fibre/PA-12 was barely changed compared to the control carbon fibre/PA-12 (165.9 GPa versus 164.9 GPa). Compared with the control carbon fibre/PA-12, the strength and the

initial failure strain of carbon fibre/PA-12 composites manufactured using fibres which passed the gas texturing process decreased, which is because the carbon fibres were damaged during the gas-texturing process (see section 2.4.1). The gas flow does not only spread the fibres but also induced surface flaws or damage by fibre-fibre contact on the surface of the fibres, causing a reduction in strength and strain to failure of the carbon fibres. However, there was no reduction in tensile strength of the non-constrained annealed carbon fibre/PA-12 composite compared with the control samples, because the carbon fibres were protected by PA-12 melt during the non-constrained annealing process.

Table 2.3 Tensile properties of control, gas-textured and non-constrained annealed carbon fibre/PA-12 composite tapes

	Modulus (GPa)	Strength (MPa)	Failure strain (%)	
			Initial	Ultimate
Control	165.9±9.7	2495±105	1.61±0.03	
Gas-textured	164.9±7.4	2313±116	1.37±0.07	1.58±0.09
Non-constrained annealed	169.6±6.6	2491±158	1.51±0.08	1.96±0.16

It is interesting to note that the tensile stress-strain curves of the gas-textured and non-constrained annealed carbon fibre/PA-12 showed a stepwise, gradual failure mode during strain controlled tensile tests instead of the usual sudden, catastrophic failure, which was observed for the control carbon fibre/PA-12 samples (Figure 2.21). During the testing of the gas-textured and non-constrained annealed carbon fibre/PA-12 tapes, part of the sample still carried some load after the first failure occurred, while the control sample completely failed in a catastrophic manner. The difference in failure mode is associated with the difference in fibre alignment between the composites manufactured using carbon fibres that passed through the gas texturing process or which were subjected to the non-constrained annealing process and the control samples. The straight fibres will carry the greater stress and so are more likely to fail first. Of the remaining fibres those with least misalignment will fail next and so the

failure process was more gradual in the gas-textured and non-constrained annealed carbon fibre/PA-12 with their large spread of fibre alignment angles. However, due to the reduction in the tensile strength and failure strain of the fibres, which were subjected to the gas-texturing process, no increase was observed in the ultimate failure strain of gas-textured carbon fibre/PA-12 composites compared with the control samples. Nevertheless it is promising that a higher ultimate failure strain was observed for the carbon fibre/PA-12 composites which were subjected to non-constrained annealing compared to the control carbon fibre/PA-12. The higher ultimate failure strain for this composite was due to the fact that non-constrained annealing introduced significant fibre misalignment and waviness (see Figure 2.22) into the composite without damaging the carbon fibres. Compared with the control carbon fibre/PA-12 composite, the non-constrained annealed carbon fibre/PA-12 composite had enhanced ductility which exhibited in its higher ultimate failure strain and a more gradual failure mode.

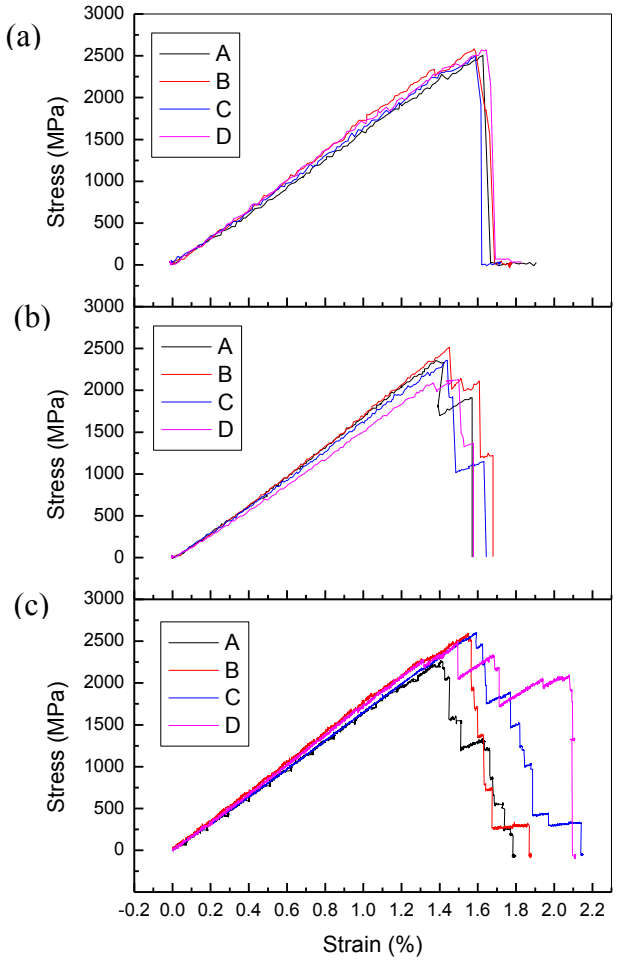


Figure 2.21 Tensile stress-strain curves of (a) control, (b) gas-textured and (c) non-constrained annealed carbon fibre/PA-12 tapes

2.4.3 The fibre alignment angle in the control, gas-textured and non-constrained annealed carbon fibre/PA-12 tapes

In order to lend support for the proposed failure mechanism of the composites, containing the fibres which passed through the gas texturing process or were subjected to non-constrained annealing, the distributions of fibre alignment angles were quantified (Figure 2.22).

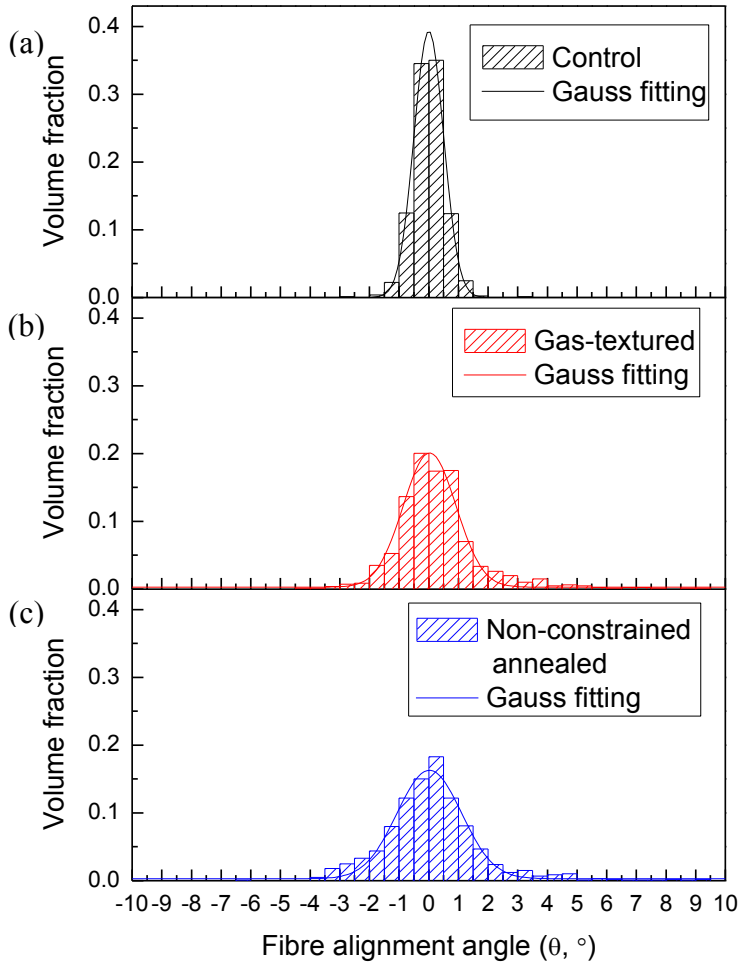


Figure 2.22 True fibre alignment angle distributions of (a) control (b) gas-textured and (c) non-constrained annealed carbon fibre/PA-12 composites

The true fibre alignment angles of the control, gas-textured and non-constrained annealed carbon fibre/PA-12 tapes ranged from -2 to 2°, -3.5 to 4° and -4 to 5°, respectively. It can be seen that the distribution are symmetric about the 0° degree position except for higher magnitude of misalignment in the gas-textured and non-constrained annealed composite. In these cases, there appears to be fewer fibres with misalignment angle less than -3°, then there are with angle greater than 3°. However, noted earlier, this is due to the difficulties with the measurement technique, fibres at angle close to -5° have major axis length which exceeded the length of the micrograph and so were not counted. Despite this loss of symmetry, the fibre

misalignment distributions of all these composites are fitted well by Gauss distribution. A Gaussian distribution as described is Equation 2.9:

$$f(\theta) = y_0 + \frac{A}{w\sqrt{\pi/2}} e^{\frac{-2(\theta-\theta_c)^2}{w^2}} \qquad \text{Equation 2.9}$$

where θ_c is the median value of the Gaussian fitting curve, y_0 the offset value in y axis of the Gaussian fitting curve, A the area between the Gaussian fitting curve and $y = y_0$ and w refer to the width of the peak in the Gaussian fitting curves. The width of the peak in the Gaussian fitting curves when $y = y_0 + (y_{max} - y_0)/2$ is $w \times \sqrt{\ln 4}$ [58]. Table 2.4 summarises the parameters of the Gaussian fitting curves of the fibre alignment angle distributions of the control, gas-textured, non-constrained carbon fibre/PA-12 composites. Compared with the control carbon fibre/PA-12, the widths of Gaussian fitting curves of the distributions of fibre alignment angles in the gas-textured and the non-constrained annealed carbon fibre/PA-12 increased by 77% and 116%, respectively. This indicates that both the annealing process and gas texturing significantly increase the variance of the fibre alignment angles in carbon fibre/PA-12 composites.

Table 2.4 Parameters of the Gaussian fitting curves of the distribution of the fibre alignment angles of control, gas-textured, non-constrained annealed carbon fibre/PA-12 composite

	θ_c (°)	w	A
Control	0.00	1.00	0.49
Gas-textured	0.03	1.77	0.44
Non-constrained annealed	0.02	2.16	0.43

Ninety five percents of the fibres in the carbon fibre/PA-12 control had less than ±1° misalignment from the fully aligned position. However, only 68.5 % of fibres in the gas-textured carbon fibre/PA-12 composites were still almost straight, i.e. the misalignment angle smaller than ±1°. The bulk of the remaining 31.5 % were misaligned up to ±3°, but some fibres were misaligned to an even greater extend. This

was caused by the gas flow during the gas-texturing treatment, which affected the arrangement of carbon fibre filaments in the tow and so caused the fibre misalignment. Similar to the gas-textured carbon fibre/PA-12, the variation of fibre alignment angle in non-constrained annealed carbon fibre/PA-12 is larger than that in control samples, but now only 57.5% of fibres are aligned within ±1°. This indicates that non-constrained annealing can be successfully used to introduce variable fibre alignment angles into a carbon fibre/PA-12 composite. In this case, the fibre waviness is caused by a combination of a) the CTE mismatch between carbon fibre and PA-12, b) CTE mismatch between composite and mould tool c) the shrinkage caused by the re-crystallisation of PA-12 and d) movement of PA-12 melt.

2.5 Summary

Two manufacturing methods, gas-texturing and non-constrained annealing, were used to introduce fibre waviness and misalignment with small fibre alignment angles into continuous UD carbon fibre reinforced PA-12. It was found that these two manufacturing methods did increase the width of the Gaussian distribution of fibre alignment angle. That means that more fibres are misaligned in these two composite compared to the control sample. In order to evaluate the effect of variation of fibre alignment on the tensile behaviour of carbon fibre/PA-12, uniaxial tensile tests were carried out on these two composites and a control. Compared with control carbon fibre/PA-12, both gas-textured and non-constrained annealed carbon fibre/PA-12 exhibited a stepwise and gradual tensile failure mode under strain control rather than a sudden and catastrophic failure, which was observed for the control sample. However, the tensile strength of the gas-textured carbon fibre/PA-12 composite decreased and no increase in its ultimate tensile failure strain was observed. The decrease in the tensile strength of the composite is due to the fact that the gas-texturing process

damaged the carbon fibres. However, for the carbon fibre/PA-12 subjected to non-constrained annealing, the ultimate tensile failure strain increased without significantly affecting the composite's tensile strength and modulus. The more gradual tensile failure mode of carbon fibre/PA-12 and the increase in the ultimate tensile failure strain are due to the difference in the fibre alignment and fibre waviness of non-constrained annealed carbon fibre/PA-12 and its control samples.

3 Intermingled carbon fibre/glass fibre thermosetting hybrid composites

3.1 Introduction

UD carbon fibre reinforced polymer composites (CFRPs) have high specific strength and stiffness, but they fail in a brittle manner at a low strain to failure (1.5-1.8%) [59]. In order to increase the strain to tensile failure of UD CFRP composites, glass fibres have been used as another reinforcement to hybridise with carbon fibre to obtain a hybrid composite [60-68]. Ideally, the carbon fibres provide the tensile stiffness in the initial loading stage, while the glass fibres result in a higher strain to failure of the hybrid composite. Fibre reinforced hybrid polymer composites have been studied since the 1970s [69]. Compared with conventional single fibre-type reinforced polymer composites, hybrid composites can offer more advanced design possibilities because their mechanical properties can be changed by changing the fibre types and the fractions of individual fibre types.

Hybrid composites can be realised by laminated hybridisation [60-68], woven hybridisation [70-73] and intermingled hybridisation [39, 74-78], which will be discussed in detail in section 3.2. The difference between these three hybrids is that the fibre types are hybridised at different levels (i.e. layer, fibre tow and fibre filament). The level of hybridisation affects the mechanical properties of hybrid composites [24, 25, 74, 78-82]. Peijs et al. [79] found that tow-to-tow carbon fibre/high performance polyethylene (HPPE) reinforced epoxy hybrid had a higher strain to failure than the control carbon fibre reinforced epoxy, while the strain to failure in sandwiched carbon fibre/HDPE hybrid composite did not increase. Pimenta and Robinson [81] also reported that the tensile strain to failure of hybrid composites improves at the finer hybridisation level. Hence, to manufacture hybrid UD

composites containing two fibre types hybridised at the filament level is a potential way to produce high-performance composites with improved strain to failure.

If two fibre types are completely hybridised at filament level, then the two fibre types should be randomly distributed within polymeric matrix. When such intermingled UD hybrid composites are subjected to longitudinal tension, the initial failure is most likely to occur in the fibre type with the lower failure strain while the nearest neighbouring fibres of the other fibre type with a larger strain to failure should still carry load and stop the failure from propagating. Such a hybrid composite therefore should have a higher strain to failure with a gradual tensile failure behaviour as compared to single fibre type composites. Some investigators attempted to use simultaneous filament winding [80, 83, 84], co-weaving [72, 73] and an air-texturing commingling process [76] to produce the fibre hybrid composites hybridised at the finer level than the conventional fibre hybrid composites that are produced by making a laminate from two prepregs of different fibre types [60-68]. There are few experimental studies in the literature which establish a relationship between the composites hybridised at different levels and the corresponding tensile behaviour [79, 81]. In addition, only few literatures were found to provide the definition and quantification of the degree of hybridisation at filament level. For instance, Summerscales [85] proposed that the contiguity index can be used to define the intimately-mixed hybrid composite. The contiguity index is the ratio of the number of changes of fibre type (along a transect of the micrograph) to the number of fibre-fibre space. However, this method is only able to quantify the degree of hybridisation in the one dimension.

In this research, an air-assisted fibre tow spreading technology was used to increase the spacing between the fibre filaments within carbon fibre and glass fibre tows

separately. After assessing the quality of the spread carbon fibre and glass fibre tows, the spread fibre tows with best quality were selected and combined by airflow to produce two types of hybrid tows. In order to evaluate the degree of hybridisation at the filament level, a model was developed to assess the hybridisation in a commingled tow consisting of two randomly distributed fibre types. In order to characterise the experimental degree of hybridisation, an image recognition programme was developed to analyse cross-sectional micrographs of the hybrid tows. By comparing modelling results with experimental results, it was possible to quantify the degree of hybridisation of two produced intermingled hybrid tows. The fibre tow with the higher degree of hybridisation was selected for the manufacture of a carbon fibre/glass fibre reinforced epoxy hybrid composite via the resin film infusion technique. Finally, the tensile behaviour of this hybrid composite and of control samples was characterised.

3.2 Literature review

3.2.1 The definition and classification of fibre hybrid composites

A hybrid composite is normally considered to be a composite which consists of at least two different reinforcements in a matrix [86]. The reinforcement can be particles, short or continuous fibres but also woven fabrics. This literature review focuses on hybrid composites which contain different types of continuous fibres, i.e. fibre hybrid composites.

Fibre hybrid composites can be classified into three types based on their structure, namely laminated hybrid composites, woven hybrid composites and intermingled hybrid composites (Figure 3.1) [87, 88]. Laminated fibre hybrid composites are the most common hybrid composites among these three types, which consist of two or more types of fibre prepregs [60-68]. Woven fibre hybrid composites consist of a

woven fabric made from different types of fibre tows. One type of fibre tow is in the weft while the other type is in the warp direction, but often there are more than two types of fibre tows even in weft or warp direction [72, 73]. However, in intermingled hybrid composites, at least two continuous fibres are aligned but randomly dispersed throughout a matrix [89]. In these three composites, the fibres are hybridised at three different levels, i.e. prepreg layer, fibre tow and single filament.

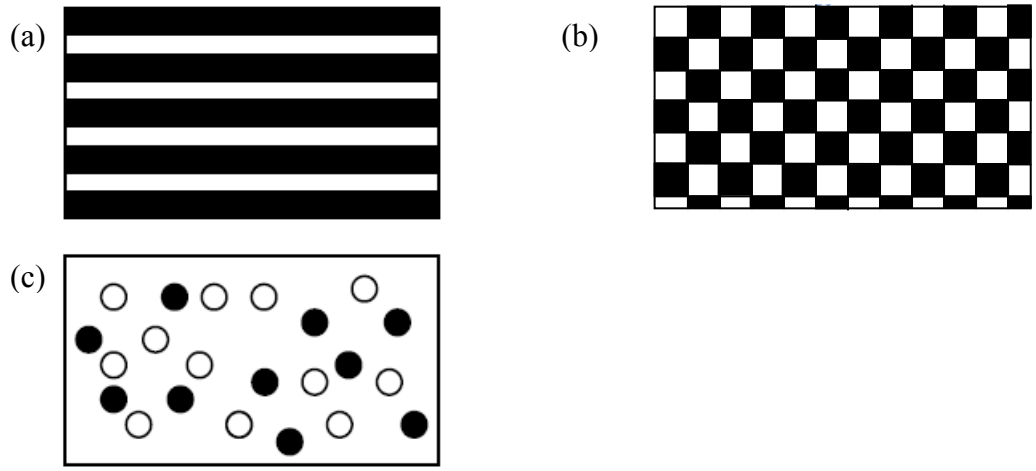


Figure 3.1 Classification of fibre hybrid composites: (a) laminated, (b) woven and (c) intermingled

3.2.2 Tensile behaviour of UD fibre hybrid composites

3.2.2.1 Hybrid effect

The purpose of manufacturing fibre hybrid composites is to create a material, which will retain the advantages of the constituent reinforcements. Because different hybrid composites have different fibre types and different fractions of individual fibre types in the total fibres, it is difficult to evaluate the synergistic effect of hybridisation on the properties of corresponding composites relative to those only containing one fibre type. Therefore, the "hybrid effect" was defined as the difference between the properties of the hybrid composites and the properties predicted by the rule of mixtures (ROM) based on the properties of the composites only containing one fibre type [84]. One requirement to applying ROM for property prediction of hybrid

composite is that the predicted property has a linear relationship with the fraction of the individual fibre types in the total reinforcement. However, some properties are not linearly dependent on the fraction of the individual fibre types in the total reinforcement. For instance, Manders et al. [63], Kretsis [86] and Peijs et al. [79] found that the tensile strength of hybrid carbon fibre/glass fibre or carbon fibre/polyethylene fibre composites is bi-linearly dependent on the volume fraction of carbon fibre in the reinforcement (considering the total fibre volume fraction in the composite is 60%).

The "hybrid effect" was re-defined as the deviation of the strain to primary failure of the hybrid composite from the strain to failure of the un-hybridised composite containing the fibres with the lower strain to failure [60]. Since the 1980s, many investigators found that hybrid composites provided additional strain to failure ranging from -5% to + 35%, which was highly dependent on the type and volume fraction of the high-elongation fibre in the composite and the hybrid structure [86]. However, Chamis et al. also observed a large negative hybrid effect when tow-by-tow hybridising high modulus carbon fibre and glass fibre [62]. Recently, Swolfs et al. pointed out the second definition of "hybrid effect" required an accurately-measured baseline, i.e. the strain to failure of the un-hybridised composite made from low-elongation fibre. This baseline is often affected by stress concentrations in the gripping areas of the test specimens. The effect of stress concentrations on low-elongation fibres was reduced when testing hybrid composites due to the protection provided by high-elongation fibres in the hybrid composite, which may result in an overestimation of the hybrid effect [88].

To sum up, both definitions of "hybrid effect" provide a method to evaluate the effectiveness of the hybridising strategy, but both definitions have their drawbacks: a)

the first definition is invalid when the properties of the hybrid composite are not linearly dependent on the fraction of individual fibre types in the total reinforcement; and b) the second definition requires an accurately-measured failure strain of low elongation fibre composite as a baseline, which is difficult to achieve due to stress concentration caused by the grips in the test. For this research project, it is more important to evaluate the effectiveness of the hybridisation based on different research aims, such as the aimed stiffness, strength, impact resistance or economic cost rather than using the terminology of "hybrid effect".

3.2.2.2 Tensile modulus of UD fibre hybrid composite

For UD fibre hybrid composites, it was found that the measured initial longitudinal tensile modulus fits the value predicted by the ROM [24, 60, 63, 65, 68, 79, 84, 90-92]. It is important to select correct fraction of individual fibre type in the total reinforcement when using ROM to estimate the tensile modulus of hybrid composites [93]. For example, the weight fraction, filament number fraction, ply fraction and volume fraction of each fibre in the total reinforcement are not always the same because the densities and diameters between the constituent fibres can be different. The initial longitudinal tensile modulus of fibre hybrid composites, E_H, is estimated using Equation 3.1 (the contribution of the polymer matrix is assumed to be neglectable),

$$E_H = \sum_{i=1}^{n} E_i V_i \qquad \text{Equation 3.1}$$

where E_i is the elastic modulus of individual constituent fibres and V_i the volume fraction of the constituent fibres in the hybrid composite. However, some papers showed that the longitudinal tensile modulus of hybrid fibre composite was smaller than the predicted value [25, 64]. This is possibly caused by fibre misalignment in the hybrid composite.

3.2.2.3 Strain to failure of UD fibre hybrid composite

a) Primary failure strain of UD fibre hybrid composite

As discussed in section 3.2.2.1, one of the definitions of the "hybrid effect" considers the deviation of the primary failure strain of the hybrid composite from the failure strain of the un-hybridised composite containing only low-elongation fibres. In this section, this definition will be used to evaluate the impact of hybridisation on the primary failure strain of UD composites, as shown in Table 3.1 [24-26, 60-63, 65, 68, 73, 79, 91]. It was found that the positive and negative hybrid effects are both present on the failure strain of UD composites. The "hybrid effect" in most of the investigations is in the range of -5% to + 35% [25, 26, 60, 61, 63, 65, 68, 73, 79, 91] despite of several exceptions such as the works carried by Chamis et al. [62] and Bakis et al. [24] (Table 3.1). Both of these two works shows a large negative hybrid effect, so Chamis et al.'s work was discarded as unrealistic in review papers on fibre hybrid composites published in 1987 [86] and 2014 [88]. However, it seems that their work has some value, because no investigators studied the hybrid effect of UD hybrid composite containing very high content of low-elongation (LE) fibre in the total reinforcement. Their work did show that a positive hybrid effect is difficult to be achieved when the majority of fibres in hybrid composites are low-elongation fibres. In Bakis' work, the very large negative hybrid effect is possibly due to the fact that the researchers used different methods to manufacture and test the control composite and hybrid composite rods.

Table 3.1 Overview of the investigations on the hybrid effect of continuous UD fibre hybrid composites

Investigators	Year	Fibre type	Volume ratio between LE and HE fibre	Hybrid structure	Hybrid effect[a] (%)	Note
Hayashi [60]	1972	CF/GF	1/3	Layer-by-layer	44	
Bunsell & Harris [61]	1974	CF/GF	1/1 & 1/2	Layer-by-layer	42 & 85	

Zweben [69]	1977	CF/Kevlar	1/1	Layer-by-layer	4	
Chamis et al. [62]	1981	LMCF/GF	9/1 & 8/2	Tow-by-tow	16 & -5	
		HMCF/GF	9/1 & 8/2		-29 & -42	
Manders et al.[63]	1981	CF/GF	1/19-4/1	Layer-by-layer	35-8.7	
			1/249-1/16	Thin layer CF sandwiched between GF	52-30	Multiple CF failure and debonding between GF layers
Peijs & Kok [79]	1992	CF/High performance-PE	3/2	Layer-by-layer	0	
				Tow-by-tow	8.5	
Qiu et al. [91]	1993	Kelvar/S-GF	4/3	Filament-by-filament	11	Hybrid seven-fibre micro-composite
Saha et al. [65]	1996	GF/PEF	1/3, 1/1 & 3/1	Layer-by-layer	15.7, 9.8 & 5.9	
Bakis et al. [24]	2001	CF/GF	1/120, 1/2.7 & 1/7	Core/surface hybridised rod	-12.5, -25 & -31.2	Suspicious baseline
You et al. [25]	2007	CF/GF	1/1.6	Core/surface hybridised rod	(9 or 27)[b]	
			1/1.6	filament-by filament hybridised rod	(14 or 33)[b]	Depends on the dispersion of two fibres
Cui et al. [26]	2009	CF/Twaron F/GF/ steel F	1/0.8/3.5/4.4	Core/surfaces hybridised rod	6	
Czél et al. [68]	2013	CF/GF	1/29,1/14.5, 1/10 & 1/7.5	Layer-by-layer	46, 37, 28 & 29	Multiple CF failure and debonding between GF layers
Swolfs et al. [73]	2014	CF/self-reinforced PP	(1/3.5)[c]	Woven CF/SRPP mat (CF/PP in 0° direction) and SRPP (in 0° & 90° direction)	-6	

Note:

a) $Hybrid\ effect = (\varepsilon_{p,H} / \varepsilon_{LE} - 1) \times 100\%$, where $\varepsilon_{p,H}$ is the primary failure strain of the hybrid composite, ε_{LE} the failure strain of un-hybridised composites containing only the low-elongation fibre;

b) Authors used ultimate failure strain of the hybrid composite to calculate the hybrid effect;

c) The ratio shown here is the volume ratio of carbon fibre in self-reinforced PP.

The enhancement in the failure strain of UD composites by hybridisation is affected by many factors, such as the volume ratio between low-elongation fibre and high-elongation fibre, the scatter of the failure strain of the low-elongation fibre and the degree of hybridisation in the composite. The larger volume ratio between low-elongation and high-elongation fibres resulted in a bigger hybrid effect [61, 63, 65, 68]. Zweben et al. found that increasing the scatter of the failure strain of low-elongation fibres can also enhance the hybrid effect [69]. Later, Fukunaga et al. [94] pointed out that the hybrid effect should be zero if the scatter of the failure strain of low-elongation fibres is zero. Swolfs et al. [88] thought the hybrid effect investigated after 1990 tended to decrease compared with that investigated in the 1970s and 1980s, which was due to the smaller scatter in the failure strain of carbon fibre. Furthermore, as discussed in section 3.1, the large degree of hybridisation in the hybrid composites is also an important factor, which contributes to the enhancement in the hybrid effect [25, 63, 81].

One of the main factors causing the hybrid effect is that the presence of high-elongation fibres in the hybrid composites changes the damage development compared to that in UD un-hybridised composites [68, 69, 81, 95, 96]. In the 1970s and 1980s, it was found that the high-elongation fibres in the hybrid fibre composites arrested the crack propagation initiated by the failure of low-elongation fibres [63, 69, 82]. Recently, Czel et al. [68] also observed that the failure of the thin carbon fibre layer was arrested by the sandwiched glass fibre blocks, which resulted in multiple carbon fibre ply fragmentation and then progressively-developing delaminations between carbon fibre and glass fibre layers in hybrid fibre composites. The damage development of such hybrid composites is different from that observed in UD un-hybridised composites, which results in a high hybrid effect [95]. Another factor

causing the hybrid effect are the different coefficients of thermal expansion (CTE) between the different fibre types in the composite resulting in residual thermal stresses in hybrid composites after curing [61, 63, 65, 69]. For instance, the typical values of the CTEs of PAN-based carbon fibre/epoxy and E-glass fibre/epoxy are -0.3×10^{-6}/°C and 6×10^{-6}/°C [3]. Due to this mismatch in CTEs of carbon fibre and glass fibre, there is a compressive thermal residual stress on carbon fibre and a tensile residual stress on glass fibre, which contributes to the positive hybrid effect under tensile load in fibre direction.

b) Ultimate failure strain of UD fibre hybrid composite

Compared with the primary failure strain of fibre hybrid composites, less attention has been paid to studying their ultimate failure strain. So far, the published papers show that the ultimate failure strain of UD fibre hybrid composites is lower than the failure strain of un-hybridised composites containing only the high-elongation fibres but is higher than that of composites containing the low-elongation fibres [60, 61, 68, 91] (see Table 3.2). The main possible failure mechanism is that: a) the stress concentrations as a result of the failure of low-elongation fibres cause the nearby high-elongation fibres to fail; followed by b) a cluster of broken low-elongation and high-elongation fibres is formed as the increasing tensile strain; then c) the fibre hybrid composites fail completely when the size of the broken fibre cluster exceeds a critical value [88, 96]. Due to this failure mechanism, the ultimate failure strain of hybrid fibre composite is smaller than the failure strains of the un-hybridised composites containing only high-elongation fibres.

Table 3.2 Comparisons of ultimate failure strain of the hybrid composites and their corresponding un-hybridised composites

Investigators	Failure strain of LE fibre composite (%)	Ultimate failure strain of fibre hybrid composite (%)	Failure strain of HE fibre composite (%)
Hayashi [60]	1.5	2.31	2.8
Bunsell & Harris [61]	0.26	1.25	1.75
Qiu et al. [91]	1.79	2.58	4.71
Czél et al. [68]	1.5	2.75	3.4

Note: the detailed information about fibre types, fibre volume ratio and structure in hybrid composite is shown in Table 3.1.

3.2.2.4 Tensile strength of UD fibre hybrid composite

As already mentioned in section 3.2.2.1, the theoretical tensile strength of UD fibre hybrid composites is bi-linearly dependent on the volume fraction of low-elongation fibre in the total fibres (shown in Figure 3.2), which is obtained by the damage development [63, 79, 86, 97]. This process is divided in to three stages: i) the low-elongation fibre and high-elongation fibre carry the tensile stress when the tensile strain of the hybrid is less than the failure strain of low-elongation fibre; ii) all low-elongation fibres fail and stop carrying any tensile stress when the tensile strain of the hybrid composite exceeds the failure strain of low-elongation fibre, while all high-elongation fibres still remain intact and continue to carry tensile stress; and finally iii) the high-elongation fibres fail when the tensile strain exceeds the failure strain of the high-elongation fibres causing complete failure of the hybrid composite. The tensile strength of such a hybrid composite is either the stress in hybrid when low-elongation fibres fail or the stress in hybrid when high-elongation fibres fail, depending on which one has a higher value.

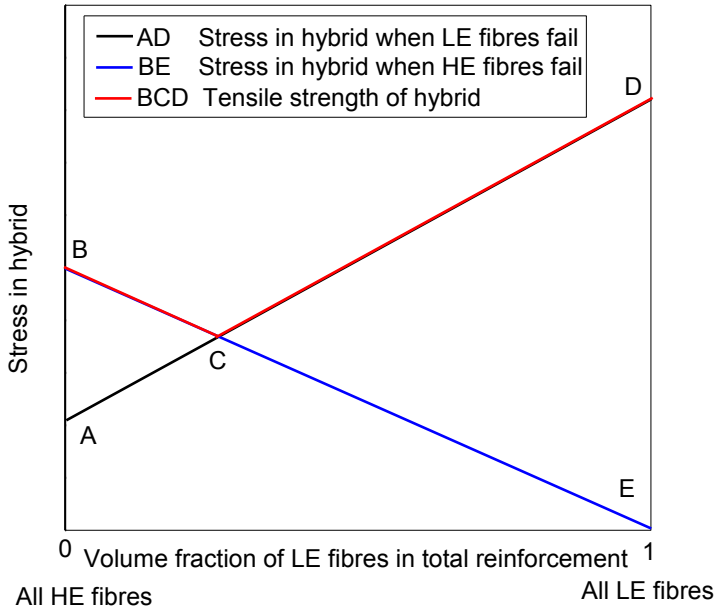


Figure 3.2 Theoretical tensile strength of fibre hybrid composite [63]

However, the experimental results show that both positive deviation [25, 63, 65, 79] and negative deviation [24, 26, 62, 68, 91, 98] from the theoretical tensile strength of hybrid composite. It is due to the fact that the damage development in the hybrid composites in the experiment is not as simple as the one stated above. Firstly, there are variations in the tensile strengths of low-elongation and high-elongation fibres, which means that not all low-elongation fibres and high-elongation fibres in the hybrid composite fail at the same time. Secondly, the stress concentration as result of the failure of low-elongation fibres possibly causes the nearby high-elongation fibres to fail at strains, which are much lower than their ultimate failure strain, as discussed in section 3.2.2.3.

3.2.3 Manufacturing of UD fibre hybrid composites

3.2.3.1 Fibre hybridisation at layer level

Layer-by-layer stacking has been a well-used technique for the production of fibre hybrid composites since the 1970s [60-68]. Hybrid composites are produced by stacking layers of prepregs containing just one fibre type followed by prepregs

containing another fibre type in the desired stacking sequence. This lay-up is then vacuum-bagged and autoclaved at the required temperature and pressure [68]. The main advantage of this technique is that it is very simple, but the degree of hybridisation in this laminated hybrid composite is limited by the thickness of the prepregs used, which is normally around 125 μm. As discussed in section 3.1 and 3.2.2, the degree of hybridisation plays an important role in controlling the tensile behaviour of UD hybrid composites. Very recently, Czél and Wisnom [68] used thin-ply carbon fibre prepregs with a ply thickness of 22 μm to hybridise with glass fibre prepregs with a ply thickness of 125 μm, which increased the degree of hybridisation compared to traditional laminated hybrid composites.

3.2.3.2 Fibre hybridisation at tow level

Simultaneous filament winding [79, 80, 83, 84, 98, 99] and weaving [70-73] are two techniques which can be used to hybridise continuous fibres at the tow level.

In simultaneous filament winding, two impregnated continuous fibre tows are simultaneous wound onto a mandrel to obtain a UD fibre hybrid prepreg [98]. Then the prepregs are stacked together and autoclaved into hybrid composites. The degree of hybridisation and the volume ratio between the fibre types in such composites are mainly controlled by the size of the fibre tows. Compared with laminated hybrid composites, the composites manufactured using this technique have a higher degree of hybridisation [79, 83]. However, fibre misalignment in hybrid prepregs can be higher than in the commercially available prepregs and pultrused products.

Woven hybrid fabrics have been commercially available for over two decades [100]. Some researchers studied the mechanical properties of woven hybrid composite containing one fibre type in the warp and another fibre type in the weft direction [70-72]. Because this chapter focuses on continuous UD fibre hybrid composite, using co-

weaving technique to manufacture such hybrid composite will not be reviewed here. It is worth noting that Swolfs et al. [73] used the co-weaving technique to manufacture woven hybrid fabrics containing carbon fibre/polypropylene tape and self-reinforced polypropylene tape in the warp and only self-reinforced polypropylene tape in the weft direction. It means that they produce a woven composite hybridised at the tow level in the warp direction.

3.2.3.3 Fibre hybridisation at filament level

Hybridising two types of fibres at filament level is very challenging, as it requires commingling and intimately mixing the two fibre tows together to form a fibre hybrid tow. In order to produce UD fibre hybrid composites, the fibre hybrid tows have to be impregnated by (thermoplastic or thermosetting) polymer and then cured or consolidated. However, the original purpose to develop commingled fibre tows was not to manufacture UD fibre hybrid composites but continuous UD fibre reinforced thermoplastic composites (an example is TWINTEX®, Fibre Glass Industries, Inc, USA). In this process, the reinforcement fibre tow and a thermoplastic fibre tow are combined by commingling and then the thermoplastic fibres within the combined tow are melted and consolidated in a pultrusion process [39].

Two techniques are available to commingle two fibre tows together, namely gas-texturing and in-situ commingling. In the former case, an air flow is used to spread a fibre tow into thousands of individual filaments and relocate the positions of different fibres, so the reinforcement fibre tow and polymer matrix fibre tow are commingled together [39, 74]. Herath et al. [76] used the gas-texturing technique to produce hybrid reinforcement tows (carbon fibre/glass fibre and carbon fibre/aramid fibre). They found that the degree of hybridisation of this hybrid yarns was higher than those made by simultaneous filament winding. Unfortunately, they did not provide sufficient

information about the tensile behaviour of their commingled UD composites. The in-situ commingling technique was first reported by Mäder et al. in 2007; they used this technique to combine and hybridise self-spun glass fibres and polypropylene fibres. In their process, the polypropylene fibres and glass fibres were spun separately and then combined. The degree of hybridisation in the glass fibre/polypropylene fibre tow can be optimised by changing the spinning speed and spinning nozzles [78]. This process did provide a fibre hybrid tow with a higher degree of hybridisation degree compared with the gas-texturing process, but it requires fibre manufacturing to be operated simultaneously with the commingling process, which is rather difficult to do especially when aiming to hybridise carbon fibre with glass fibre or polymer fibre.

3.3 Materials and methods

3.3.1 Materials

The continuous carbon fibre tows and glass fibre tows used are listed in Table 3.3 and Table 3.4, respectively. An epoxy resin film (HexPly®M21, 37g/m^2) from Hexcel Co. was used as matrix.

Table 3.3 The detail information of carbon fibres

Sample	Fibre type	Tow size	Diameter of fibre[b] (μm)	Modulus of fibre[b] (GPa)	Manufacturer
CF-A	AS4	12K	7	230	Hexcel Co., Cambridge, UK
CF-B	T700SC	12K	7	230	Toray International UK Ltd., London, UK
CF-C	M40J	12K	5	377	Toray International UK Ltd., London, UK
CF-D	T800SC	12K	5	294	Toray International UK Ltd., London, UK
CF-E	IM7-GS[a]	12K	5	276	Hexcel Co., Cambridge, UK
CF-F	IM7-TS[a]	12K	5	276	Hexcel Co., Cambridge, UK
CF-G	AS4-GS[a]	12K	7	230	Hexcel Co., Cambridge, UK
CF-H	AS4-GP[a]	12K	7	230	Hexcel Co., Cambridge, UK
CF-I	AS7-GS[a]	12K	7	241	Hexcel Co., Cambridge, UK

CF-J	Panex 35[a]	48K	7	242	Zoltek Co., St. Louis, US
CF-K	Testing[a]	3K	Unknown	Unknown	Hexcel Co., Cambridge, UK
CF-L	AS4-GS	3K	7	230	Hexcel Co., Cambridge, UK

Note: a) the information of fibre types is confidential required by Hexcel Co.
b) the information is provided by the corresponding manufacturers

Table 3.4 The detail information of glass fibres

Sample	Fibre type	Tow size (tex)	Diameter of fibre[a] (μm)	Modulus of fibre[a] (GPa)	Manufacturer
GF-A	E-T635B	2400	17	72	Taishang Fibre Glass Inc. Taian, China
GF-B	E-5744	735	15	75	AGY World Headquarters, Aiken, US
GF-C	S-2-933	675	9	94	AGY World Headquarters, Aiken, US

Note: a) the information is provided by the corresponding manufacturers

3.3.2 Air-assisted fibre tow spreading and intermingling technology

3.3.2.1 Spreading of carbon fibre and glass fibre tows

The principle of the air-assisted fibre tow spreading technology is to let air pass through a fibre tow in a low-tension or tension-free state [101, 102]. Under these conditions the space between the filaments is increased as seen in Figure 3.3, which allows filaments of another fibre type to be inserted into the increased space to form an intermingled fibre hybrid tow.

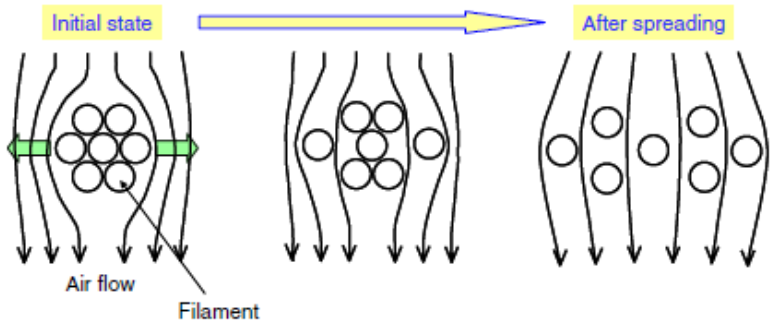


Figure 3.3 Schematic figure of air-assisted fibre spreading process [101]

The air-assisted fibre tow spreading machine (Izumi International Inc, Greenville, US) was used in this research (Figure 3.4 (a)). The spreading machine consists of four parts, namely a fibre sizing loosening system, a tension and speed control system, a vacuum system and a fibre winding system (Figure 3.4 (b)). The components, operation parameters and functions are summarised in Table 3.5.

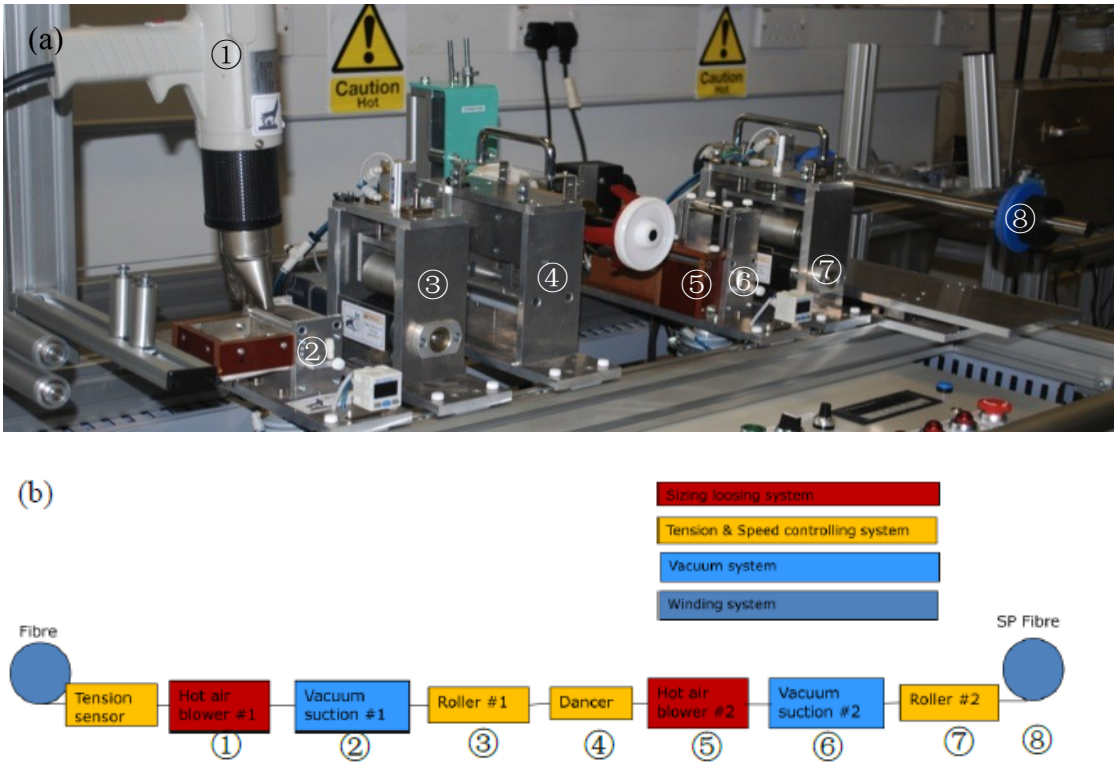


Figure 3.4 Setup of fibre tow spreading machine (a) photo (b) flow chart

Table 3.5 Summary of function, component and operating parameters of fibre tow spreading machine

	Component	Operating parameter	Function
Sizing loosening system	①⑤	Airflow rate of blower ① Air flow rate and temperature of blower ②	Hot air blowing does soften fibre sizing. The purpose of this treatment is to prevent sizing on fibres from sticking the filaments together during the spreading process.
Tension & speed controlling system	Tension sensor ③④⑦	Tension in fibre tow before blower ① Speed of process	Low tension or tension-free state in the fibre tow is essential for spreading, which allows filaments to relocate within fibre tow.
Vacuum system	②⑥	Reduced pressure Width of vacuum suction window	Vacuum suction provides airflow to pass through fibre tow to spread fibre tows.

Winding system	⑧	Winding torque Transverse travelling speed of winder	Winding torque controls the tightness of the fibre tow packing on the creel. Transverse travelling speed controls the winding pattern of the fibre tow.

In order to understand the capacity of the fibre tow spreading machine and determine the optimal spread fibre tow for the commingling of fibre tows, 12 types of carbon fibre and 3 types of glass fibre (details shown in Table 3.3 and Table 3.4) were used explored. Because tow size, fibre diameter, sizing type and sizing content on the fibre surfaces are different between these tested fibres, the manufacturing parameters had to be adjusted for each fibre type separately. By assessing the stability of the spread fibre tow and the spreadablity of the fibre tows (its details will be discussed in section 3.4.1.1), the optimal parameters for spreading each fibre type are shown in Table 3.6.

Table 3.6 The manufacturing parameters of spreading carbon fibre and glass fibre tows

Sample	Tension before ①(N)	Hot air blower ①, ⑤	Gauged vacuum pressure (kPa)*		Process speed (m/min)
			②	⑥	
CF-A	1	Off	-6.5	-11.3	1
CF-B	1	Off	-7.5	-13.5	1
CF-C	1	Off	-9.3	-16.2	1
CF-D	1	Off	-7.2	-14.0	1
CF-E	1	Off	-9.3	-15.6	1
CF-F	1	Off	-9.1	-15.4	1
CF-G	1	Off	-8.1	-11.4	1
CF-H	1	Off	-9.5	-12.8	1
CF-I	1	Off	-9.0	-12.5	1
CF-J	2	Off	-5.0	-14.5	1
CF-K	0.5	Off	-5.5	-8.2	1
CF-L	0.5	On	-5.5	-9.6	1
GF-A	1	On	-7.4	-13.6	0.75
GF-B	0.5	On	-8.5	-14.3	0.75
GF-C	0.5	On	-9.5	-15.2	0.75

3.3.2.2 Manufacturing of intermingled carbon fibre/glass fibre hybrid tows

After assessing the quality of spread carbon fibre and glass fibre tows (see Section 3.4.1.1), one type of carbon fibre (CF-B) with the best quality and two types of glass

fibre (GF-A and GF-B) were selected as base materials for manufacturing intermingled carbon fibre/glass fibre hybrid tows A and B. Fibre types, number of filaments of each fibre type and volume ratio between carbon fibre and glass fibre in the carbon fibre/glass fibre hybrid tows are shown in Table 3.7. Figure 3.5 shows the principle of the hybridizing process: the spread carbon fibre and glass fibre were firstly overlapped together and then passed through the air-assisted hybridisation unit to insert the individual fibres into the spaces created by the spreading between the filaments of the tows to create a hybrid tow.

Table 3.7 Fibre types, number of filaments of each fibre type and volume ratio between carbon fibre and glass fibre in the carbon fibre/glass fibre hybrid tows

Sample	Type		Number of filaments (K)		V_{CF}:V_{GF}
	CF	GF	CF	GF	
A	CF-B (T700SC)	GF-A (E-T635B)	12	3.87	1 : 2.14
B	CF-B (T700SC)	GF-B (E-5477)	12	1.63	1.55 : 1

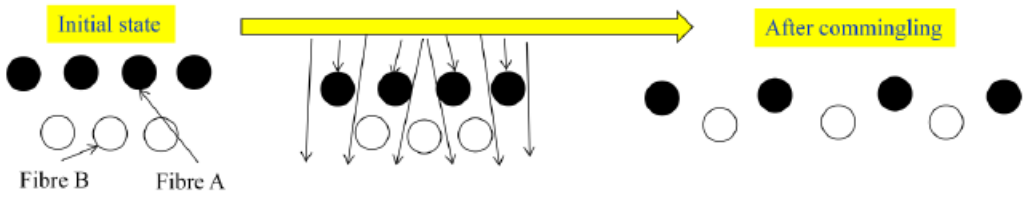


Figure 3.5 Schematic figure of air-assisted fibre hybridisation process

In order to hybridise carbon fibre tow and glass fibre tow together by air flow, the fibre tow spreading machine (Izumi International Inc, Greenville, US) was self-modified by adding tension controlled fibre creels, as shown in Figure 3.6. The E-glass fibre tows were first spread and then hybridised and commingled with T700 fibres by vacuum suction unit #2, which was initially spread by vacuum suction unit #1. In order to achieve the maximum hybridisation degree, two key requirements need to be met in this process: a) the width of the spread carbon fibre should be the same as that of the spread glass fibre before entering the hybridisation unit (vacuum suction

unit #2); b) the spread carbon fibre and glass fibre tows should fully overlap. The manufacturing parameters, therefore, were carefully set to meet these requirements, as shown in Table 3.8. In order to obtain control glass fibre tow and carbon fibre fibre tow, as-received glass fibre tow and carbon fibre tows passed through the spreading unit and then hybridising unit without adding the other fibre type. The parameters used in producing control fibre tows were same as the manufacturing parameters used for producing carbon fibre/glass fibre hybrid tow.

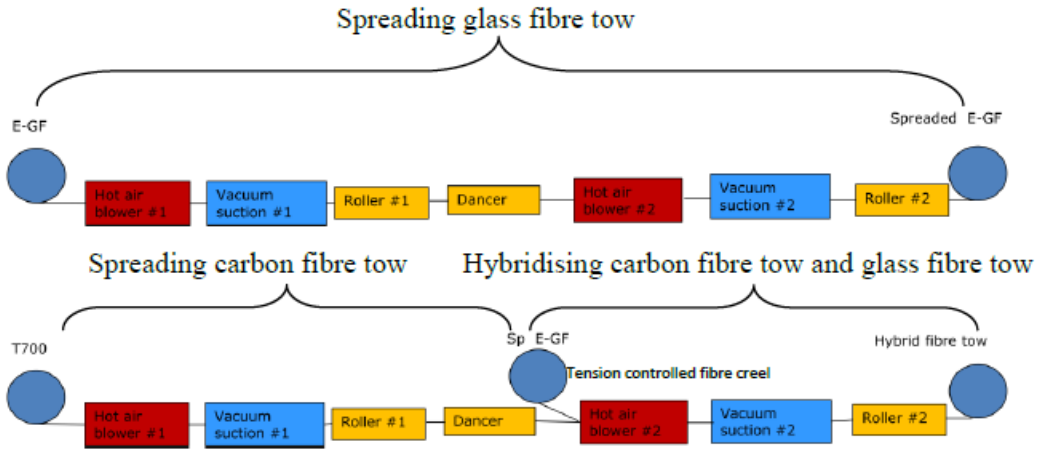


Figure 3.6 Manufacturing of intermingled carbon fibre /glass fibre tow

Table 3.8 The manufacturing parameters of hybridising carbon fibre/glass fibre tows

Process	Fibre type	Measured vacuum pressure (kPa)		Process speed (m/min)
		②	⑥	
Step 1	GF-A	-1.2	-14.0	0.75
	GF-B	-8.5	-14.3	0.75
Step 2	CF-B	-7.0 (spreading)	-18.3 (hybridising)	0.75

3.3.3 Microscopy analysis of carbon fibre/glass fibre hybrid tows

In order to evaluate the distribution of glass fibre and carbon fibre within the fibre hybrid tows, a dry carbon fibre/glass fibre hybrid tow was carefully fixed using adhesive tape between two microscope slides to minimise accidental changes to fibre arrangement within the tow. Then it was embedded in a transparent epoxy (EpoxyCure ®, Buehler Ltd., Germany) and cured at room temperature overnight.

The samples were polished (details are seen in section 2.3.5.1) and observed using a reflective microscope (AX10, Zeiss Ltd., UK) at a magnification of 20x. A typical microscopy image is shown in Figure 3.7. The micrographs were analysed using an image recognition program developed to evaluate the fibre distribution within the carbon fibre/glass fibre hybrid tow, which is discussed in section 3.4.2.2. In order to obtain a representative result, six images taken from different locations in each of the fibre hybrid tows were analysed using this program.

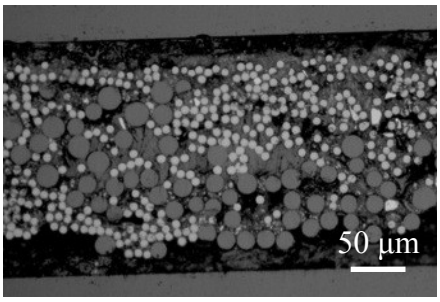


Figure 3.7 Typical micrograph of a carbon fibre/glass fibre hybrid tow (type B)

3.3.4 Determination of fibre diameters

The modified-Wilhelmy technique was used in order to determine the diameters of the fibres used. As shown in Figure 3.8, five fibres, attached to an ultramicrobalance (4504 MP8, Sartorius, Gottingen, Germany) was vertically immersed into n-dodecane (99 % purity, Fisher Scientific), which completely wets the fibres. The fibre diameter, D_F, was calculated using Equation 3.2:

$$D_F = \frac{\Delta m g}{\pi \gamma_l} \qquad \text{Equation 3.2}$$

where Δm is the recorded mass change determined during immersion into or withdrawal from the test liquid, g the acceleration due to gravity (9.8 N/kg) and γ_l the surface tension of n-dodecane (25.4 mN/m).

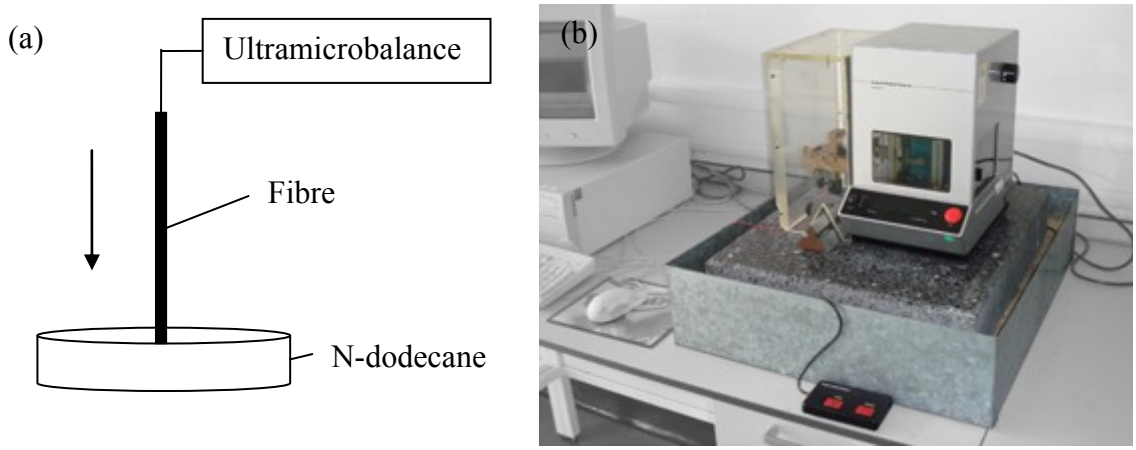


Figure 3.8 (a) Schematic diagram and (b) photo of the setup used to measure fibre diameters using the modified-Wilhelmy technique

3.3.5 Manufacturing of carbon fibre/glass fibre reinforced epoxy hybrid composite

The carbon fibre/glass fibre reinforced epoxy composites were manufactured by resin film infusion. The dry carbon fibre/glass fibre hybrid tows with a length of 200 mm and width of 20 mm were carefully laid up on the epoxy films to maintain the fibre alignment. The stacking sequence of the lay-up process was $E/(H/E)_5$, where E is epoxy resin film and H is the dry carbon fibre/glass fibre hybrid tow. Six uncured specimens were placed into a mould containing six 200 x 20 mm slots, which was coated with a mould release agent (Release agent-8185, Buehler Ltd., Germany). A schematic and photo of the mould is shown in Figure 3.9. The mould containing the uncured specimens was placed in to a hot press (Model #4126, Carver Inc, Indiana, USA) and heated up from room temperature to 180°C at a rate of 3°C/min under a pressure of 0.8 MPa. The samples were kept at 180°C and 0.8 MPa for 2.5 h and then cooled down to room temperature. The control carbon fibre reinforced epoxy and glass fibre reinforced epoxy resins were manufactured using the same method as described above. The fibre volume fractions in control carbon fibre, glass fibre and carbon fibre/GF reinforced epoxy composite are all from 30-40%.

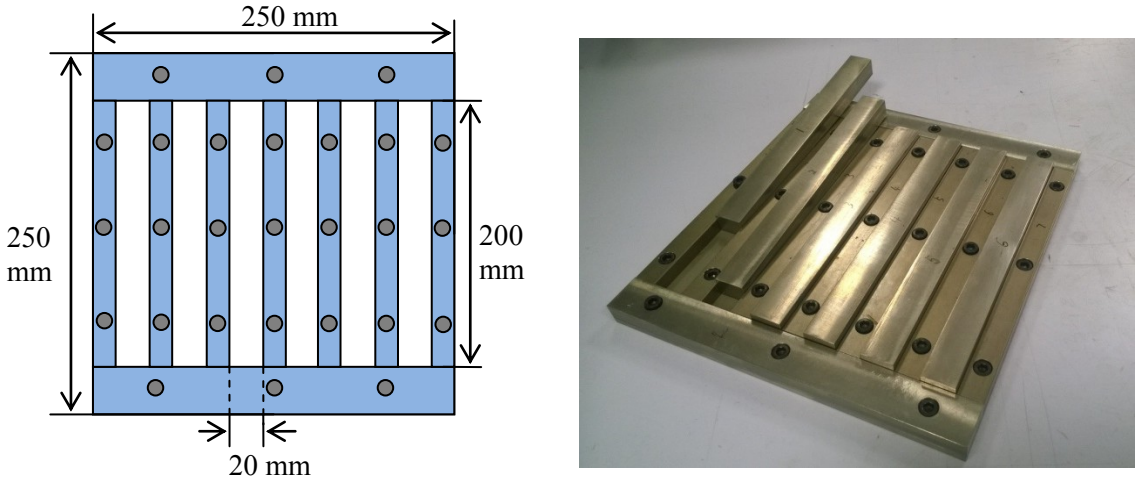
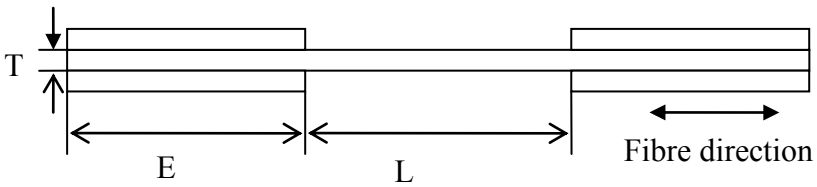


Figure 3.9 (a) Schematic and (b) photo of the mould used to manufacture carbon fibre/glass fibre reinforced epoxy hybrid composite

3.3.6 Tensile test of carbon fibre/glass fibre reinforced epoxy composite

The carbon fibre/glass fibre reinforced epoxy, control carbon fibre reinforced epoxy and control glass fibre reinforced epoxy composites were end tabbed with woven GF reinforced epoxy (Croylam®-F, Croylek Limited, Surry, UK) with a thickness of 1.5 mm and then cut to 100 x 5 mm (Figure 3.10). Five specimens of each group were tested under uniaxial tensile load (Instron 5969, Instron Ltd, Bucks, UK) at a crosshead speed of 0.5 mm/min. A video extensometer (Imetrum, Imetrum Ltd., Bristol, UK) was used to record the strain over the whole gauge length.



T =0.5 mm W= 5 mm L=50 mm E=25 mm

Figure 3.10 Dimensions of the specimen used for the tensile testing

3.4 Results and discussion

3.4.1 Spreading and comingling of carbon fibre/glass fibre tows

3.4.1.1 Effect of different fibre types on the efficiency of fibre tow spreading

Because the quality of spread fibre tow affects the degree of hybridisation of the intermingled carbon fibre/glass fibre tows, it was important to investigate the effect of different fibre types on the fibre tow spreading and select the suitable spread carbon fibre tow and glass fibre tow for hybridisation. In order to assess the quality of spread fibre tow, the "spreadability" and the "stability" were defined and used. Because the fibre tows used in this research have different tow sizes and fibre diameters, the "spreadability" (S) is defined as a function of the number of fibre filaments within a tow and the fibre diameter:

$$S = \frac{W_s}{N \times D} \qquad \text{Equation 3.3}$$

where W_s is the width of the spread fibre tow (mm), N the number of filament in a fibre tow and D the fibre diameter. Some fibre tows have a fairly high "spreadability", but the width of the spread tow is not stable during the process. Hence, a grading system (see Table 3.9) based on appearance of the spread fibre tow was designed to determine the "stability" of the spread fibre tows. The higher grade in the system means that the width of the spread fibre tow was more stable for a longer length of produced spread tow. Table 3.10 gives a summary of the width and the quality of the spread fibre tow. Figure 3.11 shows the appearance of the spread fibre tows.

Table 3.9 Grading system used to quantify stability of the spread fibre tow width

Grade	Appearance of spread fibre tow
1	Width of spread tow varies by ca. 60% within a ca. 100 mm long spread fibre tow and spread tow was split into several parts most of the time.
2	Width of spread tow varies by ca. 50% within a ca. 150 mm long spread fibre tow and spread tow was often split into several parts.
3	Width of spread tow varies by ca. 50% within a ca. 2 m long spread fibre tow and spread two was split into two parts occasionally.
4	Width of spread tow is almost stable within a ca. 5 m long spread fibre tow.
5	Width of spread tow is almost stable within a ca. 20 m long spread fibre tow.

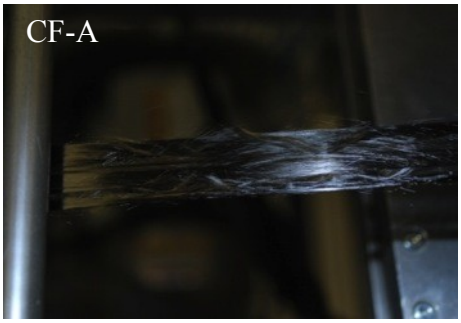
The air-assisted fibre tow spreading technology allows to spread, i.e. to increase the width of carbon fibre tows by ~5 times with a reasonable stability except for CF-G (see Table 3.10). CF-A and CF-G are the same carbon fibre type except that CF-G is sized with stiff and heavy sizing while CF-A is unsized. Because the sizing sticks the filaments within fibre tow together, the "spreadability" of CF-G is lower than that of CF-A. CF-B, CF-D, CF-I and CF-K had the most stable spread tow width and consistently good fibre arrangement in through-thickness direction of the spread tow (see Figure 3.11). There was no obvious gap or split within these four spread fibre tows. It is worth noting that CF-K had the largest "spreadability" amongst these four carbon fibre tows, which implies that these carbon fibres might be most suitable for the proposed hybridisation step. Unfortunately, CF-K is commercially confidential, so it cannot be used for the hybridisation experiments. Therefore, CF-B was selected for the hybridisation experiments considering their spreadability and availability.

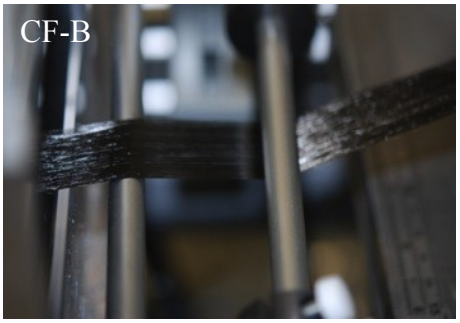
Table 3.10 Summary of the appearance of spread carbon fibre and glass fibre tows

Sample name	Original tow width (mm)	Spread tow width (mm)	Stability (Grade)	Spreadability	Fibre breakage	Comment
CF-A	5-7	25-30	3	0.30-0.36	Yes	Significant fibre entanglements and fibre misalignment
CF-B	5-7	25-30	5	0.30-0.36	No	Good fibre arrangement and alignment
CF-C	3-4	10-14	4	0.17-0.23	No	Some fibre entanglement and fibre twisting
CF-D	5-7	25-30	5	0.30-0.36	No	Good fibre arrangement and alignment
CF-E	3-4	10-14	4	0.17-0.23	No	Good fibre arrangement and alignment
CF-F	3-4	10-14	4	0.17-0.23	No	Some fibre entanglement
CF-G	5-7	8-12	4	0.09-0.14	No	Good fibre arrangement and alignment
CF-H	5-7	20-25	3	0.24-0.30	No	Non-uniform fibre arrangement through-thickness direction. Gap between the fibre filaments.
CF-I	5-7	20-25	5	0.24-0.30	No	Good fibre arrangement and alignment
CF-J	13-15	40-45	3	0.12-0.13	No	Significant fibre misalignment and entanglement
CF-K	2	8-10	5	0.38-0.48	Yes	Good fibre arrangement and alignment

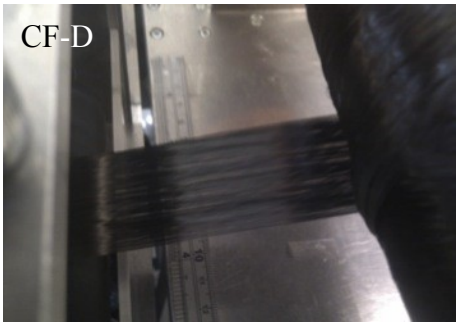
CF-L	2	5-8	3	0.24-0.38	Yes	Non-uniform fibre arrangement in through-thickness direction. Fibre tow splits in the middle.
GF-A	5-7	20-25	2	0.27-0.34	Yes	Significant fibre entanglements and fibre misalignments
GF-B	3	8-14	2	0.29-0.50	Yes	Significant fibre entanglement and fibre twisting
GF-C	3-4	8-15	1	0.21-0.36	Yes, but not as obvious as GF-A&B	Some fibre entanglement and large gap between yarns in the tow

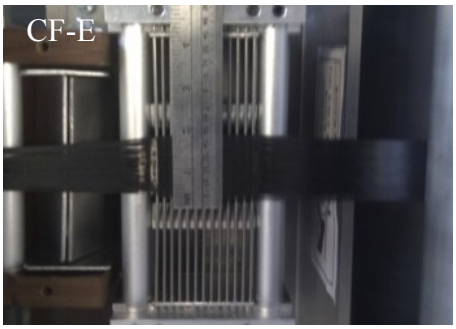
Among the three glass fibre tows, GF-C had the least stable spread tow width and smallest spreadablility. It is possibly due to the fact that this GF-C tow contains 10 yarn bundles, which consist of hundreds of individual filaments, but are not connected. Therefore the glass fibre tows readily split between these yarns during the spreading process. Whereas GF-A and GF-B tows consist of thousands of individual filaments, so it is less difficult to spread these two glass fibre tows than GF-C. The widths of GF-A and B fibre tows were increased by ~400% after spreading. Because quality of spread glass fibre tow will affect the hybridising carbon fibre and glass fibre, GF-A and B which have relatively high spreadablity, were selected as the base material for the hybridising process, which has been shown in section 3.3.2.2. However, fibre breakage was more often observed in GF-A and GF-B than in GF-C, which was probably due to the low mechanical strength of E glass fibres.

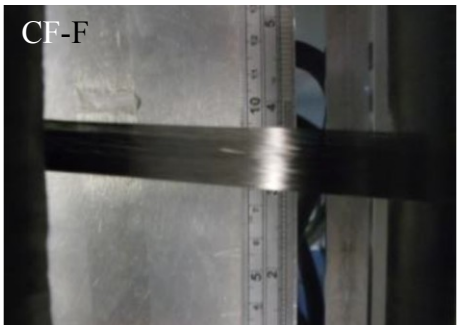

CF-A

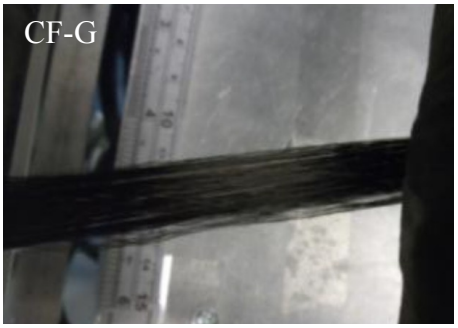

CF-B

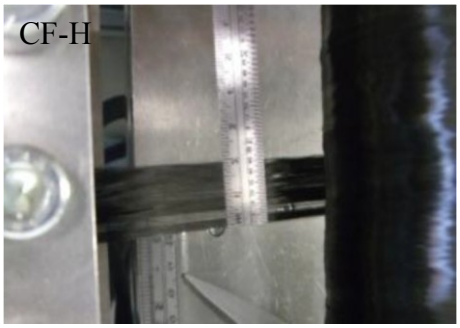

CF-C

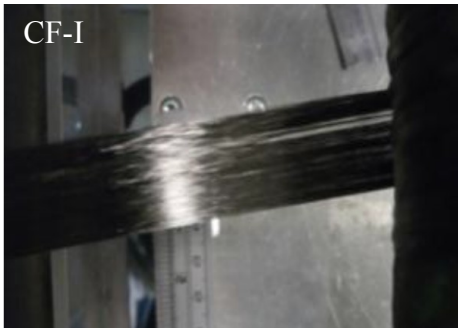

CF-D

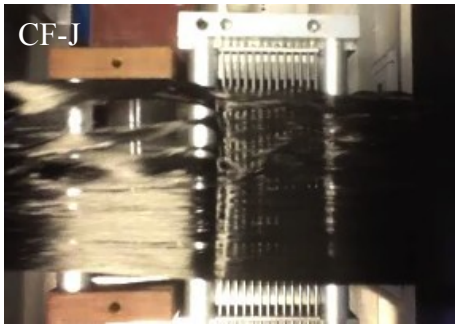

CF-E


CF-F


CF-G


CF-H


CF-I


CF-J

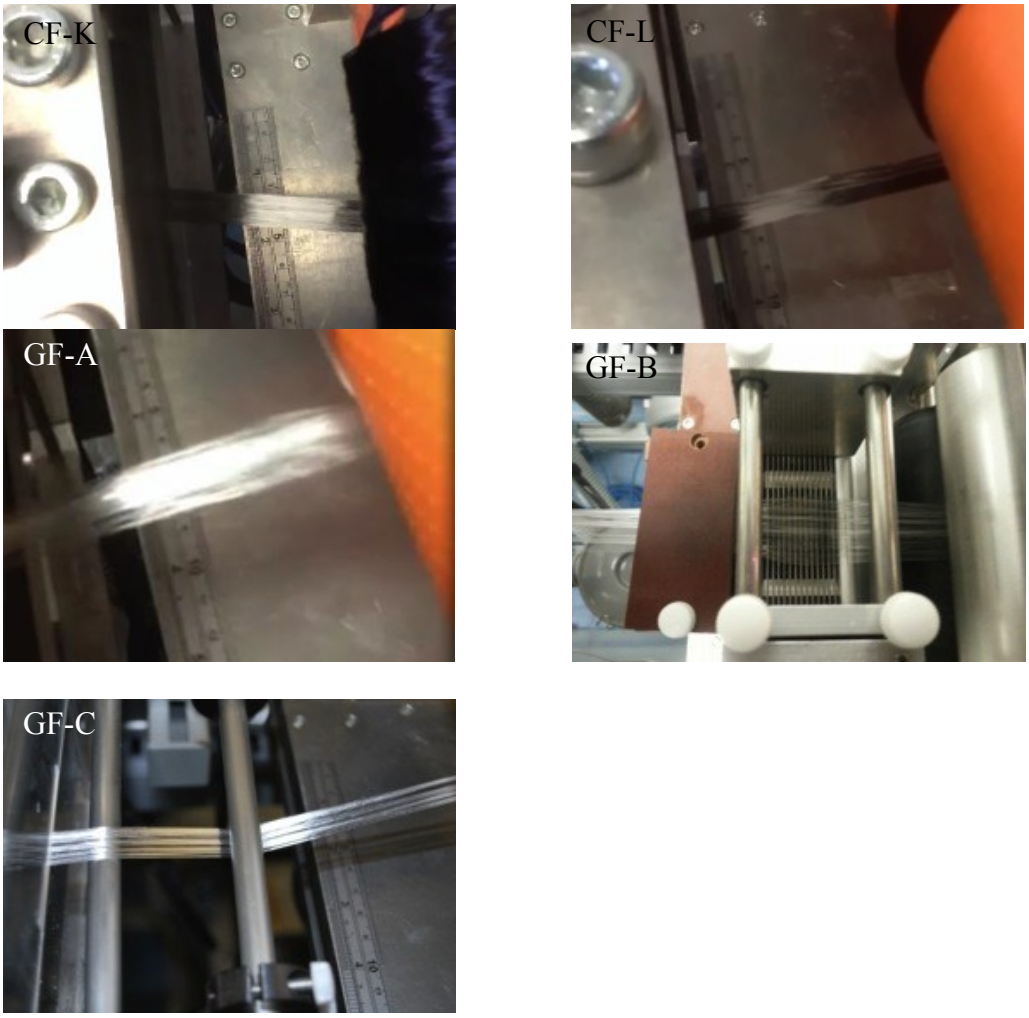


Figure 3.11 Photos of carbon fibre and glass fibre tows taken during fibre spreading

During the spreading it was found that twists, half twists and fibre entanglements within carbon fibre and glass fibre tows are the main factors affecting the stability of spread tow. Figure 3.12 shows the appearance of a spread carbon fibre tow (CF-H) with and without twisting. The width of the spread carbon fibre tow containing twists is only 1/5 of that of the twist-free tow. Unfortunately, the presence of twists within the fibre tow is unpredictable, which increases the difficulty of fibre hybridisation.

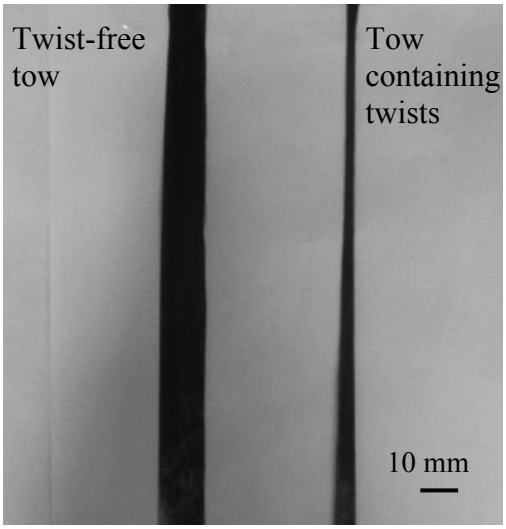


Figure 3.12 Appearance of same spread carbon fibre (CF-H) tow with and without twists

Fibre breakage was still observed for E glass fibre, which was probably caused by the low mechanical strength of the E-glass fibres. The stability of the width of the spread glass fibre tow was lower than those of all spread carbon fibre tows (CF-A to I). This is possibly due to the fact that they contained more "true twists", half twists or an uneven fibre arrangement within the glass fibre tows.

To sum up, this air-assisted fibre tow spreading technology does increase the width of carbon fibre tows by up to 5 times with a reasonable stability, while it increases the width of glass fibre tows by up to 4 times but the spread tow width was much less stable and some fibre breakage occurred. The quality of the spread fibre tows was assessed by the degree of "spreadability" of the fibre tow and the stability of the width of the spread fibre tow, which is influenced by the fibre size, the degree of twisting and the number of fibre entanglements within the fibre tow and the mechanical properties of the fibre. A heavy and stiff size on the fibre surface does reduce the "spreadability" of the fibre tow. Furthermore, the combination of twists, half-twists and fibre entanglements in the fibre tow largely affects the stability of the spread tow width. After assessing the ability to spread 12 different carbon fibre tows and 3 types

of glass fibre tows, CF-B, GF-A and GF-B were selected for the hybridisation experiments.

3.4.1.2 Hybridisation of carbon fibre and glass fibre tows

After spreading carbon and glass fibre tows individually, the spread carbon fibre tow and glass fibre tow were combined and hybridised in the air-assisted hybridising unit. Figure 3.13 shows the appearance of carbon fibre/glass fibre hybrid tows A and B. In Figure 3.13(a), the spread carbon fibre tow was barely seen from top, which means that the spread carbon and glass fibre tows were overlaid, i.e. a layer by layer hybrid tow was created rather than being commingled at filament level. On the other hand, the type B fibre hybrid tow had a larger degree of hybridisation than type A, because the spread carbon fibre tow which was originally located underneath the spread glass fibre tow could be clearly seen after hybridsation (Figure 3.13(b)).

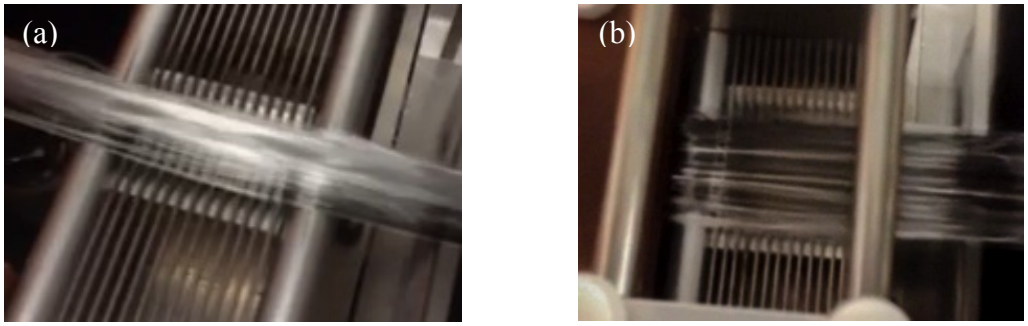


Figure 3.13 Appearance of carbon fibre/glass fibre hybrid tows (a) Type A and (b) Type B

Even though the appearance of the hybrid tows is an indication of the degree of the hybidisation, it is only a qualitative measure to assess the degree of hybridisation. The reason is that the diameters of CF-B (6.9 ± 0.1 μm), GF-A (17.5 ± 0.8 μm, used in type A fibre hybrid tow) and GF-B (14.9 ± 0.5 μm, used in type B fibre hybrid tow) are too small to observe by naked eye. The photos of hybrid CF/GF tows do not show the distribution of carbon fibres and glass fibres within the fibre tow.

3.4.2 Characterisation of the degree of the hybridisation of carbon fibre/glass fibre tows

In order to be able to quantify the degree of hybridisation of carbon fibre/glass fibre tows, a carbon fibre/glass fibre hybrid tow containing randomly-distributed carbon fibre filaments and glass fibre filaments throughout the hybrid tow was first defined and generated using a computer model (it will be discussed in detail in section 3.4.2.1). The micrographs of carbon fibre/glass fibre hybrid tows were analysed using an image recognition program (it will be discussed in detail in section 3.4.2.2). By comparing the distribution of carbon fibres in the hybrid tow determined from micrographs of the cross-sections with that of the hybrid tow containing randomly-distributed carbon fibre filaments and glass fibre filaments generated by a computer model, the degree of the hybridisation of carbon fibre/glass fibre tows could be defined and quantified (it will be discussed in detail in section 3.4.2.3).

3.4.2.1 Definition of the intermingled fibre hybrid tow: A model to describe randomly-distributed, commingled two-fibre-type tows

Some investigators used hexagonal or cubic manner as the ideal fibre pattern to model the fibre packing in UD composite [10, 11, 103-105]. If these two ideal fibre pattern are used in modelling the fibre hybrid tow containing two fibre types, the ideal hybrid tow is that each fibre is surrounded by a fibre from a different type (seen in Figure 3.14). However, the ideal intermingled hybrid tow is almost impossible to achieve in the experiment. The filament number ratios between carbon fibre and glass fibre in the ideal intermingled hybrid tow are 1:2 (in hexagonal fibre packing) and 1:1 (in cubic fibre packing), which are different from the ratios in the currently-produced hybrid tows. Therefore, the ideal intermingled fibre hybrid tow shown in the Figure 3.14 is not suitable for modelling intermingled fibre hybrid tow.

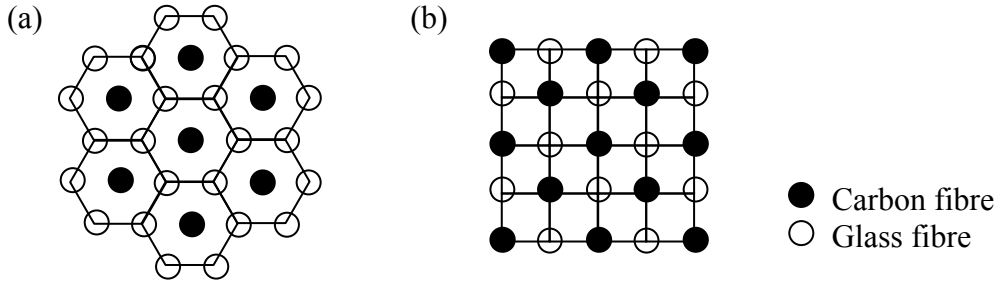


Figure 3.14 Schematic diagrams of ideal intermingled fibre hybrid tow containing two fibre types in the (a) hexagonal fibre package and (b) cubic fibre package

In order to make the model realistic and suitable for the hybrid tows with different filament number ratios between carbon fibre and glass fibres, the truly intermingled carbon fibre/glass hybrid fibre tow in the model should be one in which both carbon fibres and glass fibres are randomly distributed in the hybrid tow (seen in Figure 3.15). A computer model was built in MATLAB (seen in Appendix I) to describe this truly intermingled carbon fibre/glass fibre hybrid tow. In this model, elements A and B were randomly distributed in an m-by-m matrix. The dimension of the matrix (m) was calculated using Equation 3.4:

$$m = \text{int}(\sqrt{N_{CF} + N_{GF}}) \qquad \text{Equation 3.4}$$

where N_{CF} and N_{GF} are the numbers of carbon and glass fibre filaments in the hybrid tow.

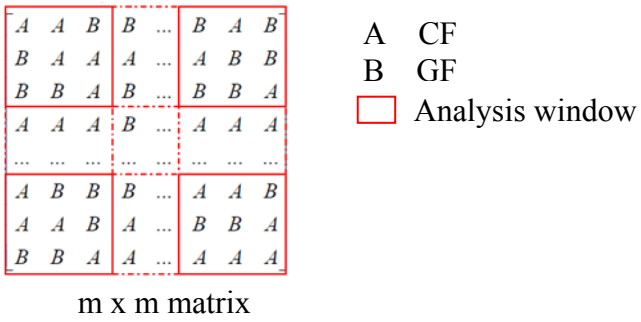


Figure 3.15 Schematic of the model to describe randomly-distributed, comingled two fibre-type hybrid tow

The number ratio between A and B in the model is the same as the corresponding hybrid tow to be produced. This matrix was subdivided into a certain number of

square analysis windows, shown in Figure 3.15. Then the proportion of the cross-sectional area of carbon fibre in the total fibre cross-sectional area in each analysis window generated by the model ($AP_{CF,Model}$) was calculated using Equation 3.5:

$$AP_{CF,Model} = \frac{N_A D_{CF}^2}{N_A D_{CF}^2 + N_B D_{GF}^2} \qquad \text{Equation 3.5}$$

where N_A and N_B are the numbers of elements A and B in each analysis window, respectively and D the fibre diameters of the fibres used to create the hybrid composite (see Table 3.11).

Table 3.11 Diameters of the fibres used in hybridisation

Hybrid tow type A		Hybrid tow type B	
CF (μm)	GF (μm)	CF (μm)	GF (μm)
6.9 ± 0.1	17.5 ± 0.8	6.9 ± 0.1	14.9 ± 0.5

Note: Fibre diameter was determined using the modified-Wihelmy technique

MATLAB was used to generate the random distribution of element A and B in this matrix. However, the distribution of A and B does vary when the model is run multiple times. Therefore the effect of running the model different numbers of times on the probability distribution of $AP_{CF,Model}$ at different sizes of analysis window had to be studied to evaluate the statistical sensitivity of this model, shown in Figure 3.16. The fibre hybrid tow type B was investigated as an example to investigate this effect. The probability distribution of $AP_{CF,Model}$ of the fibre hybrid tow barely changed with increasing number of times the model was run. It indicates that the model does provide a consistent result to describe the probability distribution of $AP_{CF,Model}$ even when the model is only run a limited number of times.

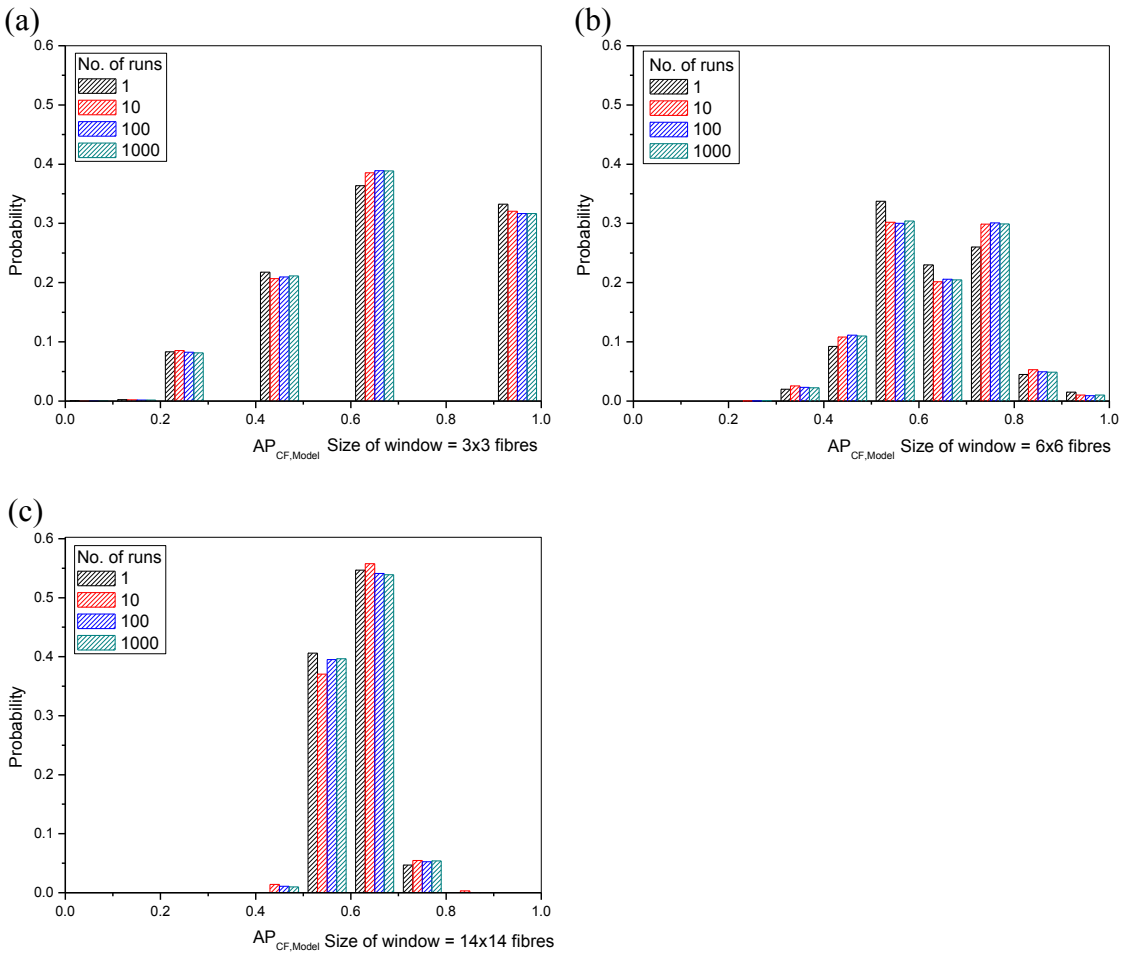


Figure 3.16 Probability distribution of $AP_{CF,Model}$ for a model fibre hybrid tow type B when the model was run 1, 10, 100 and 1000 times at the sizes of analysis windows of (a) 3x3 (b) 6x6, and (c) 14x14 fibres

The coefficient of variation (*CV*) in $AP_{CF,Model}$ as function of the size of the analysis window and the number of times the model was run is plotted in Figure 3.17. When the length of analysis window is the same, the CV in $AP_{CF,Model}$ is almost independent of the number of times the model was run, which confirms the previous statement that the probability distribution of $AP_{CF,Model}$ barely changed as the number of the model runs is increased. Furthermore, it is worth noting that the CV decreased with increasing size of the analysis window. It is due to the fact that the possibility of $AP_{CF,Model}$ in the larger analysis window closing to the mean of $AP_{CF,Model}$ is higher than that in the smaller analysis window. It suggests that the size of the analysis window in the model needs to be carefully selected to quantify the degree of

hybridisation of a real fibre hybrid tow/composite. If the analysis window in the model is too large (for example, the size of the analysis window is 14x14 fibres), the distribution of element A and B within an analysis window tends to be neglected, which is not suitable to analyse a fibre tow hybridised at the filament level. On the other hand, if the analysis window in the model is too small (for example, the size of the analysis window is 3x3 fibres), the variation of $AP_{CF,Model}$ is too large (as seen in Figure 3.16(a) and Figure 3.17 black dots) to be useful as a baseline to determine the degree of hybridisation of real hybrid tow/composite. Hence, 6x6 fibres were used as the suitable analysis window size to determine the degree of hybridisation of real hybrid tows.

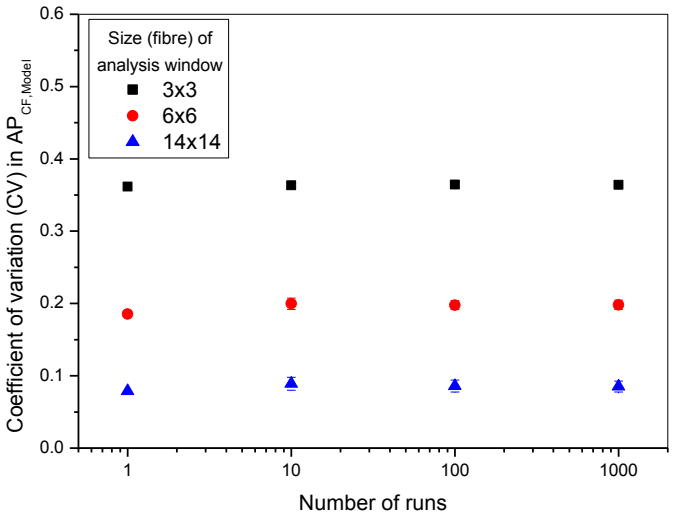


Figure 3.17 Coefficient of variation in $AP_{CF,Model}$ for fibre hybrid tow type B at as function of the size of the analysis window and number of times the model was run

3.4.2.2 Microscopy analysis of carbon fibre/glass fibre hybrid tows using image recognition

A MATLAB program (code is attached in Appendix II) was coded to evaluate the distribution of carbon fibre and glass fibre in micrographs of cross-sections of carbon fibre/glass fibre hybrid tows. The flow chart of this program is shown in Figure 3.18.

The carbon fibres and glass fibres were detected based on their image colour intensity, i.e. grey level (see Figure 3.19).

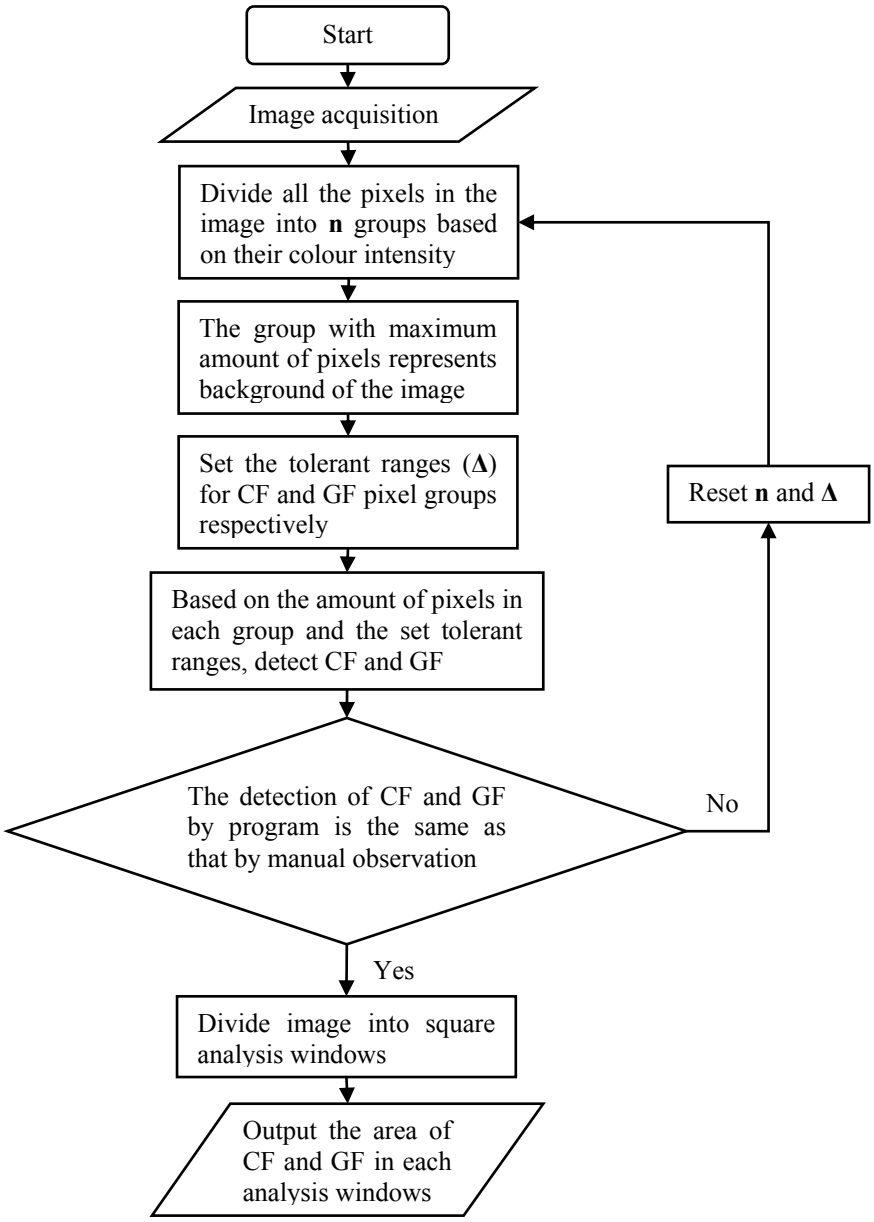


Figure 3.18 Flow chart of the program to evaluate the distribution of carbon fibre and glass fibre in micrographs of cross-sections of carbon fibre/glass fibre hybrid tows

(a)

(b)

(c)

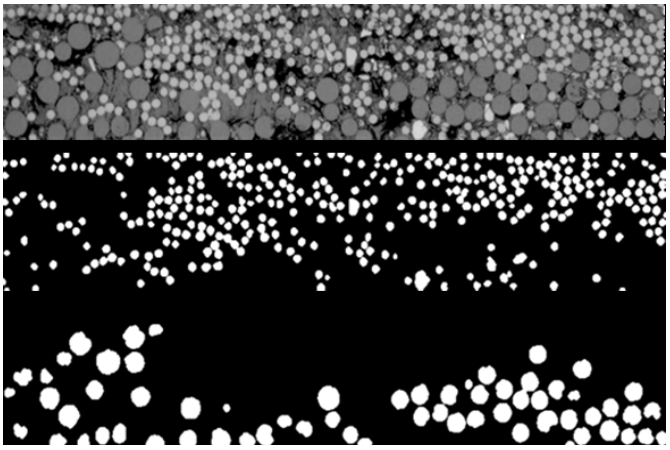


Figure 3.19 Detection of carbon fibres and glass fibres from original micrograph using an image recognition program: (a) original micrograph, (b) carbon fibre within the micrograph and (c) glass fibre within the micrograph

Two methods were used to determine the reliability of this image recognition program.

In method I, the reliability, R_I, was determined using Equation 3.6,

$$R_I = 100\% - \frac{\left| A'_{T,CF}/(A'_{T,CF}+A'_{T,GF}) - A_{T,CF}/(A_{T,CF}+A_{T,GF}) \right|}{A'_{T,CF}/(A'_{T,CF}+A'_{T,GF})} \quad \text{Equation 3.6}$$

where A is the cross-sectional area of each fibre type (as indicated by the subscript) in a typical micrograph of the fibre hybrid tow (Figure 3.19(a)), which was determined using this image recognition program and A' is the cross-sectional area of each fibre type determined by visual observation. The advantage of method I is that it can accurately assess the reliability of this program because the cross-sectional area ratio between glass fibres and carbon fibres in the typical micrograph are obtained manually and used as baseline. However, method I is very time-consuming, which is why only one characteristic micrograph was used for this reliability analysis. Method I, therefore, is suitable to analyse the local reliability of this program. The reliability obtained by method I is 93.0%, which suggests that the program does distinguish accurately between carbon fibre and glass fibre.

In method II, the reliability, R_{II}, was characterised using Equation 3.7,

$$R_{II} = 100\% - \frac{\left| N_{CF}D_{CF}^2/(N_{CF}D_{CF}^2 + N_{GF}D_{GF}^2) - \sum A_{CF}/(\sum A_{CF} + \sum A_{GF}) \right|}{N_{CF}D_{CF}^2/(N_{CF}D_{CF}^2 + N_{GF}D_{GF}^2)} \quad \text{Equation 3.7}$$

where ΣA is the total cross-sectional area of each fibre type in 6 micrographs taken at different locations in the analysed hybrid tow, which was determined using this image recognition program, N and D are number of filaments and fibre diameters of each fibre type in the hybrid tow. The advantage of method II is that it is much less time-consuming than method I and does provide a reliability analysis of all micrographs. The disadvantage of method II is that the total cross-sectional area ratio of carbon fibre and glass fibre in the analysed micrographs may be different from the volume ratio between carbon fibre and glass fibre in the hybrid tow, but it can be minimized or eliminated if sufficient micrographs are used for this analysis. Method II, therefore, is suitable to analysis the global reliability of this program. R_{II} is 95.4%, which indicates that this image recognition program is satisfactory and the number of micrographs (6) used for the analysis is sufficient to represent the degree of hybridisation in the entire fibre tow.

To sum up, by analysing the reliability of the image recognition program globally and locally, the program can be used as a reliable and accurate tool to analyse the degree of hybridisation of experimental hybrid tows.

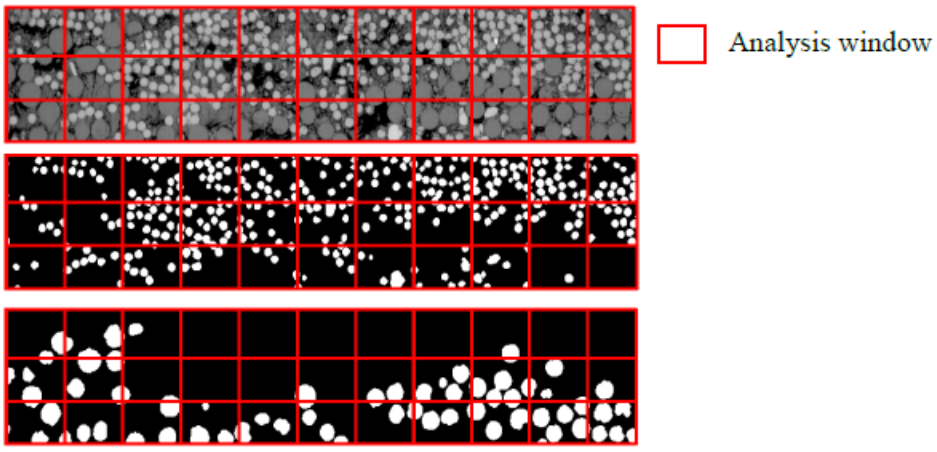


Figure 3.20 Schematic of subdividing the micrograph into square analysis windows

After the detection of carbon fibres and glass fibres in the micrographs of fibre hybrid tows, the image was subdivided into square analysis windows (see Figure 3.20). The proportion of cross-sectional area of carbon fibre in the total cross-sectional area of fibres in each analysis window in the micrographs, $AP_{CF,Experiment}$, was calculated as follows,

$$AP_{CF,Experiment} = \frac{A_{CF}}{A_{CF} + A_{GF}} \qquad \text{Equation 3.8}$$

where A is the cross-sectional area of carbon fibre or glass fibre in each analysis window. As mentioned in section 3.3.3, six images taken from different locations in the hybrid tow were analysis using this program to obtain a representative result.

3.4.2.3 Definition and quantification of the degree of hybridisation

Even though fibre hybrid composites have been investigated since the 1970s [63, 65, 68, 69, 73, 74, 98, 99, 106, 107], only very few researchers proposed a definition of the degree of hybridisation at the filament level[85]. This may be because it is difficult to manufacture such hybrid composites from conventional continuous fibre tows and, therefore, intimately intermingled unidirectional continuous hybrid fibre composites have yet to be reported. Some researchers attempted to use simultaneous filament winding [80, 83] and air-texturing [74, 78] to manufacture commingled fibre composites, which are partly hybridised at the filament level but they did not define or quantify the degree of hybridisation of their products. Here, a quantification method which is based on comparing the differences between the probability distribution of $AP_{CF,Model}$ and $AP_{CF,Experiment}$ was proposed.

In order to make this comparison, the size of the analysis window used in the model should be identical to that used for the analysis of optical micrographs of real hybrid tows. The size of analysis window in the model is based on the fibre diameter, while

in the experimental micrographs the size is based on the real length. In order to unify them, the nominal fibre diameter, $D_{nominal}$, was defined (Equation 3.9) and used as unit of the size of the analysis window for both models and experiments:

$$D_{nominal} = \sqrt{\frac{N_{CF}D_{CF}^2 + N_{GF}D_{GF}^2}{N_{CF} + N_{GF}}} \qquad \text{Equation 3.9}$$

where N and D are number of filaments and fibre diameter of each fibre type used in the hybrid tow.

When the distribution of carbon fibres and glass fibres in the hybrid tow is the same as the distribution of elements A and B in the model, the highest possible degree of hybridisation of carbon fibre/glass fibre tow was achieved. The probability distributions of $AP_{CF,Model}$ and $AP_{CF,Experiment}$ for the fibre hybrid tow type B as function of the size of the analysis window are shown in Figure 3.21. With increasing size of the analysis window, the probability distribution of $AP_{CF,Experiment}$ became closer to $AP_{CF,Model}$. However, it is clear that carbon fibres and glass fibres were not completely randomly distributed (shown in Figure 3.15) in the hybrid tow.

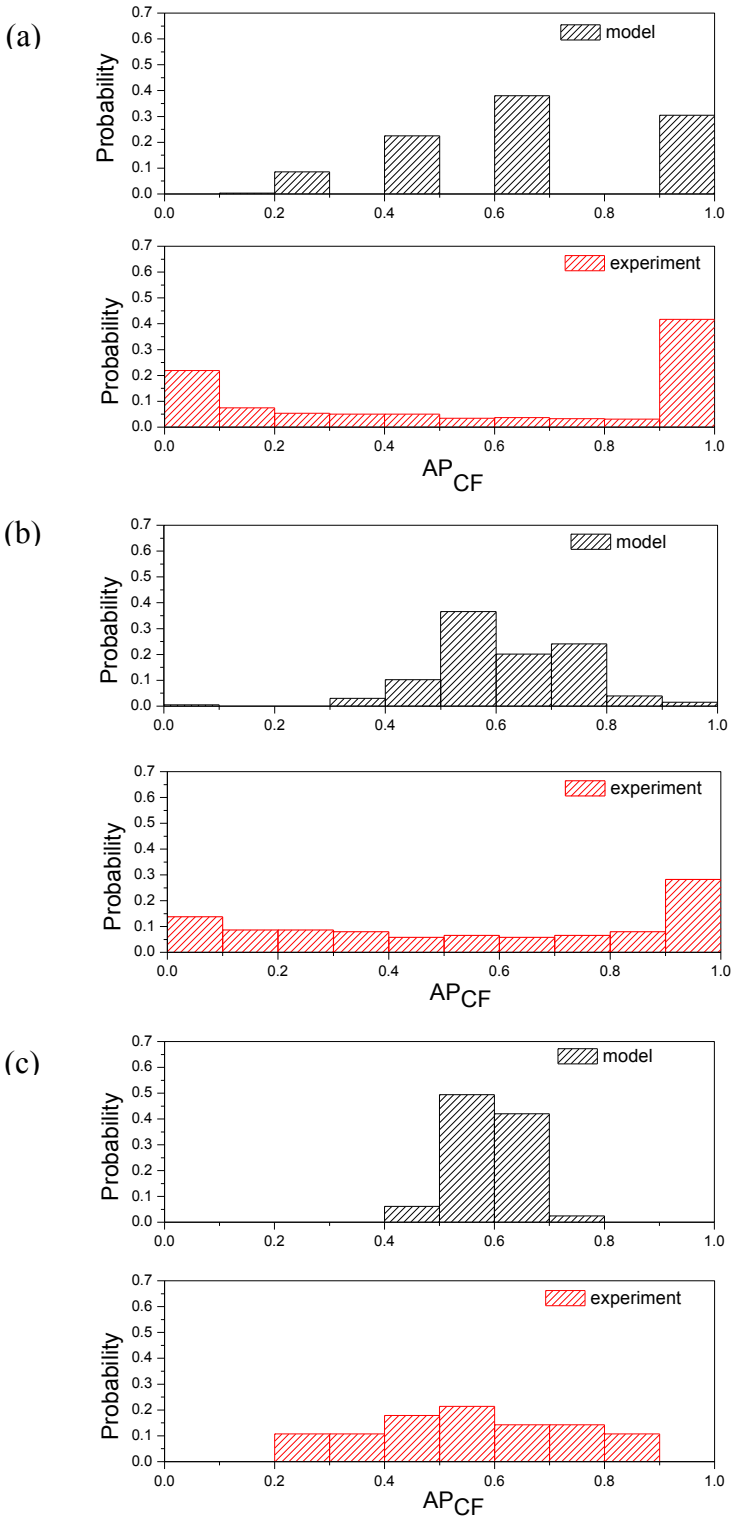


Figure 3.21 Probability distributions of $AP_{CF,Model}$ and $AP_{CF,Experiment}$ for fibre hybrid tow type B as function of the size of analysis windows (a) $(3D_{nominal})^2$, (b) $(6D_{nominal})^2$and (c) $(14D_{nominal})^2$

In order to quantify the degree of hybridisation, the coefficient of variation in $AP_{CF,Model}$ and $AP_{CF,Experiment}$ was plotted as a function of the size of the analysis

window (Figure 3.22). The CV_{Model} decreased sharply from 0.45 to 0.2 with increasing (analysis window size)$^{0.5}$ when it is less than $5D_{nominal}$. Hence, when the (size of the analysis window)$^{0.5}$ is too small (less than $5D_{nominal}$), the distribution of AP_{CF} even in the model has a large scatter. On the other hand, a larger analysis window contains many more filaments, which tends to neglect the distribution of carbon fibres and glass fibres within an analysis window. Therefore, (analysis window size)$^{0.5}$ of $6D_{nominal}$ was selected for the analysis. The degree of hybridisation, H, was calculated using:

$$H = \frac{CV_{Model}}{CV_{Experiment}} \times 100\% \qquad \text{Equation 3.10}$$

where CV_{Model} and $CV_{Experiment}$ are the coefficients of variation in $AP_{CF,Model}$ and $AP_{CF,Experiment}$ when the size of analysis window is $(6D_{nominal})^2$.

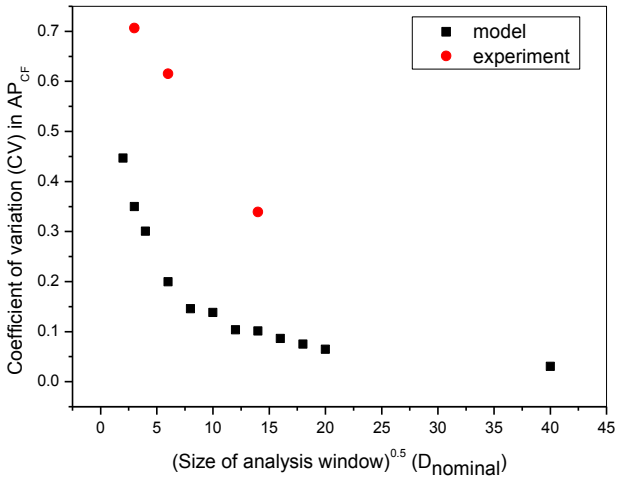


Figure 3.22 Coefficients of variation in $AP_{CF,Model}$ and $AP_{CF,Experiment}$ as a function of $\sqrt{\text{size of analysis window}}$

3.4.3 Degree of hybridisation of carbon fibre/glass fibre hybrid fibre tows

The degree of hybridisation of hybrid fibre tow type A and B were quantified using the method described in section 3.4.2. The degree of hybridisation of the hybrid fibre tow A and B was 25.4% and 32.4%, respectively, indicating that carbon fibre and glass fibre were only partly hybridised at the filament level. The difficulties of

achieving a fibre tow with a higher degree of hybridisation are: (a) a continuous hybridisation process requires that the fibre feeding and wind-up point are fixed and tension has to be applied to the fibre tow when it is wound up, which only allows the filaments to be relocated in a very limited space within the fibre tow; (b) twists, half-twists and fibre entanglements within the as-received fibre tows affected the width of spread fibre tows, which does not allow for commingling of the two fibre types.

The degree of hybridisation of hybrid tow B was increased by 28% compared with hybrid tow A, which can be seen in typical optical micrographs shown in Figure 3.23. In fact, hybrid fibre tow A (Figure 3.23(a) and (b)) was simply a combined spread fibre tow in which the carbon and glass fibre tows were mostly lying on top of each other. Only some of the carbon fibres and glass fibres in the middle of the tow were commingled (see Figure 3.23(b)). The carbon fibres and glass fibres in the hybrid tow B were better commingled than those in type A, which may be due to the fact that the spreadability of glass fibre tow (GF-B) in hybrid tow B is higher than that in the hybrid tow A (GF-A). Especially in left part of Figure 3.23(c), most of the glass fibres were surrounded by carbon fibres. By analysing the optical micrographs of tow cross-sections and comparing with the results of the image analysis and data reduction, it seems promising that the methods developed here can be used to determine the degree of hybridisation of two fibre type tows.

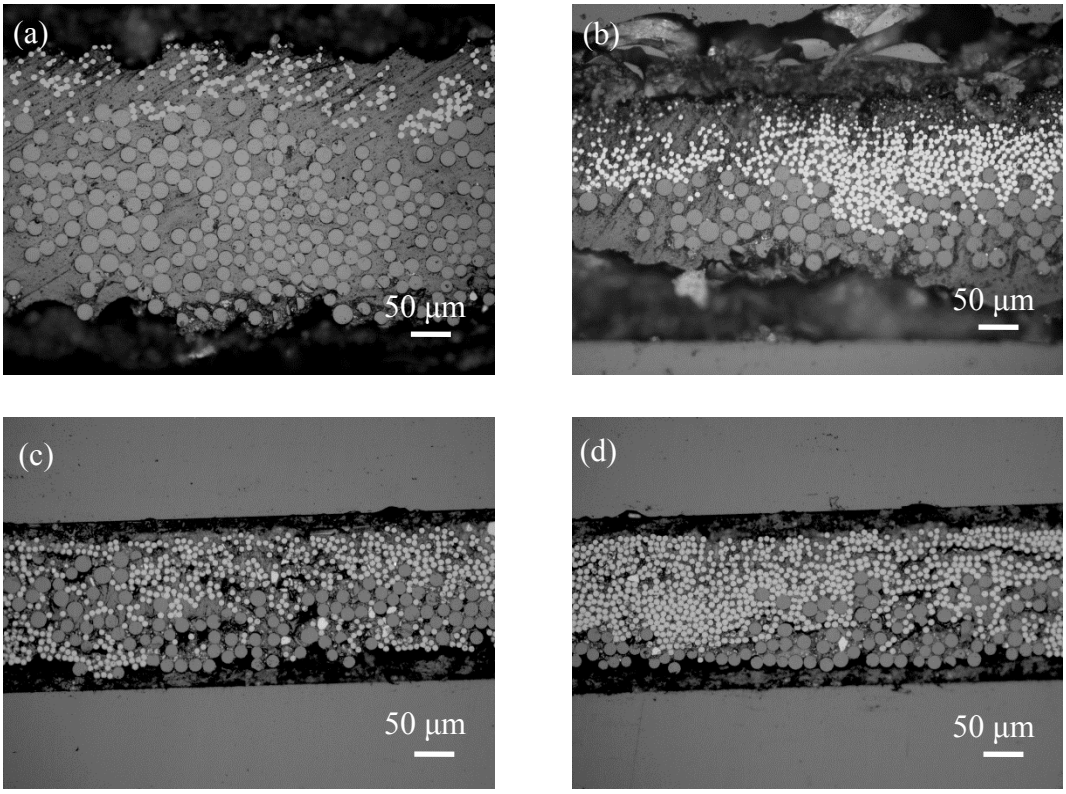


Figure 3.23 Characteristic optical micrographs of cross-sections of fibre hybrid tow A (a and b) and fibre hybrid tow B (c and d)

3.4.4 Tensile properties of carbon fibre/glass fibre reinforced epoxy composites

Fibre hybrid tow B containing commingled CF-B carbon fibre and GF-B glass fibre, having a higher degree of hybridisation, was selected for manufacturing carbon fibre/glass fibre reinforced epoxy hybrid composites. Figure 3.24 shows the typical tensile stress-strain curves of the control carbon fibre reinforced epoxy and glass fibre reinforced epoxy and hybrid composites. It is interesting to note that the hybrid composite failed more gradually than the control carbon fibre/epoxy. There are multiple drops in the tensile stress-strain curves of the hybrid composites. The ultimate failure strain of the hybrid composite was 14% higher than that of the control carbon/epoxy (Table 3.12). This improvement in ultimate failure strain and the difference in failure mode between hybrid composites and control carbon fibre/epoxy composite could be associated with the fact that glass fibre and carbon fibre were

partially commingled in hybrid composites with the degree of hybridisation of 32.45%. When some of the carbon fibres in the hybrid composite failed, the nearby glass fibres and remaining carbon fibres possibly cause the load redistribution and delayed crack propagation, which resulted in the more gradual failure of the hybrid composites. The possible damage development of this intermingled hybrid composite is that: a) carbon fibres fail when the tensile strain of the hybrid reaches their failure strain, which results in the first drop in the tensile stress-strain curve; then b) the glass fibres and remaining carbon fibres still carry the load and the nearby glass fibres delay the propagation of the crack initiated by failed carbon fibre, which causes the second increasing tendency in the stress-strain curve; finally c) more fibres fails in the hybrid as the tensile strain increases, which eventually causes the complete failure of hybrid composite. However, the stress concentration generated by the failure of carbon fibre resulted in the glass fibre in the hybrid composite failing earlier than in the pure glass fibre composite, so the ultimate failure strain of hybrid composite is lower than that of control glass fibre composite.

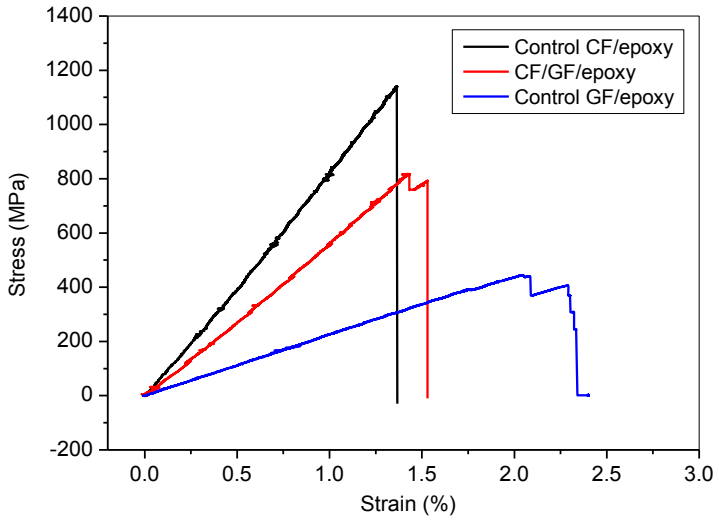


Figure 3.24 Typical tensile stress-strain curves of control carbon fibre/epoxy, carbon fibre/glass fibre/epoxy and control glass fibre/epoxy (V_f =30-40%, V_{CF}:V_{GF} = 1.55:1)

The tensile modulus of the hybrid composite (51.7 GPa) is very close to that predicted by the rule of mixtures (53.4 GPa), which indicates that the rule of mixtures can be used as a guide to design commingled hybrid fibre composites with required tensile stiffness by carefully selecting the volume ratio between carbon fibre and glass fibre. However, the tensile strength, strain to failure and failure mode of the hybrid composite cannot be easily predicted by the rule of mixtures, because the degree of hybridisation in the composite affects the load distribution after the fibres with smaller strain to failure fail. Very recently, Pimenta and Robinson [81] predicted that composites with a higher degree of hybridisation have a larger strain to failure than composites with lower degree of hybridisation even when these two composites have a same volume ratio between carbon fibre and glass fibre. The air-assisted spreading and commingling technology provides a potential manufacturing route to produce a carbon fibre/glass fibre hybrid composite with reasonable degree of hybridisation, which has a higher strain to failure and exhibits a more graceful failure mode than pure carbon fibre composites.

Table 3.12 Tensile strength, modulus, strain to initial and final failure of control CF/epoxy, CF/GF/epoxy and control GF/epoxy composites.

	Max stress (MPa)	Modulus (GPa)	Initial failure strain (%)	Ultimate failure strain (%)
CF/Epoxy	1055 ± 167	73.0 ± 8.8	1.34 ± 0.06	1.34 ± 0.06
CF/GF/Epoxy	719 ± 103	51.7 ± 5.0	1.33 ± 0.08	1.52 ± 0.05
GF/Epoxy	458 ± 14	22.9 ± 0.9	2.04 ± 0.11	2.34 ± 0.14

Note: V_F=30-40%, V_{CF}:V_{GF} = 1.55:1

3.5 Summary

Twelve different carbon fibres and 3 glass fibre tows were spread using the air-assisted fibre tow spreading technique. The "spreadability" of the fibre tows and stability of spread fibre tow width was characterised and the following fibres CF-B, GF-A and B were selected for hybridisation. Two types of unidirectional carbon fibre/glass fibre hybrid tows were successfully manufactured using air-assisted fibre

tow commingling. The degree of the hybridisation of carbon fibre/glass fibre tows was defined and determined by comparing the distribution of the fibres of a model of a hybrid tow containing randomly distributed two-fibre-types and the distribution of fibres of the manufactured hybrid tows, which was characterised by analysing optical micrographs of cross-section of hybrid tows using an image recognition program. The degree of hybridisation of type A fibre tow and type B fibre tow were 25.4% and 32.4%, respectively, which means that carbon fibres and glass fibres were partially hybridised at the filament level. The hybrid tow B containing CF-B carbon fibre and GF-A glass fibre with a higher degree of hybridisation was selected as the reinforcement to manufacture fibre reinforced epoxy hybrid composites by resin film infusion. Compared with the control carbon fibre/epoxy, the hybrid composite exhibited a more gradual tensile failure and 14% improvement in its ultimate failure strain. It indicates that the intermingled hybridisation of carbon fibre and glass fibre can enhance the ductility compared to that of the control UD CFRPs. However, the ultimate failure strain of the hybrid composite was lower than the failure strain of the control glass fibre composite due to the stress concentration caused by the failed carbon fibre.

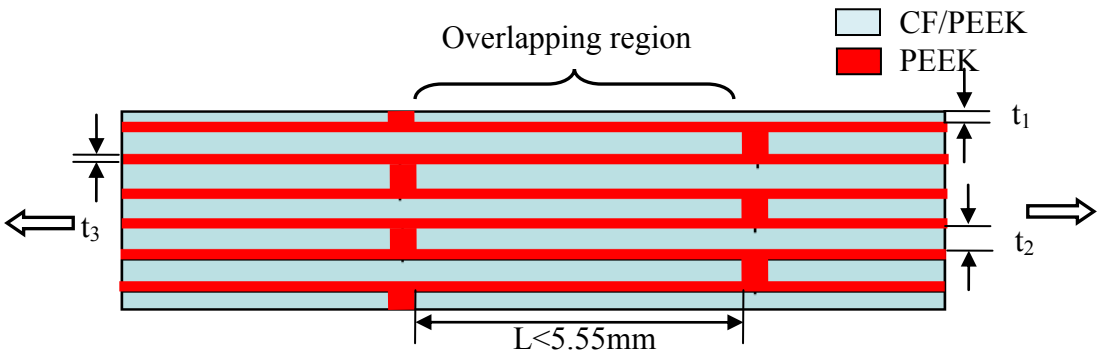
4 Ductile cut-ply interleaved carbon fibre/PEEK composites

4.1 Introduction

Two types of the most common materials which exhibit ductility are metals (such as steel and aluminium etc.) and polymer (such as polyethylene, polypropylene and polyether ether ketone etc.). Such materials can plastically deform in tension without fracture, but in mark contrast conventional continuous UD CFRPs deform elastically under tension in the fibre direction and fail suddenly without little warning and residual load-carrying capacity. The reason is that the longitudinal tensile behaviour is dominated by carbon fibre, which has a brittle tensile failure. As defined in section 1, the conventional continuous UD CFRPs have no ductility in fibre direction, which limits their application ranges. For instance, the UD CFRPs cannot be used as critical structural components in civil engineering.

One potential method of increasing the ductility of UD CFRPs is to add discontinuities to form a cut-ply UD carbon laminate (seen in Figure 4.1) though this may reduce the strength and stiffness. The cut-ply UD CFRP composite can exhibit ductility because of the shear response of the polymer matrix in the cut region and the shear deformation of the polymer matrix in the overlapping region between the cut layers. Recently, Pimenta and Robinson et al. [108, 109] proposed an analytical shear-lag model for composites with 'brick-and-mortar' architecture considering non-linear matrix response and failure. The model indicated that a ductile tensile response can be achieved by selection of a polymer matrix with suitable properties and by the careful design of the structure of the cut-ply composite (i.e. the length of overlapping region between two bricks, the thicknesses of the brick and mortar interlayer). In the research reported here, a cut-ply interleaved carbon fibre/PEEK composite (shown in Figure

4.1) was designed to achieve a ductile response. This composite was then manufactured and its tensile behaviour investigated.



Thickness of outer CF/PEEK layer (t_1) = thickness of CF/PEEK prepreg ($t_{CF/PEEK}$)= 150 μm, thickness of inter CF/PEEK layer (t_2) = 2×$t_{CF/PEEK}$ = 300 μm, thickness of PEEK layer (t_3) = 100 μm

Figure 4.1 Schematic diagram of cut-ply interleaved carbon fibre/PEEK composite

A significant challenge in this research is to create cut-ply interleaved carbon fibre/PEEK with an accurate internal structure as seen in Figure 4.1. Because PEEK is a thermoplastic material, the carbon fibre/PEEK is often manufactured via compression moulding method [100]. The solid PEEK in the prepreg and interleaved film is transformed into a very viscous liquid when it is heated up to its melting temperature. This may cause two effects: a) the melt from PEEK interleaved film can enter into carbon fibre/PEEK region, resulting in carbon fibre/PEEK layer with non-uniform fibre volume fraction; b) the melt could flow into the pre-cut region and so push the adjacent two carbon fibre/PEEK layers away from each other, which would decrease the accuracy of the pre-cut alignment in the through-thickness direction. The compression moulding process, therefore, has to be optimised to minimise these two effects.

In this research, the cut-ply interleaved carbon fibre/PEEK composite was designed based on strength and fracture energy criteria. Then, the effect of the various manufacturing parameters (the thickness of the PEEK film, the temperature and pressure used in the compression mould) on the internal structure of the resulting

composite were studied in small scale plates. After optimising the manufacturing method, the cut-ply interleaved carbon fibre/PEEK composite was manufactured at a larger scale. Specimens cut from the plate were tested in tension with a digital image correlation (DIC) camera measuring the strain over a range of the gauge lengths bridging the overlap zone between the cut layers. Finally, fracture surfaces of the cut-ply interleaved carbon fibre/PEEK composite were analysed using scanning electron microscopy (SEM).

4.2 Literature review

Previous researchers have studied cut-ply UD CFRP composite to a) improve formability of UD prepreg and decrease the difficulties in manufacturing composite structures with complex shapes [110-112]; b) avoid a single catastrophic failure of UD CFRP in a four-point bend test by replacing it with several smaller failures [113, 114]; c) study the failure mechanisms in tension of cut-ply UD CFRP with different structures [115-117], which is of particular relevance to the current research. In the early 2000s, Iarve and Kim [115, 116] developed a model to study the failure mechanism for UD discontinuous tow composite laminates (their structures are shown in Figure 4.2). They found that the failure strain of such a composite is mainly dominated by the strain to failure of the top and bottom UD discontinuous tow composite layers (contains multiple cuts in a single layer). The geometry (width, thickness and length) of the tow section had a significant effect on failure strain of this composite, but they did not report the stress-strain curves of their composites. Baucom et al. [117] also studied a tiled composite, which contained continuous carbon fibre in the outer layers and cut-ply CFRP (only one cut in each layer) in the middle layers. They found that the strength of such composite was influenced by the spacing distance between the resin pockets in the adjacent cut-ply layers.

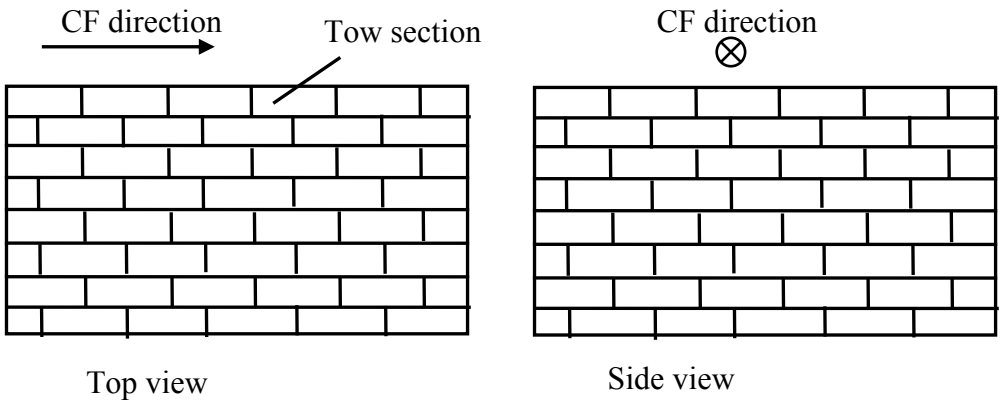


Figure 4.2 Schematic diagrams of UD discontinuous tow composite laminates [116]

However, these works do not specifically address the aim of the current research which is to assess the potential of a cut-ply UD composite to exhibit ductility experimentally. The thermoplastic polymer matrix, PEEK, is used in this research rather than the thermosetting matrix, epoxy, in the previous published works [110-117]. Compared with epoxy, the PEEK is a more ductile polymer, which exhibits a non-linear tensile stress-strain response. The ductility of the PEEK interleaf layers is key to achieving ductility in the cut-ply interleaved carbon fibre/PEEK composite.

4.3 Materials and method

4.3.1 Materials

Carbon fibre/PEEK composite prepreg with a thickness of 150 μm (APC-2, VF = 53.9% measured by reflective microscopy with the magnification of 20 x) and PEEK films with thicknesses of 100 μm and 50 μm (APTIV ® 1000-100G and 1000-050G, supplied by Victrex Plc., UK) were used to manufacture cut-ply interleaved carbon fibre/PEEK composites.

Table 4.1 Properties of carbon fibre/PEEK prepreg and PEEK [7, 118]

Melting point of PEEK (°C) [118]	Thickness of CF/PEEK prepreg, $t_{CF/PEEK}$ (mm)	0° tensile properties of CF/PEEK [7]		Mode II fracture toughness of CF/PEEK, G_{IIc} (kJ/m^2) [7]	Shear strength of PEEK, $\hat{\tau}_{PEEK}$ (MPa) [118]
		Modulus, $E_{CF/PEEK}$ (GPa)	Strength, $\hat{\sigma}_{CF/PEEK}$ (MPa)		
346	0.15	138 *	2070 *	2	50.3

*Note: Values listed above are typical for the composite with a V_F of 60%. The actual V_F in the carbon fibre/PEEK prepreg used in this research is 53.9%, so $E_{CF/PEEK}$ and $\hat{\sigma}_{CF/PEEK}$ are corrected to 124 GPa and 1860 MPa, respectively.

4.3.2 Cut-ply interleaved carbon fibre/PEEK design

Since it is shearing of the PEEK interleaf that will result in ductility, it is important to ensure that shear failure of the PEEK interleaf occurs before tensile failure of the whole laminate. Assuming that shear failure is due to yielding, and using the configuration shown in Figure 4.1, then the shear failure can be ensured if the overlap length L satisfies Equation 4.1(its derivation is attached in Appendix III) ,

$$L < \frac{\hat{\sigma}_{cut-ply} \times t_{total}}{\hat{\tau}_{PEEK} \times n_{PEEK}} \qquad \text{Equation 4.1}$$

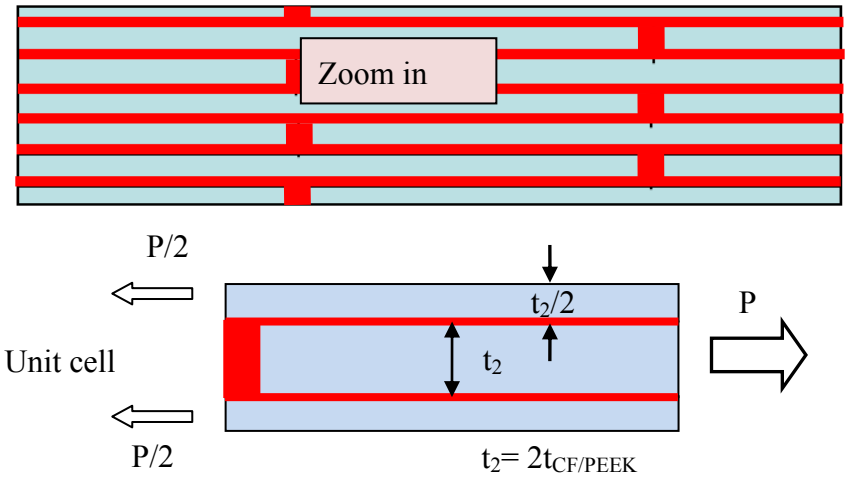
where $\hat{\sigma}_{cut-ply}$ is the tensile strength of the cut-ply interleaved carbon fibre/PEEK assuming no shear failure of the PEEK interleaf, t_{total} the thickness of the composite , $\hat{\tau}_{PEEK}$ the shear strength of PEEK and n_{PEEK} is number of PEEK interleaves in the composite. Assuming the tensile load carried by the PEEK interleaf is negligible, then $\hat{\sigma}_{cut-ply}$ can be referred to the tensile strength of carbon fibre/PEEK by Equation 4.2,

$$\hat{\sigma}_{cut-ply} \times t_{total} = \hat{\sigma}_{CF/PEEK} / 2 \times n_{PEEK} \times n'_{CF/PEEK} \times t_{CF/PEEK} \qquad \text{Equation 4.2}$$

where $n'_{CF/PEEK}$ is the number of carbon fibre/PEEK prepregs in the inter CF/PEEK layer, $\hat{\sigma}_{CF/PEEK}$ and $t_{CF/PEEK}$ are the tensile strength and the thickness of continuous unidirectional carbon fibre/PEEK prepreg. By substituting Equation 4.2 into Equation

4.1, the critical overlapping length between carbon fibre/PEEK layers ($L_{critical}$) can be obtained via Equation 4.3,

$$L_{critical} \leq \frac{\hat{\sigma}_{CF/PEEK} \times t_{CF/PEEK}}{\hat{\tau}_{PEEK}} \qquad \text{Equation 4.3}$$



w is the width of specimen, which is in the through-plane direction

Figure 4.3 Analysis of the unit cell in the cut-ply interleaved carbon fibre/PEEK composite

To ensure delamination growth does not occur prior to failure, the elastic strain energy release rate when the interleaved composite fails should be less than the critical mode-II fracture toughness ($G_{II,c}$) of UD carbon fibre/PEEK composite. The mechanical response of the entire composite can be analysed through the unit cell shown in Figure 4.3. The elastic strain energy release rate (G) of this unit cell is determined by Equation 4.4,

$$G = \frac{1}{2w}\left[\frac{2 \times (P/2)^2}{2E_{CF/PEEK} w \times t_2/2} - \frac{P^2}{2E_{CF/PEEK} \times 2t_2 w}\right] < G_{II,c} \qquad \text{Equation 4.4}$$

where $E_{CF/PEEK}$ is the tensile modulus of UD carbon fibre/PEEK composite, w the width of specimen and P the load applied on this unit cell. P can be determined by Equation 4.5.

$$P/2 = \hat{\sigma}_{CF/PEEK} \times t_2/2 \times w \qquad \text{Equation 4.5}$$

By substituting Equation 4.5 into Equation 4.4, the critical thickness of carbon fibre/PEEK prepreg ($t_{CF/PEEK,critical}$), below which delamination will not occur, can be obtained via Equation 4.6,

$$t_{CF/PEEK,critial} = \frac{4 \times E_{CF/PEEK} \times G_{IIc}}{\hat{\sigma}^2_{CF/PEEK}} \qquad \text{Equation 4.6}$$

According to the properties shown in Table 4.1, the $L_{critical}$ and $t_{CF/PEEK,critical}$ are 5.55 mm and 0.286 mm respectively. Considering the tolerances involved in cutting and laying-up the carbon fibre/PEEK prepregs, the designed overlapping length between carbon fibre/PEEK layers was set as 4 mm. The carbon fibre/PEEK prepreg used in this research has a thickness of 0.15 mm, which is less than the critical thickness of the prepreg.

4.3.3 Manufacturing method of cut-ply interleaved carbon fibre/PEEK

As stated in section 4.1, the key challenge in this research is to avoid or minimise PEEK melt from the interleaved film entering the carbon fibre/PEEK and the cut region, so the product can have a distinct interleaved polymer region and a well-controlled carbon fibre/PEEK region, as seen in Figure 4.1. In order to meet this challenge, the interleaved samples were initially produced at small-scale to optimise the manufacture process. This process was then scaled up to produce cut-ply interleaved carbon fibre/PEEK composite panel from which tensile specimen could be prepared.

4.3.3.1 Optimisation of compression moulding process

a) Small-scale interleaved carbon fibre/PEEK manufacturing

The carbon fibre/PEEK prepregs (C) and PEEK films (P) were cut to 150 mm x10 mm and laid up in the sequence of $[C/(P/C_2)_2P/C]_s$ in stainless steel mould (as seen in Figure 4.4) covered with mould release film (Upilex® 25S, UBE Industries Ltd.,

Tokyo, Japan). The assembly was then put in a hot pressing machine (Model #4126, Carver Inc., Indiana, USA). The processing consists of three steps:

- pre-heating (step A): the laminate was pre-heated at a temperature of magnitude Temp A for 15 mins without applying pressure;
- hot pressing (step B): pressure of magnitude Pres B was applied to the laminate for 8 mins;
- consolidation (step C): the laminate was finally consolidated at a temperature of Temp C and pressure of Pres C for 10 mins.



Figure 4.4 Photo of the mould for manufacturing small-scale interleaved carbon fibre/PEEK composite

In order to determine the satisfactory manufacturing parameters, various combination of the thickness of PEEK film, temperature and pressure, as shown in Table 4.2, were used in compression moulding to manufacture the small-scale interleaved carbon fibre/PEEK composite. The effect of the thickness of PEEK film, the temperature and pressure in compression moulding will be discussed in section 4.4.1.

Table 4.2 Manufacturing parameters of compression moulding of small-scale interleaved carbon fibre/PEEK composite

Sample	Thickness of PEEK film (μm)	Pre-heating (step A)	Hot pressing (step B)	Consolidation (step C)	
		Temp A (°C)	Pres B (MPa)	Temp C (°C)	Pres C (MPa)
S-1	100	400	1.3	200	1.6
S-2	100	400	0.65	200	0.78
S-3	100	360	1.3	180	1.6
S-4	100	360	0.65	180	0.78
S-5	50	400	1.3	200	1.6

S-6	50	400	0.65	200	0.78
S-7	50	360	1.3	180	1.6
S-8	50	360	0.65	180	0.78

b) Microscopy analysis on the small-scale interleaved carbon fibre/PEEK composite

In order to assess the quality of the small-scale interleaved carbon fibre/PEEK composite, the thicknesses of PEEK layers between carbon fibre/PEEK regions were measured at 20 locations in each of five microscopy images (at 5x magnification) of the longitudinal section of interleaved carbon fibre/PEEK composite.

4.3.3.2 Cut-ply interleaved CF/PEEK composite panel manufacturing

After optimising the compression moulding process by manufacturing the small-scale interleaved carbon fibre/PEEK composite, the dimensions of the composite sample were increased up to 150 mm x 150 mm. In order to create the cut-ply interleaved carbon fibre/PEEK composite with an accurate internal structure (as shown in Figure 4.1), it is important that: a) the locations of the cut in alternate carbon fibre/PEEK layers should be same; and b) the cut-ply carbon fibre/PEEK layers do not move in the mould. The mould, therefore, was carefully designed as shown in Figure 4.5. This mould was used not only during the compression moulding of the composite but also during the lay-up and cutting process. One dowel was located near each of the four corners of the mould to help ensure that each layer of carbon fibre/PEEK would not move during the lay-up and cutting processes. Two alternative cutting templates were designed (shown in Figure 4.6) to help position the cut in each carbon fibre/PEEK layer according to Figure 4.1 with an intended overlap of 4.5 mm. Specimens were manufactured using both templates and the structures of these specimens were examined to establish which cutting template was more effective.

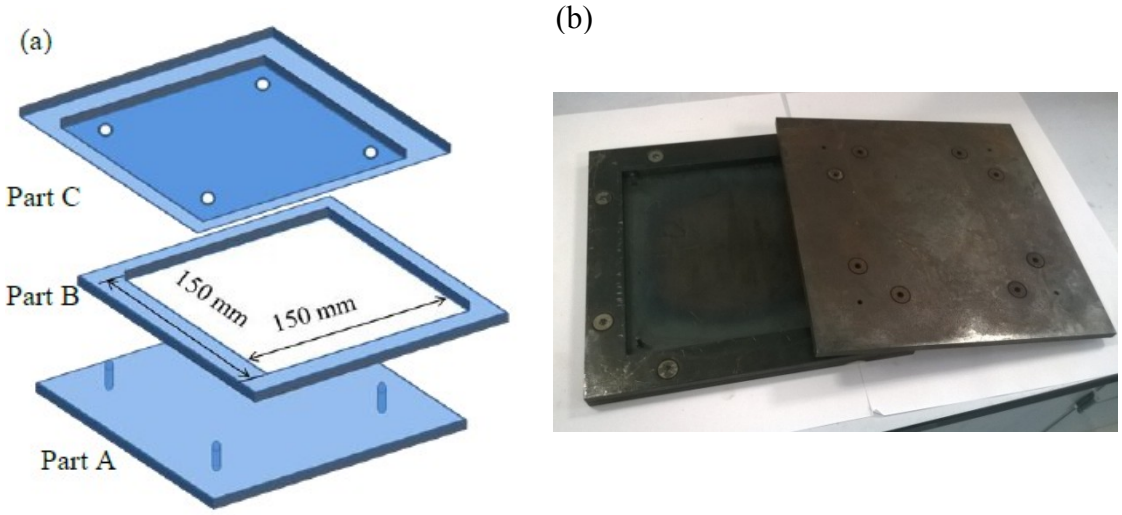


Figure 4.5 (a) Schematic diagram and (b) photo of the mould for manufacturing large-scale cut-ply interleaved carbon fibre/PEEK composite

The steps of the cutting and lay-up processes for making cut-ply interleaved carbon fibre/PEEK composite were as follows:

1. All the prepregs and PEEK films were cut into 150 mm x 150 mm by a scalpel and punched at the corners by a hole-puncher with the aid of the cutting templates.

2. The prepreg was put into the mould Part A which was previously covered with mould release film (Upilex® 25S, UBE Industries Ltd., Tokyo, Japan). Then the discontinuous cutting pattern was created with a scalpel by cutting through the slot (as shown in Figure 4.6) in the cutting template.

3. The cutting template was removed from the mould Part A. The prepreg in the mould was cleaned by air duster to remove any residual debris from the cut.

4. Another prepreg was put into the mould Part A and cut in the same way stated in step 2. Before cutting, a thick cardboard layer was put between the two prepreg plies to avoid cutting the prepreg below and this was removed after cutting. The carbon fibre/PEEK prepregs and PEEK films were laid up in the sequence of $[C/(P/C_2)_2P/C]_s$.

5. Mould Part B and Part C were assembled with mould Part A.

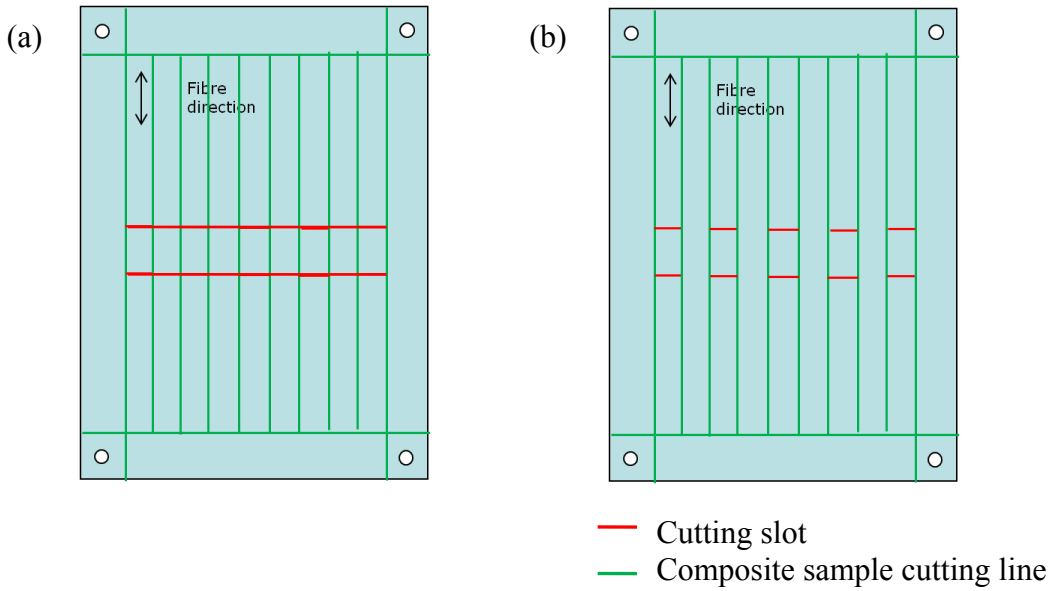


Figure 4.6 Schematic diagrams of cutting template (a) A and (b) B

As discussed in section 4.4.1.1, the manufacturing parameters determined in the small-scale fabrication trials were used to make the large-scale cut-ply interleaved carbon fibre/PEEK composite panels. The mould, complete with prepregs and polymer films, was pre-heated at the temperature of 360 °C for 15 mins, then subjected to a pressure of 0.65 MPa for 8 mins and finally consolidated at the temperature of 180 °C and a pressure 0.78 MPa for 10 minutes. The composite panel was taken from the mould after it was cooled down to room temperature. The panel was cut into 8 mm x 120 mm specimens by a disc saw (DIADISC-5200, Mutronic GmbH & Co, Germany). The structures of these specimens were examined by a reflective microscope to assess which cutting template gave the composite a more accurate cut-ply interleaved structure. The tensile properties of the composite made via the more effective optimal cutting template were then tested in tension.

4.3.4 Tensile test method of cut-ply interleaved carbon fibre/PEEK

Both side edges of the cut-ply interleaved carbon fibre/PEEK samples (dimension: 8 mm x 2.4 mm x120 mm) were polished using SiC paper (CarbiMet®-S-P320 and

P1200, Buehler Ltd., Düsseldorf, Germany) and then painted to create a black-white speckle pattern. The samples were tested under a uniaxial tensile load (Model 5969, Instron Ltd, Bucks, UK) at a crosshead speed of 0.1mm/min. The strain on both edges of each sample was measured by two 2D digital image correlation (DIC) cameras (ARAMIS ®, GOM UK Ltd., Coventry, UK). The distance between the grips was 20 mm. Gauge lengths of 6, 8, 10, 12 mm (as shown in Figure 4.7 (a)) were used in the DIC strain-measuring program to evaluate the effect of gauge length on the strain to failure and tensile modulus of the composite. The tensile test setup is shown in Figure 4.7(b).

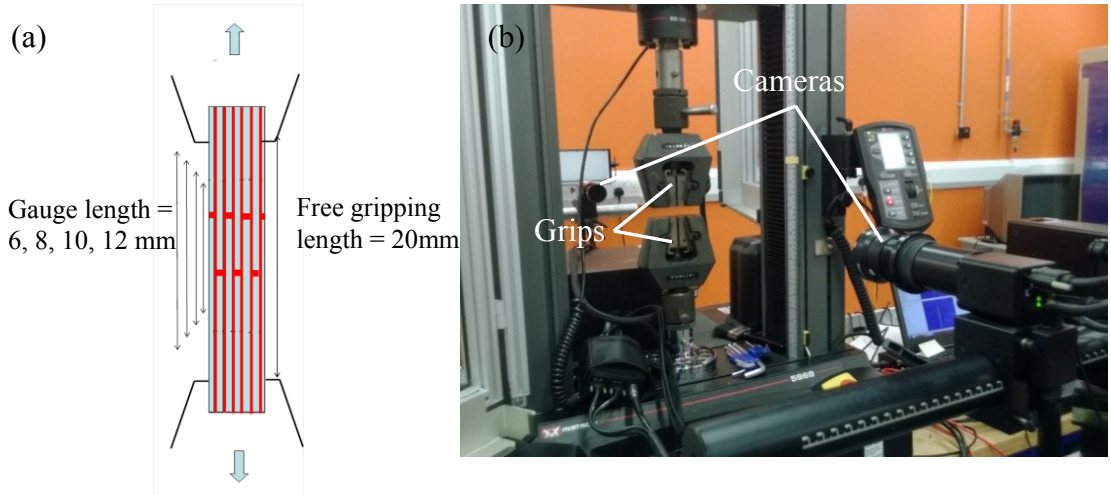


Figure 4.7 (a) Schematic diagram from the side view and (b) photo of the tensile test setup

The tensile modulus is the slope of the best-fit straight line of the stress-strain curve in the strain interval from 0.1% to 0.25%. The yield stress (σ_y) and yield strain (ε_y) are the stress and strain at the "yield" point (marked as the blue point in Figure 4.8). It is found by drawing a parallel line to the linear-fitting line of the initial stress-strain curve, but offset by a strain of 0.1%. The point of intersection between the tensile stress-strain curve and the offset parallel line is defined as the "yield" point. Ductile strain (ε_d) is calculated based on the definition of the ductility of material [9-11]

shown in Figure 4.8, which is the difference between the strain to failure (ε_u) and the strain at a stress equal to 95% of tensile strength based on the initial modulus.

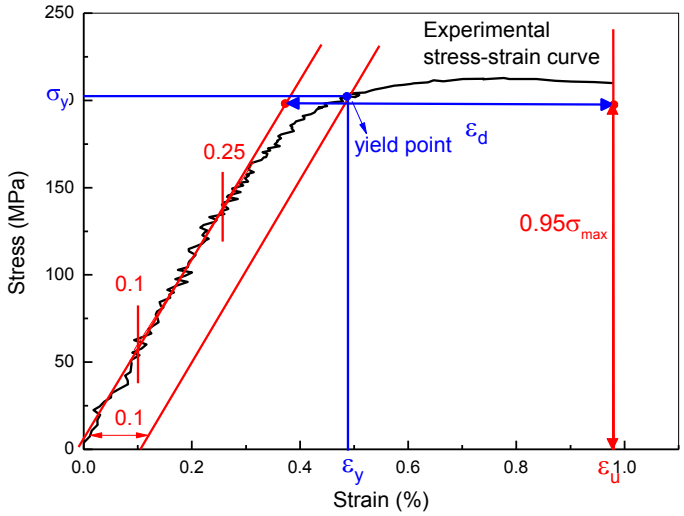


Figure 4.8 Definition of initial modulus, σ_y, ε_y, ε_u and ε_d

4.3.5 Fractography

The fracture surface of the specimen (schematic in Figure 4.9) was gold sputtered then observed by a scanning electron microscope (S-3700N, Hitachi High-Technology Co., Japan) at the magnification of 1000x and 1600x with an acceleration voltage of 5 kV.



Figure 4.9 Schematic diagram of fracture surface of cut-ply interleaved carbon fibre/PEEK

4.4 Results and discussion

4.4.1 The micro-structure of cut-ply interleaved carbon fibre/PEEK composite

4.4.1.1 The effect of manufacturing parameters on the micro-structure of small-scale interleaved carbon fibre/PEEK composite

Figure 4.10 shows the thicknesses of the PEEK region between the carbon fibre/PEEK regions in the composite fabricated via the various manufacturing parameters shown in Table 4.2. Compared with the original thickness of PEEK film, the thickness of the PEEK interleaf region in all the samples was reduced after compression moulding. For the composite made from the PEEK film with an initial thickness of 50 μm, the PEEK interleaf thickness was reduced to 30 μm, causing the boundaries between interleaved PEEK regions and carbon fibre/PEEK regions to become indistinct as shown in Figure 4.11 (a). These indistinct boundaries and very thin polymer regions could possibly cause non-uniform shear load transfer between carbon fibre/PEEK regions and lead to a premature failure of the composite. On the other hand, the composite made from the PEEK film with a thickness of 100 μm had a distinct boundary between PEEK interleaf region and carbon fibre/PEEK region, seen in Figure 4.11 (b). The PEEK film with the thickness of 100 μm, therefore, was selected to manufacture large-scale cut-ply interleaved carbon fibre/PEEK composite panels.

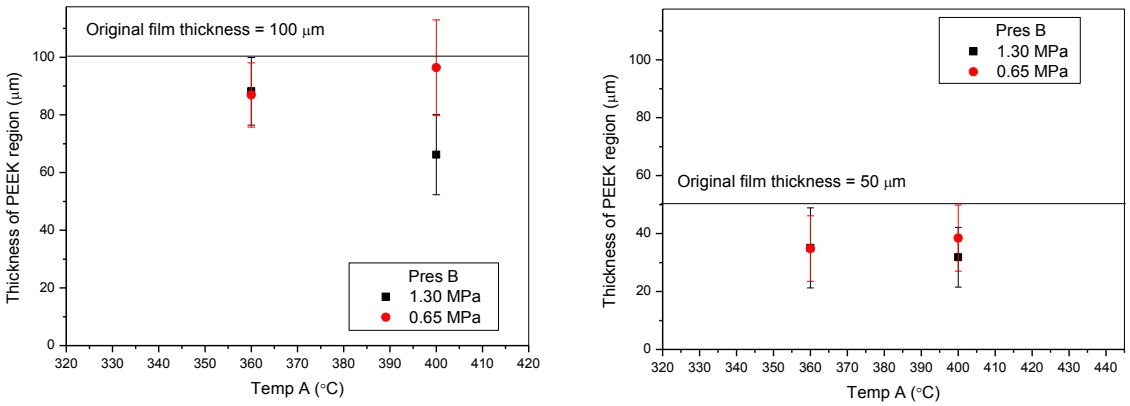


Figure 4.10 The thicknesses of PEEK region in small-scale interleaved carbon fibre/PEEK composites manufactured from the PEEK films with the thicknesses of (a) 100 μm and (b) 50 μm via various temperature and pressure used in compression moulding

When the temperature of step A and B (Temp A) in compression moulding was 400 °C, the thickness of PEEK region fabricated under 1.3 MPa (Pres B) was 35% less (for the composite made from 100-μm-thick PEEK film) and 25% less (for the composite made from 50-μm-thick PEEK film) than those manufactured under 0.65 MPa. However, when Temp A was 360 °C, the thickness of the PEEK region was almost the same for these two pressures. This possibly means that liquid PEEK melt predominately remained in its original location at 360 °C. Also, the thickness of the PEEK region in the composite manufactured under a pressure of 0.65 MPa was less variable than that manufactured under 1.3 MPa. This suggests that the lower pressure allows the PEEK melt in the interleaf region and in the carbon fibre region to move more evenly. Considering these two factors, 360 °C and 0.65 MPa were selected as the optimal Temp A and Pres B to be used in compression moulding. As seen in Figure 4.11(b), the interleaved carbon fibre/PEEK composite manufactured under such parameters has a distinct PEEK interleaf region with an average thickness of 86 μm and no obvious voids.

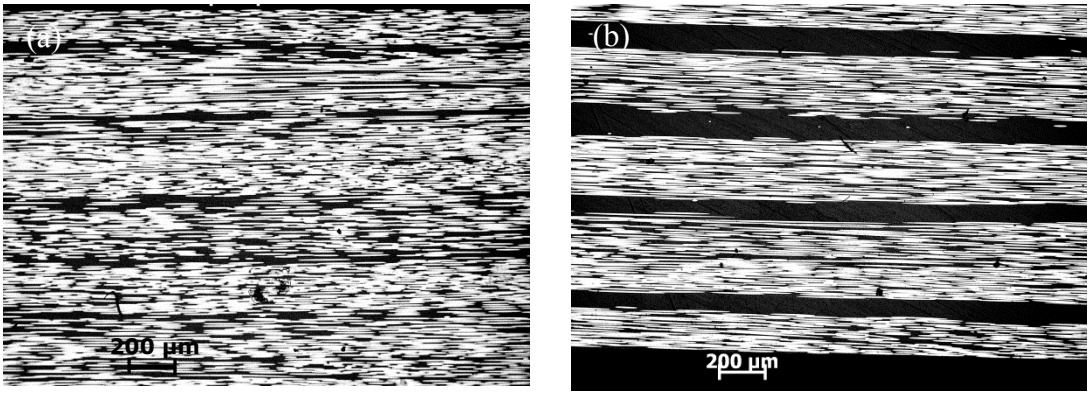


Figure 4.11 The micrographs of small-scale interleaved carbon fibre/PEEK composites made from (a) 50-µm-thick PEEK film (sample: S-8)and (b) 100-µm-thick PEEK film (sample :S-4)

4.4.1.2 The effect of cutting template on the micro-structure of large-scale cut-ply interleaved carbon fibre/PEEK composite

Figure 4.12 shows the micro-structures of the large-scale cut-ply interleaved carbon fibre/PEEK composite obtained using the two different cutting templates. When using cutting template A, all the carbon fibre/PEEK layers in the interleaved composite were dislocated after the compression moulding, as seen in Figure 4.12(a). The length of PEEK pocket in the cut region was 8-9 mm, which was even larger than the carbon fibre/PEEK layer overlapping length of 4.5 mm. It was possibly due to the fact that the cutting template A had a 120-mm-long cut, which allowed the carbon fibre/PEEK layers near the cut region to be easily pushed away from each other by the melt PEEK pocket. On the other hand, using cutting template B with the discontinuous cut (shown in Figure 4.6(b)) significantly improved the micro-structure of cut-ply interleaved carbon fibre/PEEK composite, as seen in Figure 4.12(b), so the composite obtained via using cutting template B was selected in the further investigation.

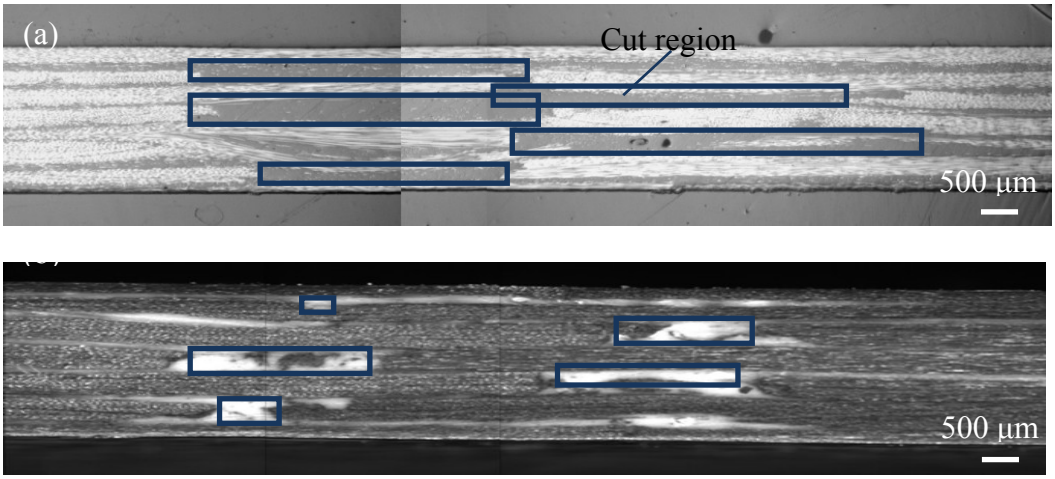


Figure 4.12 The micro-structure of the large-scale cut-ply interleaved carbon fibre/PEEK composites obtained using cutting templates (a) A and (b) B

4.4.1.3 Comparison of the micro-structure of the manufactured cut-ply interleaved carbon fibre/PEEK composite with the designed structure

As seen in Table 4.3, the thicknesses of the carbon fibre/PEEK layer and PEEK layer in the cut-ply interleaved carbon fibre/PEEK composites were 288 ± 31 and 87 ± 11 µm respectively, which were less than the thicknesses of the as-received carbon fibre/PEEK prepreg (300 µm) and the PEEK film (100 µm). These thickness losses were probably caused by the polymer melt flow during the compression moulding. In particular, some PEEK melt from the PEEK film and the carbon fibre/PEEK prepreg flowed to the cut region and formed a polymer pocket, as seen in Figure 4.13. Furthermore, the overlaps between the carbon fibre/PEEK lengths were less than the intended value of 4.5 mm achieved in the lay-up process, indicating that the carbon fibre/PEEK layers were possibly pushed away by the PEEK pocket. Due to the variation of the micro-structure of manufactured carbon fibre/PEEK compared with the design structure, the actual dimensions of the micro-structure of cut-ply interleaved carbon fibre/PEEK (shown in Table 4.3) were used to analysis its tensile behaviour.

Table 4.3 The micro-structure of cut-ply interleaved carbon fibre/PEEK (produced by cutting templates and measured in the micrographs)

Thickness of the carbon fibre/PEEK layer (μm)	288 ± 31
Thickness of the PEEK layer (μm)	87 ± 11
Overlapping length between the carbon fibre/PEEK (μm)	2241 ± 752
Length of the PEEK pocket (μm)	1530 ± 781

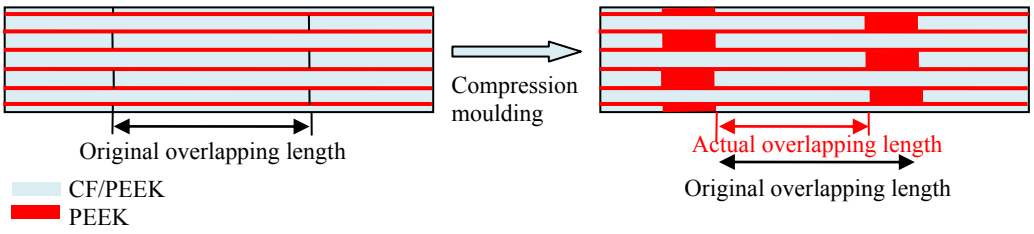


Figure 4.13 The schematic diagram of micro-structural changes in cut-ply interleaved carbon fibre/PEEK composite caused by compression moulding

4.4.2 Tensile behaviour of cut-ply interleaved carbon fibre/PEEK composite

Table 4.4 shows the tensile properties of cut-ply interleaved carbon fibre/PEEK composite. As seen in Figure 4.14, there is a non-linear relationship between the tensile stress and strain of the cut-ply interleaved carbon fibre/PEEK composites. At the initial stage of tensile testing, the stress in the specimen was linearly increased with increasing strain. After the tensile strain reached the 0.45-0.50%, the slope of the stress-strain plot gradually reduced. During this stage, no obvious damage or cracking was observed in the tested specimen. When the tensile strain was ~0.85%, the complete composite failure occurred, which resulted in a crack along the PEEK interleaves and pockets.

Table 4.4 The tensile properties of cut-ply interleaved carbon fibre/PEEK composite

Strength (σ, MPa)	230 ± 22
Initial Modulus (E, GPa)	47.6± 5.5
Strain to failure (ε_f, %)	0.84 ± 0.25
"Yield" stress (σ_y, MPa)	215 ± 23
"Yield" strain (ε_y, %)	0.50 ± 0.09
Ductile strain (ε_d, %)	0.40 ± 0.23

Note: the strain recorded in this table was measured at the gauge length of 10 mm.

The non-linearity of the shear behaviour of PEEK interleaf layers caused the non-linear tensile stress-strain behaviour of the entire composite. Assuming that complete

composite failure occurred when the shear stress in the interleaved PEEK region exceeded the shear strength of the PEEK, then the average shear strength of the interleaved PEEK ($\hat{\tau}$) is calculated by Equation 4.7,

$$\hat{\tau} = \frac{F_{\max}}{w \times L \times n_{PEEK}} = \frac{\hat{\sigma} \times t}{L \times n_{PEEK}} \qquad \text{Equation 4.7}$$

where F_{max} is the maximum tensile load applied to the specimen, n_{PEEK} is the number of PEEK interleaves in the specimen, $\hat{\sigma}$ is the tensile strength of the cut-ply interleaved carbon fibre/PEEK, L in the average overlapping length between carbon fibre/PEEK layers, w and t are the width and thickness of the specimen. Using Equation 4.7, the measured shear strength of PEEK, 40.7 ± 4.8 MPa, which is less than the value of 50.3 MPa reported by the manufacturer of the PEEK film (Victrex Plc., UK) [7]. This may be due to: a) there is a shear stress concentration zone near the cut region, which means that the local shear stress in the cut region when the complete composite failure occurred was higher than the measured average shear strength of PEEK; b) the shear strength of PEEK is affected by its degree of crystallinity, which is influenced by heating/cooling history in the compression moulding process.

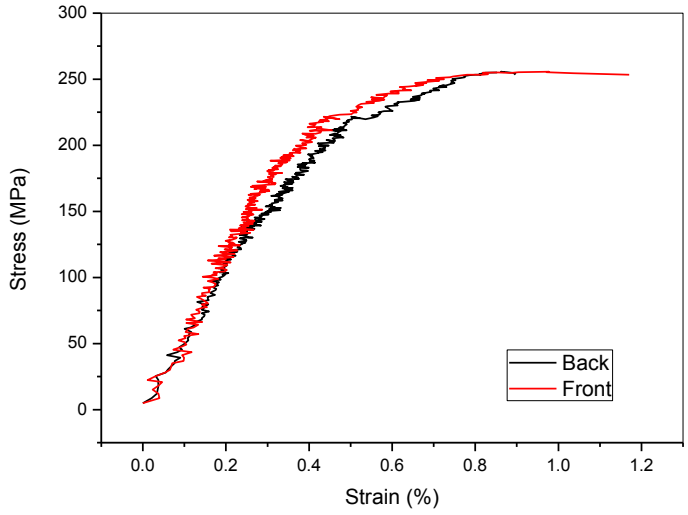


Figure 4.14 The typical tensile stress-strain curves measured from the front and back view at the gauge length of 10 mm

Figure 4.14 shows the typical tensile stress-strain curves measured from the front and back view. At the initial stage of the tensile testing, the two curves are almost identical, indicating that the initial tensile modulus of such composite obtained via measuring the strain changes from the front and back views are the same. However, the strains to failure of the cut-ply interleaved carbon fibre/PEEK composite measured from the front (1.17%) and back (0.90%) views have a 30 % difference. The main possible reason is that the micro-structures of this specimen observed from the front and back views are not exactly the same, as seen in Figure 4.15. Such difference in the micro-structures from the front and back causes the different displacement as the carbon fibre/PEEK layers pull out from the nearby interleaf PEEK layers, which in turn affects the strain changes measured from the front and back view. However, it is promising to see that the specimen measured from the both views had a ductile behaviour.

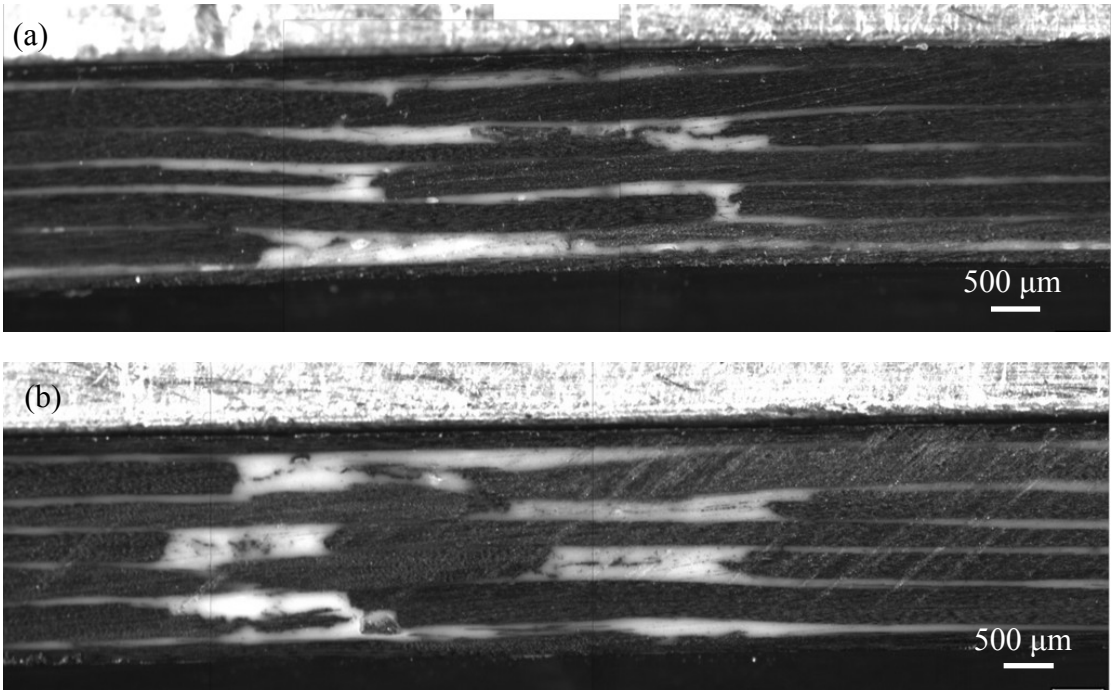


Figure 4.15 The micrographs of a cut-ply interleaved carbon fibre/PEEK composite observed from the (a) front and (b) back views

The gauge length also affects the strain to failure of the composite. As seen in Figure 4.16, the strain to failure decreased with increasing gauge length and the modulus

increased. This indicates that the strain change along the gauge length is not uniform. For a short gauge length, the majority of the strain change is produced by shear strain of the interleaf PEEK layer in the overlapping region. As the gauge length is increased, the significance of the strain in the overlapping region is reduced in comparison to the overall strain in the gauge length.

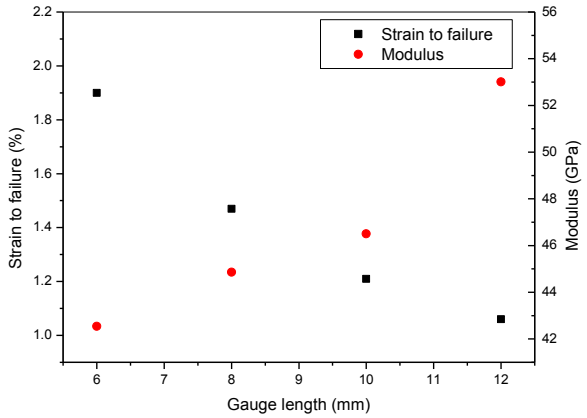


Figure 4.16 A typical plot of the effect of the gauge length on the strain to failure and modulus of the cut-ply interleaved carbon fibre/PEEK composite

This effect can also be seen in Figure 4.17 which shows that the non-linear region in the tensile stress-strain curve becomes smaller as the gauge length is increased. This suggests that the gauge length should be equal to the overlapping length between carbon fibre/PEEK layers in the ideal case to obtain the maximum ductile strain. In these experiments it was not possible to reduce the gauge length to the overlap size due to the limitation of the DIC camera.

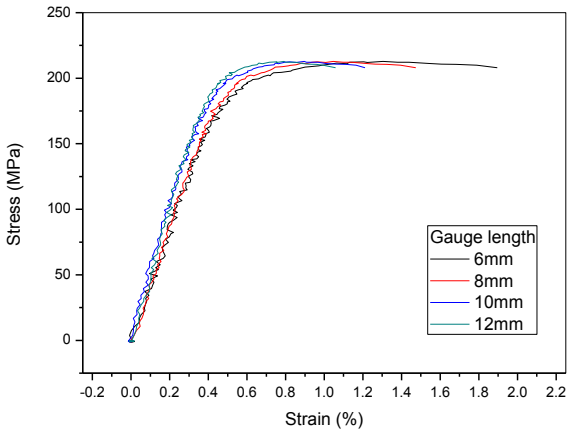


Figure 4.17 The typical tensile stress-strain curves of cut-ply interleaved carbon fibre/PEEK composite at the gauge length of 6,8 10 and 12mm

4.4.3 Fractographic analysis of the cut-ply interleaved carbon fibre/PEEK composite

Fractographic analysis of the cut-ply interleaved carbon fibre/PEEK composite confirms that the shear fracture occurred in the PEEK interleaf region, as seen in Figure 4.18. The likely failure mechanism is: a) the PEEK in the interleaved region was plastically deformed and then cracked in shear; b) then the PEEK was smeared by abrasion during the subsequent relative movement of the fracture surfaces. The PEEK fracture surface (shown in Figure 4.18) exhibits edges overlapping like fish scales from right bottom of the image to the left top, which indicates the direction of the shear loading (which is aligned with the global shear direction). Similar fracture surfaces of PEEK were reported by Purslow in 1988 [119].

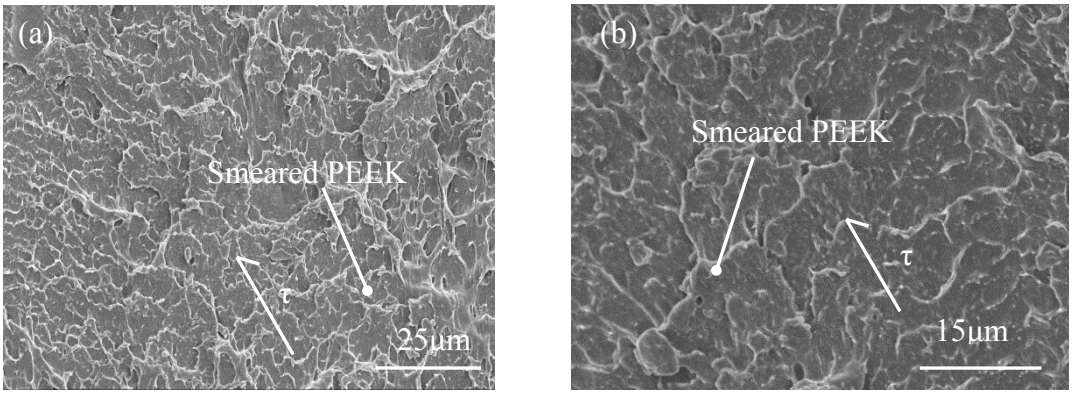


Figure 4.18 The SEM images of PEEK fracture surface of cut-ply interleaved carbon fibre/PEEK composite at the magnifications of (a) 1000 x and (b) 1600 x

4.5 Summary

In order to manufacture a cut-ply interleaved carbon fibre/PEEK composite, small-scale compression moulding trials were conducted at a range of temperatures and pressures with PEEK films of various thicknesses. By evaluating the thickness of the interleaved PEEK layer in the small-scale samples, optimised compression moulding parameters were obtained. A manufacturing method involving the optimised compression moulding and a novel cutting and layup design was developed for

making a larger scale cut-ply interleaved carbon fibre/PEEK composite panel. By measuring the longitudinal strain on both edges of the cut-ply interleaved carbon fibre/PEEK composite during tensile testing, it was found that there was a softening non-linear relationship between the tensile stress and strain for this type of the composite i.e. the composite exhibits ductility. The ductility of this composite is provided by the shear yielding of the interleaved PEEK region between the carbon fibre/PEEK layers. SEM inspection confirmed that abrasive PEEK shear failure characteristics could be observed on the fracture surface of the cut-ply interleaved carbon fibre/PEEK composite.

5 Conclusions and future work

5.1 Summary of findings

In the present investigation, three approaches were explored to create UD CFRP composites with enhanced ductility. The findings described in this thesis provide a better understanding of the mechanisms that can be used to introduce a more graceful, gradual failure in UD CFRP composites subjected to uniaxial tension load in fibre direction. The main findings and achievements from three research packages are summarized below.

5.1.1 Introducing fibre waviness into UD composites

Two manufacturing methods, gas-texturing and non-constrained annealing, were used to introduce fibre waviness into continuous UD carbon fibre/PA-12 composites. The fibre alignment angle and tensile behaviour of the manufactured composite tapes and the unmodified control samples were characterised. The findings are listed below.

- The width of Gaussian distribution of fibre alignment angle in carbon fibre/PA-12 tapes was increased by gas-texturing and non-constrained annealing methods and inferred that fibre waviness had been successfully introduced.
- The fibre waviness resulted in a more gradual tensile failure mode of the composites under uniaxial tension rather than the single, catastrophic failure, which was observed for the control samples.
- Ultimate tensile failure strain of carbon fibre/PA-12 was increased by non-constrained annealing in comparison to the control sample. This increase was caused by fibre waviness in the composite, but there was no improvement in failure strain of gas-textured carbon fibre/PA-12 due to the damage of the carbon fibre caused by gas-texturing process.

5.1.2 Intermingled UD carbon fibre/glass fibre hybrid composites

Twelve types of carbon fibre tows and 3 types of glass fibre tows were spread via an air-assisted fibre tow spreading technique. After assessing their "spreadabilty" and the stability of the width of spread fibre tows, the carbon fibre tow with highest spreadabilty and stability was separately mixed with two glass fibre tows with largest spreadabilty via air-assisted tow commingling to produce two types of continuous intermingled carbon fibre/glass fibre hybrid tows. Finally, a hybrid carbon fibre/glass fibre/epoxy composite was manufactured via resin film infusion. The main achievements of this research are summarized below.

- The air-assisted fibre tow spreading technology does allow the increase of the width of carbon fibre and glass fibre tows by up to 5 and 4 times, respectively. The "spreadability" of the fibre tow and the stability of the spread tow width were affected by the sizing on the fibre tow, the number of tow twists and fibre entanglements in the fibre tow as well as the tensile properties of the fibres.
- A characterisation method was developed to quantify the degree of hybridisation (at filament level) in UD carbon fibre/glass fibre hybrid tows.
- Two continuous intermingled UD carbon fibre/glass fibre tows with the degree of hybridisation of 32.5% and 25.4% were successfully manufactured via air-assisted commingling process.
- Compared with carbon fibre/epoxy composite, the intermingled carbon fibre/glass fibre hybrid composite exhibited a more gradual failure mode under tension. Intermingled hybridising increased the ultimate failure strain of the composite by 14%.

5.1.3 Interleaved cut-ply carbon fibre/PEEK composites

A cut-ply interleaved carbon fibre/PEEK composite panel was manufactured. The structure of the interleaved, cut ply composite was influenced by the thickness of the interleaved PEEK film, and the temperature and pressure used during compression moulding. The key findings are shown below.

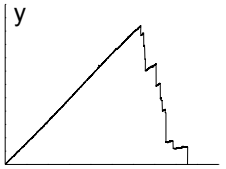
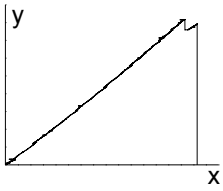
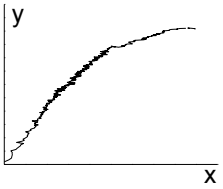
- The resulting composite exhibits non-linear tensile behaviour with a ductile strain of 0.40%, which is mainly caused by the shear yielding of the PEEK interleaves between the adjacent carbon fibre/PEEK layers in the overlapping area.
- Abrasive PEEK shear failure characteristics were observed by SEM inspection of the fracture surface of the cut-ply interleaved carbon fibre/PEEK composite.

5.1.4 Comparison of the three approaches to produce CFRP with enhanced ductility

The three approaches explored in this thesis did result in CFRP with enhanced ductility. The tensile properties of the composites produced by three approaches are summarised in Table 5.1. The tensile behaviour of the composites produced by the first two approaches (introducing fibre waviness and intermingling carbon fibre and glass fibre) is similar: the stress linearly increases with increasing strain followed by several load drops when the tensile strain is close to the ultimate failure strain. The hybrid shows a final massive stress drop (catastrophic failure) and in comparison the wavy fibre specimens show a much more progressive failure process, but the stress carried by the wavy composite after initial failure is lower than that carried by hybrid composite. However, the cut-ply interleaved carbon fibre/PEEK composite exhibits a different behaviour: a stress plateau was observed following the linear elastic region, indicating no drop in the load carrying capacity of the cut-ply interleaved composite. Regarding to the value of failure strain, tensile strength and modulus, the UD CFRP

composite containing fibre waviness has the highest values amongst these three composites. Compared to the control sample, the wavy fibre composites have improved ultimate failure strain without significantly changing its tensile strength and modulus. The hybridisation of carbon fibre with glass fibre tows did also result in an increase of the ultimate failure strain of the carbon fibre composite but with reduction in the tensile strength and modulus. In the case of interleaved cut-ply carbon fibre/PEEK, it has obviously a much lower tensile strength and modulus than other two types of composites even though it exhibited a ductile strain of 0.4%.

Table 5.1 The tensile properties of the composites produced using wavy fibres, hybrid tows and by ply cutting and interleaving

		UD composite containing wavy fibres	UD hybrid carbon/glass composites	Cut-ply interleaved CF/PEEK composites
Schematic of stress (y)-strain (x) curve				
Failure strain	Initial value (%)	1.51±0.08	1.33 ±0.08	0.50 ± 0.09 (yield strain)
	Ultimate value (%)	1.96±0.16	1.52 ± 0.05	0.84 ± 0.25
	Improvement (%) [ab]	21	14	N/a (Ductile strain = 0.4%)
Tensile strength	Value (MPa)	2491±158	1438 [c]	230 ± 22
	Improvement (%) [a]	0	-32	N/a
Tensile modulus	Value (GPa)	169.6±6.6	103.4 [c]	47.6 ±5.5
	Improvement (%) [a]	0	-29	N/a

Note: a) $\text{Improvement} = (\frac{\text{certain property of produced composite}}{\text{certain property of its control composite}} - 1) \times 100\%$

b) Improvement in ultimate failure strain

c) Because the fibre volume fraction of the hybrid composites made in this study is only about 30%, its tensile strength and modulus were normalised to that of composites with fibre volume fraction of 60%.

To conclude, all of these three investigated approaches hold some promise in enhancing the ductility of UD CFRP composites, but they all have weaknesses. Specifically, the UD composite containing wavy fibres has the largest improvement in ultimate failure strain among these three composite without significantly changing the tensile strength and modulus, but it can only carry very limited stress after the first failure occurs. The intermingled hybridisation of carbon fibre and glass fibre also offers an enhanced failure strain but decreases the tensile strength and modulus compared with carbon fibre composite. Cut-ply interleaved carbon fibre composite has most promising tensile stress-strain curve among these three types, but its tensile strength and modulus are much lower than those of the other two.

5.2 Suggestions for future work

The work discussed in this thesis opens up new possibilities to create UD CFRP composites with enhanced ductility. It is worthy studying the unloading tensile, compressive and flexural behaviours of currently-developed materials (i.e. non-constrained annealed carbon fibre/PA-12, intermingled carbon fibre/glass fibre hybrid composite and cut-ply interleaved carbon fibre/PEEK composite) in the future. Further investigations derived from the three individual work packages are discussed in the following sections.

5.2.1 Introducing fibre waviness into UD composites

In order to gain a better understanding of the failure mechanism of UD composites containing wavy fibres, a micro-level UD composite containing tens of wavy and straight fibres should be tested under tension while being monitored using micro-CT or SEM to observe the initial individual fibre breaks and subsequent behaviour. Then a model of the tensile behaviour of such manufactured composite should be developed

to optimise the fibre waviness (i.e. content, wavelength, amplitude and location) in the composite.

Another research direction derived from this work package is to develop a new technique to manufacture the UD composite with a range of fibre waviness in a controllable manner, such as partially overfeeding a carbon fibre tow into composite production line. The fibre waviness should be created because the length of overfed carbon fibres in the composite is larger than the length of produced composite tape. It is anticipated that the fibre waviness can be controlled by the overfeeding ratio of carbon fibres and the speed of composite production. Compared with the currently-used method, non-constrained annealing of thermoplastic (it was demonstrated for carbon fibre/PA-12) tapes, the proposed method is less time-consuming and has better control of the fibre waviness. However, the challenge of designing overfeeding fibre system in the current composite tape production line is foreseen in the future investigation.

5.2.2 Intermingled UD carbon fibre/glass fibre hybrid composites

Inspired by the fact that hybridising continuous glass with carbon fibre tows can increase the failure strain of composites, hybrid composites with the same volume ratios of carbon fibre/glass fibre but the different degrees of hybridisation should be investigated to further understand the failure mechanism of intermingled carbon fibre/glass fibre composites under tension. These results can be used to develop and validate the modelling of the tensile behaviour of intermingled hybrid composites, which can be then used to explore the optimisation of the degree of the hybridisation and carbon fibre content in the hybrid composite.

The spreading and hybridising process can be modified to improve the degree of hybridisation of the UD hybrid tow. So far, the largest width of the current produced

fibre tow is only 28mm, which is limited by the width of the vacuum window in the equipment. Enlarging the size of vacuum window in the future investigation will increase the width of the spread fibre tow, which can reduce the difficulties of intermingling two spread fibre tows together. Another modification in the manufacturing process is to build an automatic resin film feeding or resin impregnation system, which will follow the air-assisted fibre tow commingling unit. Instead of manually laying up hybrid fibre tow and resin film together to produce hybrid composite, the modified process will produce intermingled hybrid carbon fibre/glass fibre/resin prepreg of consistent quality. More importantly, using resin impregnation or an in-situ resin film feeding (i.e. producing and feeding feed resin film simultaneously) system can potentially apply smaller amount of resin on the hybrid tow than the resin film infusion method, which will result an increase in the total fibre volume fraction in the hybrid composite.

5.2.3 Interleaved cut-ply carbon fibre/PEEK composite

It was found that interleaved cut-ply carbon fibre/PEEK composite exhibited a softening non-linear tensile behaviour with a ductile strain of 0.4%. The ductility of such a composite is mainly the result of shearing of the PEEK interleaf in the overlapping region. However, the produced composite in this work package only contains one overlapping region, so overcoming the manufacturing challenges of producing interleaved cut-ply carbon fibre/PEEK composites containing multiple overlapping regions (shown in Figure 5.1) might result in composites which exhibit progressive failure and enhanced ductile strain, which could be potentially be used in damage tolerant structures.



Figure 5.1 Schematic diagram of interleaved cut-ply carbon fibre/PEEK composite containing multiple overlapping regions

There are significant difficulties presented by such configuration. One is the manufacturing difficulty of ensuring the overlap geometry is consistently produced. This difficulty was not completely resolved for the single overlap configuration tested in this work and it can be anticipated that this will only become more complex for the multiple overlap configuration shown in Figure 5.1. One strategy might be to replace the cuts in each ply with partial cuts or perforations. Another difficulty is that the tensile stress-strain response for the single overlap specimens described in this thesis reached a plateau and this means that if the same materials are used in the configuration shown in Figure 5.1 then this multiple overlap specimen will suffer from localisation of failure subjected to uniaxial tension and the overall ductility will be very low. To improve this, some mechanism is required to ensure that after one overlap (the weakest) has undergone its plastic shear distortion that this overlap can then carry an increased load to enable the next weakest overlap position to start failing and so on that all overlaps undergo plastic deformation prior the final failure. To achieve this one approach is to investigate other but shear strain-hardening polymers for the interleaf and matrix materials.

Appendix I

MATLAB codes of a program to define the truly intermingled hybrid fibre tow (i.e. a model to describe randomly-distributed, commingled two-fibre-type tows) and obtain the $AP_{CF,Model}$ from the defined model are shown below.

i) Code of main program

```
% ------------------------------------------------- Initialization
close all;
clear all;
% ------------------------------------------------- Define parameters
A_size = 120;
F_A = 3;
F_B = 22;
stepR_window = 10;
stepC_window = 10;
run_number = 5;
D_A = 14.95;
D_B = 6.9;
% -------------------------------------------------Define output matrix
% ................................ Define dimension of output matrix
Output_number_ratio_0 =
zeros((floor(A_size/stepR_window))^2,run_number);
% ..............................Define output_number_ratio_0 matrix
for i = 1:run_number
    column_ratio_0 =
Random_H_Anlys(A_size,F_A,F_B,stepR_window,stepC_window);
    for j = 1:(floor(A_size/stepR_window))^2
        Output_number_ratio_0(j,i) = column_ratio_0(j,1);
    end
end
% ..............................Define output_area_ratio_1(CF) matrix
Output_area_ratio_1 = zeros(size(Output_number_ratio_0));
for i = 1:(floor(A_size/stepR_window))^2
   for j = 1:run_number
       Output_area_ratio_1(i,j)= (1-
Output_number_ratio_0(i,j))*D_B^2/((1-
Output_number_ratio_0(i,j))*D_B^2+Output_number_ratio_0(i,j)*D_A^2);
   end
end
% ------------------Change the format of Output_area_ratio_1 into txt
R_Output_area_ratio_1 = Output_area_ratio_1';    % reverse the matrix
% ..................................................Define file name
str_window_size = num2str(stepR_window);
str_run_number = num2str(run_number);
Filename = strcat(str_window_size,'x',str_run_number,'.txt');
Fid = fopen(Filename,'wt');
[L,W] = size(R_Output_area_ratio_1);
textformat = [repmat('%f,',1,L),'\n'];
fprintf(Fid,textformat,R_Output_area_ratio_1);
fclose all;
% -------------------------------------------------Histrogram count
Histro_count =
Hist(Output_area_ratio_1,[0.05,0.15,0.25,0.35,0.45,0.55,0.65,0.75,0.8
5,0.95]);
```

ii) Code of function “Random_H_Anlys.m”

```
function [ column_ratio_0 ] =
Random_H_Anlys(A_size,F_A,F_B,stepR_window,stepC_window )
%Random_H_Anlys
% 1 Input = A_size(H matrix size), F_A(number of GF),F_B(number of
% CF),stepR_window(length of anlys window),stepC_window(width anlys
window)
% 2 Output = column_ratio_O (one-column matrix show the number %
fraction of GF/(CF+GF))
% ------------------Define two-fibre-type,randomly-distributed matrix
A = zeros(A_size,A_size);
% .. Generate randomly matrix (consider whether number of elements in
matrix is exactly divided by F_A+F_B)
if mod(A_size^2,F_A+F_B) == 0
    A = Random_Hmatrix(A_size,F_A,F_B);
else
    for i = (A_size*(F_A+F_B)):(-1):A_size
        if mod(i^2,F_A+F_B)== 0
            trans_A_size = i;
        end
    end
    trans_A = Random_Hmatrix(trans_A_size,F_A,F_B);
    for i = 1:A_size
        for j = 1:A_size
            A(i,j)= trans_A(i,j);
        end
    end
 end
 % ------------------Divide fibre_matrix A into windows and calculate
 % number CF/(CF+GF) in each window
 % ......................... Define analysis window and output matrix
 n_window_row = floor(A_size/stepR_window);
 n_window_column = floor(A_size/stepC_window);
 M_ratio_0 = zeros (n_window_row,n_window_column);
 M_ratio_1 = zeros (n_window_row,n_window_column);
 % ............................... Rule of Indexing indexR and indexC
 % ..................................Rule of Indexing indexR indexC
 %[     1               2               ...          n_window_column]
 %[n_window_column+1 n_window_column+2  ...        2*n_window_column]
 %[    ...             ...             ...        k*n_window_column]
 %[    ...             ...          ...  n_window_row*n_window_column]
 for i = 1:n_window_row*n_window_column
     window = zeros(stepR_window,stepC_window);
     indexR = ceil(i/n_window_column);
     if mod(i,n_window_column)== 0
         indexC = n_window_column;
     else
         indexC = mod(i,n_window_column);
     end
 % ............put elements in fibre_matrix into window(indexR,indexC)
     R_u = stepR_window*(indexR-1)+1;
     R_b = stepR_window*indexR;
     C_l = stepC_window*(indexC-1)+1;
     C_r = stepC_window*indexC;
     window = A(R_u:R_b,C_l:C_r);
 % ................calculate the number ratio in window(indexR,indexC)
     sum_0 = 0;
     sum_1 = 0;
```

```
    for m = 1:(R_b-R_u+1)
        for n = 1:(C_r-C_l+1)
            if window(m,n)== 0
                sum_0 = sum_0+1;
            else
                sum_1 = sum_1+1;
            end
        end
    end
    M_ratio_0(indexR,indexC)=sum_0/stepR_window/stepC_window;
    M_ratio_1(indexR,indexC)=sum_1/stepR_window/stepC_window;
 end
 %              End here we get matrix of number ratio in each window
 % ------------------------------transfer matrix M_ratio into column
 column_ratio_0 = zeros(indexR*indexC,1);
 column_ratio_1 = zeros(indexR*indexC,1);
 for i = 1:indexR
    for j = 1:indexC
        column_ratio_0((i-1)*indexC+j,1) = M_ratio_0(i,j);
        column_ratio_1((i-1)*indexC+j,1) = M_ratio_1(i,j);
    end
 end
end
```

iii) Code of function “Random_Hmatrix. m”

```
function
[Random_Hmatrix]=Random_Hmatrix(matrix_size,number_A,number_B)
% Function Random_Hmatrix
% 1 Generate a square matrix (Length = matrix_size) which only
contains element 1 and 0. Element 1 and 0 randomly distributed in
this Random_Hmatrix
% 2 Number ratio element 0/ element 1 = number_A/number_B
% 3 Note: mod(matrix_size^2, number_A+number_B) == 0
Random_Hmatrix = zeros(matrix_size, matrix_size);
% ..........................Form a random integer (1 to matrix_size^2)
Initial_matrix_R = randperm(matrix_size^2);
for i = 1:matrix_size^2
    if Initial_matrix_R(1,i)<=
number_A*matrix_size^2/(number_A+number_B)
        Initial_matrix_R(1,i) = 0;
    else
        Initial_matrix_R(1,i) = 1;
    end
end
for i = 1:matrix_size
    for j = 1:matrix_size
        Random_Hmatrix(i,j) = Initial_matrix_R(1,(i-1)*matrix_size+j);
    end
end
end
```

Appendix II

MATLAB codes of image recognition program for detecting carbon fibre and glass fibre and obtaining $AP_{CF,\ Experiment}$ from micrographs of hybrid carbon fibre/glass fibre tow are shown below.

i) Code of main program

```
close all
clear all
% ---------------------------------------------------- INITIALIZATION
% .....................................................Input Image
I = imread('33.jpg');
% ---------------------------------------------------- IMAGE HISTOGRAM
Id    = im2double(I)% convert image to double precision to use 'hist'
nbins = 16;                          % scalar, use nbins number of bins
n     = hist(Id(:),nbins);% vector of [1,nbins], count elements in
each bin
p     = n./sum(n); % calculate the percentage of elements in each bin
% ---------------------------------------------------- SEPARATE FIBRES
% ..................................................... General Settings
top = 520;
bottom = 560;                  % parameters for cutting the blank area
step   = round(256/nbins);                        % capacity of each bin
                              % choose the highest bin of elements
[pm,pi] = max(p);                  % pi is the index of the chosen bin
% ..................................... carbon fibre separation
Itmp1 = I;                % duplicate for carbon fibre and cut blanks
Itmp1 = Itmp1(top:end-bottom,:);
delta = 2;                          % tolerant range small blob selection
bound = (pi+delta)*step;                          % upper tolerant scale
Itmp1(Itmp1<bound) = 0;  % eliminate grey blobs with intensity <bound
es1 = strel('ball',8,8);
Itmp1 = imopen(Itmp1,es1);                                % denoising
Itmp1 = im2bw(Itmp1);                % dual-value black-white image
% ..................................... Large grey blobs separation
Itmp2 = I;                % duplicate for large blobs and cut blanks
Itmp2 = Itmp2(top:end-bottom,:);
deltaU = 1;                         % Upper bound of large blob selection
deltaL = 1;                         % Lower bound of small blob selection
boundU = (pi+deltaU)*step;
boundL = (pi-deltaL-1)*step;
Itmp2(Itmp2<boundL) = 0;
Itmp2(Itmp2>boundU) = 0;
                                                          % denoising
level = graythresh(Itmp2);
Itmp2 = im2bw(Itmp2,level);          % dual-value black-white image
figure();imshow(Itmp1);
figure();imshow(Itmp2);
% ---------------------------------------------- RATION CALCULATION
nbinR = 5;
nbinC = 5;
ratio1 = subsections(Itmp1,nbinR,nbinC);          % see subsections.m
ratio2 = subsections(Itmp2,nbinR,nbinC);
```

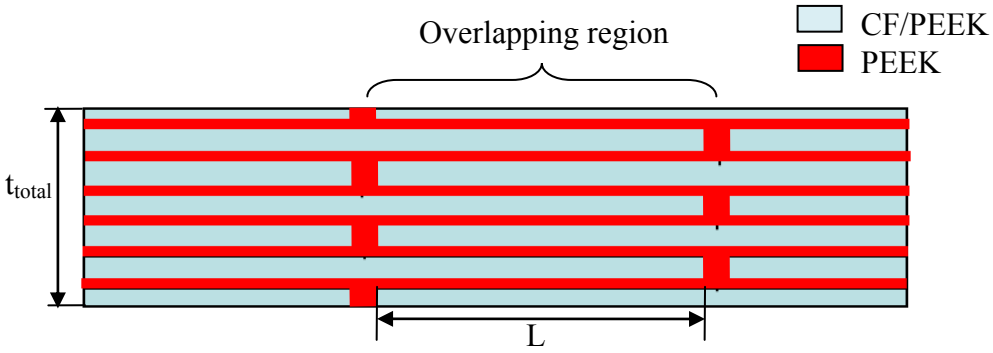
ii) Code of function “subsections.m”

```
function ratioM = subsections(Ibw, nbinR, nbinC)
[r,c] = size(Ibw);
stepR = round(r/nbinR);
stepC = round(c/nbinC);
area  = stepR*stepC;
nbins = nbinR*nbinC;

ratioM = zeros(nbinR,nbinC);

for i = 1:nbins
    % Rule of Indexing
    % [   1        2       3    ...     nbinC  ]
    % [ nbinc+1 nbinC+2 nbinC+3 ...   2*nbinC  ]
    % [   ...      ...     ...   ...   k*nbinC  ]
    % [   ...      ...     ...   ... nbinR*nbinC]
    indexR = ceil(i/nbinC);
    indexC = mod(i,nbinC);
    if indexR == 1
        R_u = 1;                    % R_u, upper bound of subsections
        R_b = stepR;                % R_b, lower bound of subsections
    elseif indexR == nbinR
        R_u = stepR*(nbinR-1)+1;
        R_b = r;
    else
        R_u = stepR*(indexR-1)+1;
        R_b = stepR*indexR;
    end
    if indexC == 1
        C_l = 1;                     % C_l, left bound of subsections
        C_r = stepC;                % C_r, right bound of subsections
    elseif indexC == 0
        C_l = stepC*(nbinC-1)+1;
        C_r = c;
        indexC = nbinC;             % mod(10,5)=0 which makes no sense
    else
        C_l = stepC*(indexC-1)+1;
        C_r = stepC*indexC;
    end
    Mtmp = Ibw(R_u:R_b,C_l:C_r);
    % Caution: Ibw should be a black-white image to continue
    ratioM(indexR,indexC) = sum(Mtmp(:))/area;
end
end
```

Appendix III



w is the width of specimen, which is in the through-plane direction

Figure Schematic of cut-ply interleaved CF/PEEK composite

Because aim of designing this structure is to allow the shear failure of the PEEK interleaf in the overlapping region occur before the tensile failure of the entire specimen, overall force causing shear failure (F_{shear}) should be less than the force causing the tensile failure ($F_{tensile}$) in the whole laminate.

So

$$F_{shear} < F_{tensile}$$

$$\hat{\tau}_{PEEK} \times L \times n_{PEEK} \times w < \hat{\sigma}_{cut-ply} \times t_{total} \times w$$

$$L < \frac{\hat{\sigma}_{cut-ply} \times t_{total}}{\hat{\tau}_{PEEK} \times n_{PEEK}}$$

where $\hat{\sigma}_{cut-ply}$ is the tensile strength of the cut-ply interleaved carbon fibre/PEEK assuming no shear failure of the PEEK interleaf, n_{PEEK} is the number of PEEK interleaves in the composite, t_{total} the thickness of the composite and $\hat{\tau}_{PEEK}$ the shear strength of PEEK.

References

[1] *Carbon fibers & carbon fiber reinforced plastics (CFRP) –a global market overview* [Report] 2013. Accessed on 2014 15/09; Available from: http://industry-experts.com/verticals/chemicals-and-materials/carbon-fibers-and-carbon-fiber-reinforced-plastics-cfrp-a-global-market-overview.

[2] *Glass fiber reinforcements – a global market overview*, [Report] 2012. Accessed on 2014 15/09; Available from: http://industry-experts.com/verticals/chemicals-and-materials/glass-fiber-reinforcements-a-global-market-overview.

[3] Matthews, F.L. and Rawlings, R.D., *Composite Materials: Engineering and Science*. 2002, Cambridge: Woodhead Publishing Ltd.

[4] *Data sheet of HexPly 8552*, [Data sheet] 2013. Accessed on 2014 15/09; Available from: http://www.hexcel.com/Resources/DataSheets/Prepreg-Data-Sheets/8552_us.pdf.

[5] *Data sheet of HexPly 913*, [Data sheet] 2014. Accessed on 2014 15/09; Available from: http://www.hexcel.com/Resources/DataSheets/Prepreg-Data-Sheets/913_eu.pdf.

[6] *Data sheet of TORAYCA T700S*, 2013. Accessed on 2014 15/09; Available from: http://www.toraycfa.com/pdfs/T700SDataSheet.pdf.

[7] *Technical data sheet of APC-2 PEEK thermoplastic polymer*, 2012. Accessed 14/12/2012; Available from: www.cemselectorguide.com/pdf/APC-2_PEEK_031912.pdf.

[8] Bank, L., *Progressive failure and ductility of FRP composites for construction: review.* Journal of Composites for Construction, 2013. **17**(3): p. 406-419.

[9] Davis, J.R., *Tensile Testing*. 2004, Ohio: A S M International.

[10] Pascoe, K.J., *An Introduction to the Properties of Engineering Materials*. 1978: Springer Netherlands.

[11] Davis, H.E., Troxell, G.E., and Hauck, G.F.W., *The Testing of Engineering Materials*. 1982: McGraw-Hill.

[12] Gibson, R.F., *A review of recent research on mechanics of multifunctional composite materials and structures.* Composite Structures, 2010. **92**(12): p. 2793-2810.

[13] Asp, L.E. and Greenhalgh, E.S., *Structural power composites.* Composites Science and Technology, 2014. **101**: p. 41-61.

[14] O'Brien, D.J., Baechle, D.M., Yurchak, O.B., and Wetzel, E.D., *Effect of processing conditions and electrode characteristics on the electrical properties of structural composite capacitors.* Composites Part A: Applied Science and Manufacturing, 2015. **68**: p. 47-55.

[15] Shirshova, N., Qian, H., Shaffer, M.S.P., Steinke, J.H.G., Greenhalgh, E.S., Curtis, P.T., Kucernak, A., and Bismarck, A., *Structural composite supercapacitors.* Composites Part A: Applied Science and Manufacturing, 2013. **46**(0): p. 96-107.

[16] Summerscales, J., Hall, W., and Virk, A.S., *A fibre diameter distribution factor (FDDF) for natural fibre composites.* Journal of Materials Science, 2011. **46**(17): p. 5876-5880.

[17] Summerscales, J., Dissanayake, N., Virk, A., and Hall, W., *A review of bast fibres and their composites. Part 2 - Composites.* Composites Part A: Applied Science and Manufacturing, 2010. **41**(10): p. 1336-1344.

[18] Virk, A.S., Hall, W., and Summerscales, J., *Modulus and strength prediction for natural fibre composites.* Materials Science and Technology, 2012. **28**(7): p. 864-871.
[19] Dicker, M.P.M., Duckworth, P.F., Baker, A.B., Francois, G., Hazzard, M.K., and Weaver, P.M., *Green composites: a review of material attributes and complementary applications.* Composites Part A: Applied Science and Manufacturing, 2014. **56**: p. 280-289.
[20] Lee, K.-Y., Buldum, G., Mantalaris, A., and Bismarck, A., *More than meets the eye in bacterial cellulose: Biosynthesis, bioprocessing, and applications in advanced fiber composites.* Macromolecular Bioscience, 2014. **14**(1): p. 10-32.
[21] Hahn, H.T. and Tsai, S.W., *Nonlinear elastic behavior of unidirectional composite laminate* Journal of Composite Materials, 1973. **7**: p. 102-118.
[22] Sun, C.T. and Yoon, K.J., *Elastic-plastic analysis of AS4/PEEK composite laminate using a one-parameter plasticity model.* Journal of Composite Materials, 1992. **26**(2): p. 293-308.
[23] Sun, C.T. and Zhu, C., *The effect of deformation-induced change of fibre orientation on the non-linear behavior of polymeric composite laminates.* Composites Science and Technology, 2000. **60**: p. 2337-2345.
[24] Bakis, C.E., Nanni, A., Terosky, J.A., and Koehler, S.W., *Self-monitoring, pseudo-ductile, hybrid FRP reinforcement rods for concrete applications.* Composites Science and Technology, 2001. **61**(6): p. 815-823.
[25] You, Y.-J., Park, Y.-H., Kim, H.-Y., and Park, J.-S., *Hybrid effect on tensile properties of FRP rods with various material compositions.* Composite Structures, 2007. **80**(1): p. 117-122.
[26] Cui, Y.-H. and Tao, J., *A new type of ductile composite reinforcing bar with high tensile elastic modulus for use in reinforced concrete structures.* Canadian Journal of Civil Engineering, 2009. **36**(4): p. 670-673.
[27] Jones, R.M., *Mechanics of Composite Materials*. 1999, London: Taylor & Francis
[28] Manders, P.W. and Kowalski, I.M. *The effect of small angular fibre misalignments and tabbing techniques on the tensile strength of carbon fibre composites*. in *32nd International SAMPE Symposium and Exhibition*, 1987: Tokyo, Japan.
[29] Chou, T.W. and Takahashi, K., *Non-linear elastic behaviour of flexible fibre composites.* Composites, 1987. **18**(1): p. 25-34.
[30] Chun, H.-J., Shin, J.-Y., and Daniel, I.M., *Effects of material and geometric nonlinearities on the tensile and compressive behavior of composite materials with fiber waviness.* Composites Science and Technology, 2001. **61**(1): p. 125-134.
[31] Chen-ming, K., Takahashi, K., and Tsu-wei, C., *Effect of fiber waviness on the nonlinear elastic behavior of flexible composites.* Journal of Composite Materials, 1988. **22**(11): p. 1004-1025.
[32] Khan, B., Potter, K., and Wisnom, M. *Simulation of process induced defects in resin transfer moulded woven carbon fibre laminates and their effect on mechanical behaviour*. in *The 8th International Conference on Flow Processes in Composite Materials (FPCM8)*, 2006: Douai, France.
[33] Wisnom, M.R. and Atkinson, J.W., *Fibre waviness generation and measurement and its effect on compressive strength.* Journal of Reinforced Plastics and Composites, 2000. **19**(2): p. 96-110.

[34] Potter, K., Langer, C., Hodgkiss, B., and Lamb, S., *Sources of variability in uncured aerospace grade unidirectional carbon fibre epoxy preimpregnate.* Composites Part A: Applied Science and Manufacturing, 2007. **38**(3): p. 905-916.

[35] Wang, J., Potter, K.D., Hazra, K., and Wisnom, M.R., *Experimental fabrication and characterization of out-of-plane fiber waviness in continuous fiber-reinforced composites.* Journal of Composite Materials, 2012. **46**(17): p. 2041-2053.

[36] Wang, J., Potter, K.D., Wisnom, M.R., and Hazra, K., *Failure mechanisms under compression loading in composites with designed out-of-plane fibre waviness.* Plastics, Rubber and Composites, 2013. **42**(6): p. 231-238.

[37] Mrse, A.M. and Piggott, M.R., *Compressive properties of unidirectional carbon fibre laminates: II. The effects of unintentional and intentional fibre misalignments.* Composites Science and Technology, 1993. **46**(3): p. 219-227.

[38] O'Hare, A.D. and Hyer, M.W., *Effects of layer waviness on the compression strength of thermoplastic composite laminates.* Journal of Reinforced Plastics and Composites, 1993. **12**(4): p. 414-429.

[39] Svensson, N., Shishoo, R., and Gilchrist, M., *Manufacturing of thermoplastic composites from commingled yarns - a review.* Journal of Thermoplastic Composite Materials, 1998. **11**(1): p. 22-56.

[40] Lauke, B., Bunzel, U., and Schneider, K., *Effect of hybrid yarn structure on the delamination behaviour of thermoplastic composites.* Composites Part A: Applied Science and Manufacturing. **29A**: p. 1397-1409.

[41] Potter, K., Khan, B., Wisnom, M., Bell, T., and Stevens, J., *Variability, fibre waviness and misalignment in the determination of the properties of composite materials and structures.* Composites Part A: Applied Science and Manufacturing, 2008. **39**(9): p. 1343-1354.

[42] Potter, K., *Manufacturing defects as a cause of failure in polymer matrix composites*, in *Failure Mechanisms in Polymer Matrix Composites: Criteria, Testing and Industrial Applications*, P. Robinson, E. Greenhalgh, and S. Pinho, Editors. 2012, Woodhead Publishing Limited: Cambridge.

[43] Kugler, D. and Moon, T.J., *Identification of the most significant processing parameters on the development of fiber waviness in thin laminates.* Journal of Composite Materials, 2002. **36**(12): p. 1451-1479.

[44] Nairn, J.A., *Thermoelastic analysis of residual stresses in unidirectional, high-performance composites.* Polymer Composites, 1985. **6**(2): p. 123-130.

[45] Cohen, A., Calhoun, D.R., Adams, M.E., and Campbell, G.A. *Experimental investigation of fiber buckling during fabrication of thermoplastic matrix composites*. in *Proceedings of the 1993 ASME Winter Annual Meeting, November 28, 1993 - December 3, 1993*, 1993: New Orleans, LA, USA: Publ by ASME.

[46] Bogetti, T.A., Gillespie, J.W., and Lamontia, M.A., *Influence of ply waviness with nonlinear shear on the stiffness and strength reduction of composite laminates.* Journal of Thermoplastic Composite Materials, 1994. **7**(2): p. 76-90.

[47] Chun, H.J. and Jang, P.S., *Nondestructive evaluation of degree of fiber waviness in thick composites.* Key Engineering Materials, 2000. **183**: p. II/.

[48] Hsiao, H.M. and Daniel, I.M., *Effect of fiber waviness on stiffness and strength reduction of unidirectional composites under compressive loading.* Composites Science and Technology, 1996. **56**(5): p. 581-593.

[49] Pain, D. and Drinkwater, B., *Detection of Fibre Waviness Using Ultrasonic Array Scattering Data.* Journal of Nondestructive Evaluation, 2013. **32**(3): p. 215-227.
[50] Yurgartis, S.W., *Measurement of small angle fiber misalignments in continuous fibre composites.* Composites Science and Technology, 1987. **30**: p. 279-293.
[51] Clarke, A.R., Archenhold, G., and Davidson, N.C., *A novel technique for determining the 3D spatial distribution of glass fibres in polymer composites.* Composites Science and Technology, 1995. **55**: p. 75-91.
[52] Creighton, C.J., Sutcliffe, M.P.F., and Clyne, T.W., *A multiple field image analysis procedure for characterisation of fibre alignment in composites.* Composites Part A: Applied Science and Manufacturing, 2001. **32**: p. 221-229.
[53] Barwick, S.C. and Papathanasiou, T.D., *Identification of fibre misalignement in continuous fibre composites.* Polymer Composites, 2003. **24**(3): p. 475-486.
[54] Sutcliffe, M.P.F., Lemanski, S.L., and Scott, A.E., *Measurement of fibre waviness in industrial composite components.* Composites Science and Technology, 2012. **72**(16): p. 2016-2023.
[55] Ho, K.K.C., Shamsuddin, S.R., Riaz, S., Lamorinere, S., Tran, M.Q., Javaid, A., and Bismarck, A., *Wet impregnation as route to unidirectional carbon fibre reinforced thermoplastic composites manufacturing.* Plastics, Rubber and Composites, 2011. **40**(2): p. 100-107.
[56] BS ISO 11566,*Carbon fibre - Determination of tensile properties of single-filament*,1996
[57] Bunsell, A.R., *Handbook of Tensile Properties of Textile and Technical Fibres*. 2009, Cambridge: Woodhead Publishing Limited.
[58] Woods, J. and Stark, H., *Probability, Statistics, and Random Processes for Engineers*. Fourth Edition ed. 2011: Pearson Education.
[59] Hull, D. and Clyne, T.W., *An Introduction to Composite Materials*. 2nd Edition ed. 1996, Cambridge: Cambridge University Press.
[60] Hayashi, T. *On the improvement of mechanical properties of composites by hybrid composition*. in *8th International Reinforced Plastic Conference*, 1972: Brighton, UK.
[61] Bunsell, A.R. and Harris, B., *Hybrid carbon and glass fibre composites.* Composites, 1974. **5**(4): p. 157-164.
[62] Chamis, C.C., Lark, R.F., and Sinclair, J.H., *Mechanical Property characterization of intraply hybrid composites*, in *Test Methods and Design Allowables for Fibrous Composites*, C.C. Chamis, Editor. 1981, ASTM. p. 261-280.
[63] Manders, P.W. and Bader, M.G., *The strength of hybrid glass/carbon fibre composites Part 1: failure strain enhancement and failure mode.* Journal of Materials Science, 1981. **16**(8): p. 2235-2248.
[64] Stevanović, M.M. and Stecenko, T.B., *Mechanical behaviour of carbon and glass hybrid fibre reinforced polyester composites.* Journal of Materials Science, 1992. **27**(4): p. 941-946.
[65] Saha, N., Banerjee, A.N., and Mitra, B.C., *Tensile behaviour of unidirectional polyethylene-glass fibres/PMMA hybrid composite laminates.* Polymer, 1996. **37**(4): p. 699-702.
[66] Taketa, I., Ustarroz, J., Gorbatikh, L., Lomov, S.V., and Verpoest, I., *Interply hybrid composites with carbon fiber reinforced polypropylene and self-*

reinforced polypropylene. Composites Part A: Applied Science and Manufacturing, 2010. **41**(8): p. 927-932.

[67] Dong, C., Duong, J., and Davies, I.J., *Flexural properties of S-2 glass and TR30S carbon fiber-reinforced epoxy hybrid composites.* Polymer Composites, 2012. **33**(5): p. 773-781.

[68] Czél, G. and Wisnom, M.R., *Demonstration of pseudo-ductility in high performance glass/epoxy composites by hybridisation with thin-ply carbon prepreg.* Composites Part A: Applied Science and Manufacturing, 2013. **52**: p. 23-30.

[69] Zweben, C., *Tensile strength of hybrid composites.* Journal of Materials Science, 1977. **12**(7): p. 1325-1337.

[70] Peijs, A.A.J.M., Venderbosch, R.W., and Lemstra, P.J., *Hybrid composites based on polyethylene and carbon fibres Part 3: Impact resistant structural composites through damage managment.* Composites, 1990. **21**(6): p. 522-530.

[71] Peijs, A.A.J.M. and Van Klinken, E.J., *Hybrid composites based on polyethylene and carbon fibres Part V Energy absorption under quasi-static crash conditions.* Journal of Materials Science Letters, 1992. **11**: p. 520-522.

[72] Pegoretti, A., Fabbri, E., Migliaresi, C., and Pilati, F., *Intraply and interply hybrid composites based on E-glass and poly(vinyl alcohol) woven fabrics: tensile and impact properties.* Polymer International, 2004. **53**(9): p. 1290-1297.

[73] Swolfs, Y., Crauwels, L., Breda, E.V., Gorbatikh, L., Hine, P., Ward, I., and Verpoest, I., *Tensile behaviour of intralayer hybrid composites of carbon fibre and self-reinforced polypropylene.* Composites Part A: Applied Science and Manufacturing, 2014. **59**: p. 78-84.

[74] Lauke, B., Bunzel, U., and Schneider, K., *Effect of hybrid yarn structure on the delamination behaviour of thermoplastic composites.* Composites Part A: Applied Science and Manufacturing, 1998. **29**: p. 1397-1409.

[75] Herath, C.N., Hwang, B.B., Ham, B.S., Seo, J.M., and Kang, B.C., *An analysis on the tensile strength of hybridized reinforcement filament yarns by commingling process.* Materials Science Forum, 2007. **539-543**(1): p. 974-978.

[76] Herath, C.N., Kang, B.C., Hwang, B.B., Min, K.H., Seo, J.M., Lee, I.C., Ruchiranga, J.V., and Lim, J.Y., *Microscopic evaluation and analysis on the tensile strength of hybridized reinforcement filament yarns by the commingling process.* Advanced Composite Materials, 2008. **17**(3): p. 225-233.

[77] Kravaev, P., Stolyarov, O., Seide, G., and Gries, T., *A method for investigating blending quality of commingled yarns.* Textile Research Journal, 2013. **83**(2): p. 122-129.

[78] Mäder, E., Rothe, C., and Gao, S.-L., *Commingled yarns of surface nanostructured glass and polypropylene filaments for effective composite properties.* Journal of Materials Science, 2007. **42**(19): p. 8062-8070.

[79] Peijs, A.A.J.M. and De Kok, J.M.M., *Hybrid composites based on polyethylene and carbon fibres Part 6: Tensile and fatigue behaviour.* Composites, 1993. **24**(1): p. 19-32.

[80] Martone, A., Giordano, M., Antonucci, V., and Zarrelli, M., *Enhancing damping features of advanced polymer composites by micromechanical hybridization.* Composites Part A: Applied Science and Manufacturing, 2011. **42**(11): p. 1663-1672.

[81] Pimenta, S. and Robinson, P. *Modelling the tensile response of unidirectional hybrid composites*. in *16th European Conference on Composite Materials*, 2014: Seville, Spain.
[82] Short, D. and Summerscales, J., *Hybrids — a review: Part 2. Physical properties.* Composites, 1980. **11**(1): p. 33-38.
[83] Peijs, A.A.J.M. and Venderbosch, R.W., *Hybrid composites based on polyethylene and carbon fibres Part IV Influence of hybrid design on impact strength.* Journal of Materials Science Letters, 1991. **10**: p. 1122-1124.
[84] Marom, G., Fischer, S., Tuler, F.R., and Wagner, H.D., *Hybrid effects in composites: conditions for positive or negative effects versus rule-of-mixtures behaviour.* Journal of Materials Science, 1978. **13**(7): p. 1419-1426.
[85] Summerscales, J., *The mechanical properties of carbon fibre with glass fibre hybrid reinforced plastics.* Department of Mechanical Engineering, Plymouth Polytechnic, 1983. **PhD Degree**.
[86] Kretsis, G., *A review of the tensile, compressive, flexural and shear properties of hybrid fibre-reinforced plastics.* Composites, 1987. **18**(1): p. 13-23.
[87] Summerscales, J. and Short, D., *Carbon fibre and glass fibre hybrid reinforced plastics.* Composites, 1978. **9**(3): p. 157-166.
[88] Swolfs, Y., Gorbatikh, L., and Verpoest, I., *Fibre hybridisation in polymer composites: A review.* Composites Part A: Applied Science and Manufacturing, (in press).
[89] Parratt, N.J. and Potter, K.D. *Mechanical behavior of intimately-mixed hybrid composites* in *International Conference on Composite Materials*, 1980: Paris, Fr: Pergamon Press, (Int Ser on the Strength and Fract of Mater and Struct).
[90] Aveston, J. and Sillwood, J.M., *Synergistic fibre strengthening in hybrid composites.* Journal of Materials Science, 1976. **11**(10): p. 1877-1883.
[91] Qiu, Y. and Schwartz, P., *Micromechanical behavior of Kevlar-149/S-glass hybrid seven-fiber microcomposites: I. Tensile strength of the hybrid composite.* Composites Science and Technology, 1993. **47**(3): p. 289-301.
[92] Hine, P.J., Bonner, M., Ward, I.M., Swolfs, Y., Verpoest, I., and Mierzwa, A., *Hybrid carbon fibre/nylon 12 single polymer composites.* Composites Part A: Applied Science and Manufacturing, 2014. **65**(0): p. 19-26.
[93] Phillips, M.G., *Composition parameters for hybrid composite materials.* Composites, 1981. **12**(2): p. 113-116.
[94] Fukunaga, H., Tsu-Wei, C., and Fukuda, H., *Strength of intermingled hybrid composites.* Journal of Reinforced Plastics and Composites, 1984. **3**(2): p. 145-160.
[95] Jalalvand, M., Czél, G., and Wisnom, M.R., *Numerical modelling of the damage modes in UD thin carbon/glass hybrid laminates.* Composites Science and Technology, 2014. **94**(0): p. 39-47.
[96] Swolfs, Y., Gorbatikh, L., and Verpoest, I., *Stress concentrations in hybrid unidirectional fibre-reinforced composites with random fibre packings.* Composites Science and Technology, 2013. **85**(0): p. 10-16.
[97] Short, D. and Summerscales, J., *Elastic and thermal properties of composites*, in *Fibre Composite Hybrid materials*, N.L. Hancox, Editor. 1981, Applied science publishers Ltd: London.
[98] Ren, P., Zhang, Z., Xie, L., Ren, F., Jin, Y., Di, Y., and Fang, C., *Hybrid effect on mechanical properties of M40-T300 carbon fiber reinforced bisphenol a dicyanate ester composites.* Polymer Composites, 2010. **31**(12): p. 2129-2137.

[99] Peijs, A.A.J.M., Catsman, P., Govaert, L.E., and Lemstra, P.J., *Hybrid composites based on polyethylene and carbon fibres Part 2: influence of composition and adhesion level of polyethylene fibres on mechanical properties.* Composites, 1990. **21**(6): p. 513-521.
[100] Åström, B.T., *Manufacturing of Polymer Composites*. 1997, London: Chapman & Hall.
[101] Sihn, S., Kim, R., Kawabe, K., and Tsai, S., *Experimental studies of thin-ply laminated composites.* Composites Science and Technology, 2007. **67**(6): p. 996-1008.
[102] Mankodi, H. and Patel, P., *Study the effect of commingling parameters on glass/polypropylene hybrid yarns properties.* AUTEX Research Journal, 2009. **9**(3): p. 70-74.
[103] Summerscales, J., Guild, F.J., Pearce, N.R.L., and Russell, P.M., *Voronoi cells, fractal dimensions and fibre composites.* Journal of Microscopy, 2001. **201**(2): p. 153-162.
[104] Shan, Y. and Liao, K., *Environmental fatigue behavior and life prediction of unidirectional glass–carbon/epoxy hybrid composites.* International Journal of Fatigue, 2002. **24**(8): p. 847-859.
[105] Pearce, N.R.L., Guild, F.J., and Summerscales, J., *The use of automated image analysis for the investigation of fabric architecture on the processing and properties of fibre-reinforced composites produced by RTM.* Composites Part A: Applied Science and Manufacturing, 1998. **29**(7): p. 829-837.
[106] Fukuda, H., *An advanced theory of the strength of hybrid composites.* Journal of Materials Science, 1984. **19**(3): p. 974-982.
[107] Thanomsilp, C. and Hogg, P.J., *Penetration impact resistance of hybrid composites based on commingled yarn fabrics.* Composites Science and Technology, 2003. **63**.
[108] Pimenta, S., Robinson, P., Czel, G., Wisnom, M., Diao, H., and Bismarck, A. *Discontinuous-ply composites for enhanced ductility*. in *6th International Conference on Composites Testing and Model Identification*, 2013: Aalborg, Denmark.
[109] Pimenta, S. and Robinson, P., *An analytical shear-lag model for brick-and mortar composites considering non-linear matrix response and failure.* Composites Science and Technology, 2014.
[110] Taketa, I., Okabe, T., and Kitano, A., *A new compression-molding approach using unidirectionally arrayed chopped strands.* Composites Part A: Applied Science and Manufacturing, 2008. **39**(12): p. 1884-1890.
[111] Taketa, I., Okabe, T., Matsutani, H., and Kitano, A., *Flowability of unidirectionally arrayed chopped strands in compression molding.* Composites Part B: Engineering, 2011. **42**(6): p. 1764-1769.
[112] Li, H., Wang, W.-X., Takao, Y., and Matsubara, T., *New designs of unidirectionally arrayed chopped strands by introducing discontinuous angled slits into prepreg.* Composites Part A: Applied Science and Manufacturing, 2013. **45**(0): p. 127-133.
[113] Malkin, R., Yasaee, M., Bond, I.P., and Trask, R.S. *Ductility in composites: Influence of ply-cuts on the flexural behavior of carbon fibre reinforced polymer (CFRP)*. in *2nd Joint US-Canada Conference on Composites - American Society for Composites, 26th Annual Technical Conference: Canadian Association for Composite Structures and Materials, September 26,*

2011 - September 28, 2011, 2011: Montreal, QC, Canada: DEStech Publications Inc.

[114] Malkin, R., Yasaee, M., Trask, R.S., and Bond, I.P., *Bio-inspired laminate design exhibiting pseudo-ductile (graceful) failure during flexural loading.* Composites Part A: Applied Science and Manufacturing, 2013. **54**(0): p. 107-116.

[115] Iarve, E.V. and Kim, R., *Three-dimensional fracture analysis and experimental investigation of model unidirectional discontinuous tow composite laminates.* Journal of Thermoplastic Composite Materials, 2002. **15**(6): p. 469-476.

[116] Iarve, E.V. and Kim, R., *Strength prediction and measurement in model multilayered discontinuous tow reinforced composites.* Journal of Composite Materials, 2004. **38**(1): p. 5-18.

[117] Baucom, J.N., Thomas, J.P., Pogue, W.R., III, and Qidwai, M.A.S., *Tiled composite laminates.* Journal of Composite Materials, 2010. **44**(26): p. 3115-3132.

[118] *Data sheet of Victrex PEEK gerneral purpose*, Accessed 13/01/2013; Available from: http://www.matweb.com/search/datasheet.aspx?MatGUID=ffc10b084c4e4dd6975438d9968e1292.

[119] Purslow, D., *Matrix fractography of fibre-reinforced thermoplastics, part 2. shear failures.* Composites, 1988. **19**(2): p. 115-126.